On the Prediction of Gas Hold-up in Ebullated Bed Reactors

by

Amir Mowla

A thesis
presented to the University of Waterloo
in fulfillment of the
thesis requirement for the degree of
Doctor of Philosophy
in
Chemical Engineering

Waterloo, Ontario, Canada, 2019

Examining Committee Membership

The following served on the Examining Committee for this thesis. The decision of the Examining Committee is by majority vote.

External Examiner:	Arturo Macchi Professor, Dept. of Chemical and Biological Engineering University of Ottawa
Supervisor(s):	Marios A. Ioannidis Professor, Dept. of Chemical Engineering University of Waterloo
Internal Member:	Nasser Mohieddin Abukhdeir Associate Professor, Dept. of Chemical Engineering University of Waterloo
Internal Member:	Hector M. Budman Professor, Dept. of Chemical Engineering University of Waterloo
Internal-External Member:	Zhongchao Tan Professor, Dept. of Mechanical and Mechantronics Engineering University of Waterloo

This thesis consists of material all of which I authored or co-authored: see Statement of Contributions included in the thesis.

I understand that my thesis may be made electronically available to the public.

Statement of Contributions

I hereby declare that I am the sole author of this thesis. I have designed and constructed the pilot scale multiphase flow system used in this study. I have performed the experimental studies and subsequent data analysis and I have written all of the chapters contained in this thesis.

My supervisor, Prof. Marios Ioannidis provided continual support and guidance throughout this work. He also contributed with many helpful editorial comments and corrections. My committee members, Prof. Nasser Abukhdeir and Prof. Hector Budman provided valuable guidances in developing the CFD simulations used in Chapter 2 and contributed in data analysis in Chapter 4.

Dr. Mehrez Agnaou contributed in developing CFD simulations of Chapters 2 and 3. Also, Dr. Tanyakarn Treeratanaphitak contributed in data analysis of Chapter 4.

Abstract

Commercial ebullated bed reactors (EBRs) are three-phase fluidized bed systems used for hydroprocessing (upgrading) of bitumen, a major Canadian resource. The objective of this thesis is to improve the understanding of the hydrodynamics of the EBRs through a combination of experimental investigation and CFD modeling. The experiments were conducted in a transparent cold-flow pilot scale reactor (inner diameter of 15.2 cm and total height of 2.2 m) and were focused on the most important parameter in the design and operation of fluidized bed systems, *i.e.*, the overall (average) gas hold-up. The pilot scale setup was operated in both two-phase (gas-liquid) and three-phase (gas-liquid-solid) modes in order to investigate the fluid dynamics in the bed and the freeboard regions present in EBRs.

In two-phase flow mode, experiments were performed with and without internal gas/liquid separators (recycle cups connected to a recycle line). The recycle cups were fabricated on the basis of designs proposed in the patent literature using a desktop 3-D printer. Different concentrations of ethanol were added to distilled water in order to reproduce the conditions of high gas hold-up and foaming frequently observed in commercial EBRs. The two-phase systems were also simulated with the Euler-Euler model using a finite volume method in the `OpenFOAM` toolbox. The average bubble size is a key input to this model and must be representative of the physical system. Provided this condition is met, the Euler-Euler model can predict the average gas hold-up under conditions of homogeneous (dispersed) two-phase flow to within 10% of the experimental values, regardless of the mode of operation (co-current vs. bubble column). Predictions of the gas hold-up under conditions of co-current heterogeneous two-phase flow are, however, less accurate (22% average error) - a result likely linked to limitations of the available empirical swarm correction models. Experiments in the systems with recycle cups showed that the performance of the cups in gas/liquid separation deteriorated in foaming systems. Also increasing the inlet liquid flow rate and/or recycle liquid flow increased the amount of entrained gas in the recycle stream. Simulation of these experiments highlighted the strengths and limitations of the Euler-Euler model.

As far as three-phase systems are concerned, a meta-analysis of a large body of published data produced a set of empirical correlations for predicting the overall gas hold-up data for systems operating with water and spherical particles. Experiments conducted to investigate the effect of particle wettability on the gas hold-up in a three-phase fluidized bed demonstrated the limitations of such an empirical approach. For the system operating with hydrophilic particles, gas hold-up values of up to 15% were predicted with less than 25% error by the most accurate correlations. For the system of hydrophobic particles, however, the correlations failed in prediction of gas hold-up and the average error

was more than 56%. Experiments demonstrated that rendering the particles hydrophobic decreased the gas hold-up by more than 20%. This was found to be the result of larger bubble size distribution in the bed of hydrophobic particles. In these systems, adhesion of bubbles to particles formed bubble-particle agglomerates with less apparent density than bare particles. Such gas-padded particles have less ability to penetrate and break-up the bubbles. Consequently, the average bubble size was larger in the bed of hydrophobic particles and also in the freeboard region above the bed. According to the semi-empirical models on foam height dynamics, steady state foam thickness is inversely proportional to the bubble diameter. Therefore, foam thickness is expected to be smaller for the system of hydrophobic particles. The foam thickness measurements in this study were consistent with the findings of the semi-empirical models.

Acknowledgements

Foremostly, I would like to express my sincere gratitude to my supervisor Prof. Marios Ioannidis. Not only this work could not happen without his continuous encouragement and support, but his guidance open doors to learn how to tackle a challenge.

I would like to thank my examining committee: Prof. Arturo Macchi (University of Ottawa), Prof. Zhongchao Tan, Prof. Nasser Mohieddin Abukhdeir, and Prof. Hector Budman for their time and effort in reading my Ph.D. thesis and for their valuable comments.

I thank my fellow labmates and colleagues, especially Dr. Mehrez Agnaou and Dr. Tanyakarn Treeratanaphitak for the stimulating discussions, for the sleepless nights we were working together before deadlines, and for all the fun we have had in the last five years.

I would also like to thank Mr. Bert Habicher, the mechanical systems designer in the Chemical Engineering department, for his great help and insightful comments in design and construction of the pilot scale multiphase flow system.

The Natural Sciences and Engineering Research Council of Canada (NSERC), University of Waterloo, Shell Canada, and the Department of Chemical Engineering are all acknowledged for their financial support of this project. Compute Canada is also acknowledged for providing computational facilities.

I want to thank all of my dear friends, especially Navid, Rasool, Kazem, Mina, Sepeher, Ehsan and Mahshad for all their help, support, and valuable hints.

In the end, my special thanks go to my family. My lovely wife, has been extremely supportive of me throughout this entire process and has made countless sacrifices to help me get to this point. My kind parents and my great brothers who always have supported me in ups and downs of this path.

Dedication

To my wife, Forough, for her continuous love, support and encouragement!

and,

To my parents, Dariush and Giti, who always picked me up on time and encourage me to go on every adventure, especially this one!

Table of Contents

List of Tables

List of Figures

Nomenclature

Acronyms

AARE	Average Absolute Relative Error
ABS	Acrylonitrile butadiene styrene
AC	Alternating current
AIC	Akaike's Information Criterion
ANN	Artificial Neural Network
CFD	Computational Fluid Dynamics
EBR	Ebullated Bed Reactor
ID	Inner diameter
LES	Large eddy simulation
OTS	Octadecyltrichlorosilane
RSM	Reynolds stress model
SSR	Residual Sum of Square

Greek Symbols

α	Time-averaged local phase volume fraction
β_g	Gas-liquid density ratio ($\frac{\rho_g}{\rho_l}$)
β_p	Solid-liquid density ratio ($\frac{\rho_p}{\rho_l}$)

ϵ	Overall phase hold-up
γ_b	Scaled bubble diameter ($\frac{d_b}{D_c}$)
μ_l	Liquid dynamic viscosity
ν	Kinematic viscosity
ω	Akaike weight
ρ_g	Gas density
ρ_l	Liquid density
ρ_p	Particle density
σ_r	Scale parameter in Rayleigh probability function
σ_ϵ^2	Estimated variance
$\sigma_{g,l}$	Liquid surface tension
$\boldsymbol{\tau}$	Stress tensor
$\boldsymbol{u}$	Phase velocity
ν_t	Turbulent viscosity

Roman Symbols

$2a$	Bubble major axis in Eq.2.3
$2b$	Bubble minor axis in Eq.2.3
Δz	Height difference
$\langle l_v \rangle$	Average bubble chord length
$\boldsymbol{g}$	Gravitational acceleration
$\boldsymbol{M}$	Inter-phase momentum transfer term
$\boldsymbol{R}_q$	Reynolds stress tensor
A_c	Cross-sectional area

C_l	Lift coefficient
C_d	Drag coefficient
C_{vm}	Virtual mass coefficient
D	Diffusion coefficient of gas in liquid
d_b	Bubble diameter
D_c	Column diameter
d_p	Particle diameter
d_r	Scaled particle diameter ($\frac{d_p}{D_c}$)
Eo	Eotvos number ($\frac{g(\Delta\rho)d_b^2}{\sigma_{g,l}}$)
Fr_l	Liquid-phase Froude number ($\frac{u_{sl}^2\rho_l}{g\Delta\rho D_c}$)
G	Electrical conductance
h	Swarm correction factor in Eq.2.14
H_e	Expanded bed height
H_∞	Steady state foam thickness
I	Turbulent Intensity
$l_v(r)$	Time-smoothed chord length at a radial position r
l_{vc}	Time-smoothed chord length at center of the column
l_{vw}	Time-smoothed chord length at the wall of the column
Mo_l	Liquid-phase Morton number ($\frac{g\mu_l^4}{\rho_l\sigma_{g,l}^3}$)
P	Pressure
$P(l_v, \sigma_r)$	Probability density function of bubble chord length
R	Column radius in Eq.4.1

R^2	Coefficient of correlation
R_r	Recycle ratio
Re_p	Particle Reynolds number ($\frac{\rho_l u_{sl} d_p}{\mu_l}$)
Re_l	Liquid-phase Reynolds number ($\frac{\rho_l D_c u_{sl}}{\mu_l}$)
S	Dimensionless Ostwald coefficient of solubility
t	Time
u_o	Bubble terminal velocity
u_r	Gas-liquid velocity ratio ($\frac{u_{sg}}{u_{sl}}$) in chapter 4 and relative velocity in chapters 2 and 3
u_{lmf}	Minimum fluidization velocity
u_{sg}	Gas superficial velocity
u_{sg}^{min}	Gas superficial velocity at the onset of foaming
u_{sl}	Liquid superficial velocity
V	Volume of computational domain
W	Work of adhesion
W_s	Mass of solid particles
We_l	Liquid-phase Weber number ($\frac{\rho_l D_c u_{sl}^2}{\sigma_l}$)
ν_m	Mixture velocity

Chapter 1

Introduction

1.1 General Overview

Upgrading is the term given to a process which converts bitumen, heavy oil or vacuum residue to an improved quality synthetic crude oil [68]. The upgrading process can improve the quality of crude oil via viscosity reduction, density reduction, contaminant (particularly sulfur and nitrogen) removal or all of the above. Bitumen is upgraded by either hydrogen addition (hydroprocessing) and/or carbon rejection (fluid bed coking) technologies. Compared to coking, hydroprocessing offers higher liquid yields, better distillate qualities and lower emission levels of sulfur dioxide. The main feedstock for any upgrader is a low-quality heavy oil, whereas the product is a lighter crude oil with higher value. The produced crude oil is then sent to refineries for further processing into a wide range of higher-value liquid products, such as lubricants and petrochemicals [68].

Co-current fluidized or *ebullated* beds of catalyst-impregnated porous pellets are used for hydroprocessing of heavy oils and bitumen. Two licensed process are available for ebullated bed technology: LC-Fining and H-Oil [200]. The difference between these two technologies is mainly in the location of the recycle pump (see Fig. 1.1). The ebullated bed reactors (EBRs) are three-phase fluidized bed reactors in which the hydrogen gas and liquid feed are introduced into a plenum chamber below the distributor grid, mixed with a recycled liquid stream and transported upward through an expanded bed of catalysts [134]. Hydrocarbon vapors and excess hydrogen exit from the top of the reactor. Part of the liquid is also withdrawn as liquid product. The catalyst used for this process is usually porous alumina pellets with Ni/Mo or Co/Mo as the active metals [127]. A recycle line connected to a recycle cup, helps to recycle the stream of liquid which is pumped through

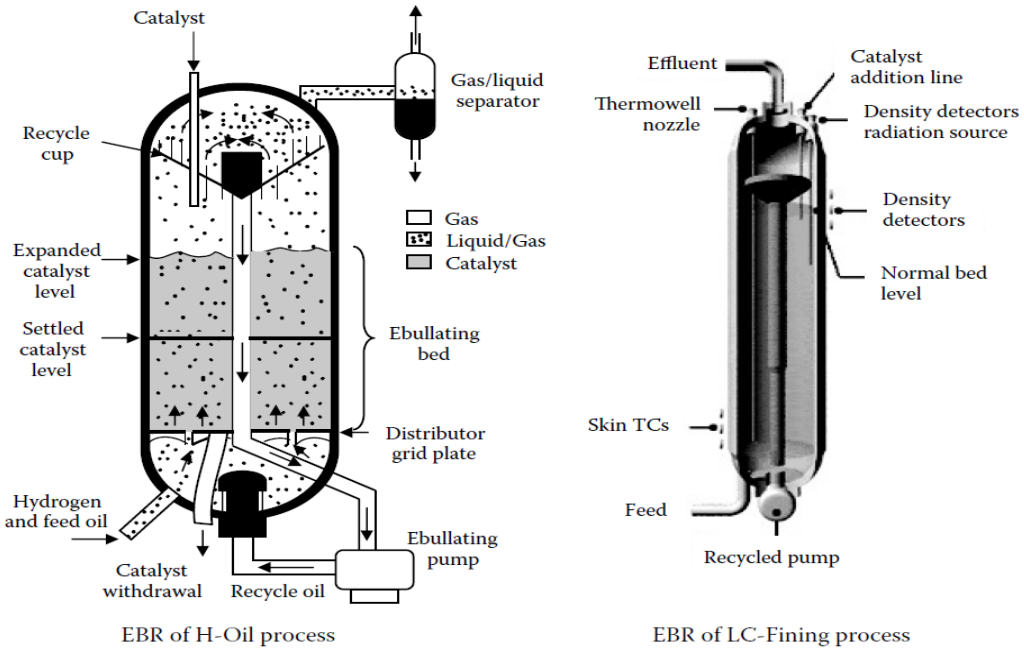

Figure 1.1: H-Oil and LC-Fining ebullated bed reactors (EBRs) [10]

a distributor at the bottom of the EBR. The operating temperature and pressure in the EBR are about 420-450 °C and 10-15 MPa, respectively. The level of expanded bed is monitored using gamma-ray density detectors. The EBR technology has been effective in processing of heavy oil and bitumen and the following advantages have been reported in the literature in connection with its utilization:

- Flexibility in addition and removal of catalyst particles which permits long term operation without system shutdown,
- Great heat transfer rates and minimal temperature gradients in the reactor, mainly due to the recycled liquid stream which provides vigorous mixing in the reactor,
- Absence of bed plugging which enables the hydroconversion of feeds with solid particles.

In the hydroprocessing of bitumen using EBRs, the presence of a minimum quantity of gas phase is necessary to perform the catalytic reactions. However, high gas hold-up values (more than 25%) have been observed in the industrial scale EBRs [54, 134]. The excess

hydrogen and vapor products decrease the effective volume and bitumen residence time in the reactor. Additionally, the presence of gas phase in the recycle stream decreases the efficiency of the recycle pump and disturbs the ebullated bed stability [34]. Entrainment of gas in the recycle line is a major contributor to high gas hold-up values in the EBR, limiting the conversion of bitumen. Foam formation in the EBRs further aggravates gas entrainment in the recycle line [201, 134].

Clearly, development of techniques to reduce the circulating gas are of great interest. Previous studies on gas hold-up reduction led to addition of an internal gas/liquid separator, called recycle cup, in the freeboard region of the reactor. Implementation of the recycle cup is an effort to improve the gas/liquid disengagement in the freeboard region, such that a smaller amount of gas is entrained in the recycle line [108]. Determination of an optimum recycle cup design has been a concern in the last 50 years and several cup designs have been developed and patented [74, 130, 69, 38, 32, 181, 201, 34, 31, 45, 28, 61]. These studies have been focused on geometric modification of the recycle cups to improve their efficiency. A few of recycle cup designs are shown in Fig. 1.2. In addition to design and implementation of the recycle cups, suppression of foam in the freeboard region of the EBRs could also decrease the amount of entrained gas in the recycle line. Given the low surface tension of the liquid phase and the likely presence of surface-active substances (such as naphthenic acid [68]), foaming is inherent to hydroprocessing reactors [201, 72]. Small solid particles present in the liquid may also act as strong foam stabilizers if they adsorb at the gas/liquid interface. The use of chemical foam control agents is not practical in the case of EBRs, since these agents are cracked under the severe operating conditions in the hydroprocessing units. A few studies have attempted to provide foam suppression methods, mainly by adjusting the surface properties of particles in simple bubble columns reactors [72, 128].

The design of an EBR is a challenging task that is presently accomplished mainly on the basis of empirical correlations which provide estimates for critical hydrodynamic parameters, such as the overall gas hold-up [53]. These correlations, have been difficult to generalize and their reliability for predicting the behavior of industrial units is questionable [134, 195]. Neglect of the role of important hydrodynamic properties, such as gas density, is a potential cause of the failure of the empirical correlations. A great number of published studies reported attempts to predict the hydrodynamic behavior of EBRs over a wide range of operating conditions using a single unified correlation [53, 188]. Considering the complexity of bubble-particle interactions, it is not surprising that these attempts have been met with limited success as significant differences remain between predictions and experimental measurements.

Due to the high cost and practical difficulties with conducting experiments in EBRs at

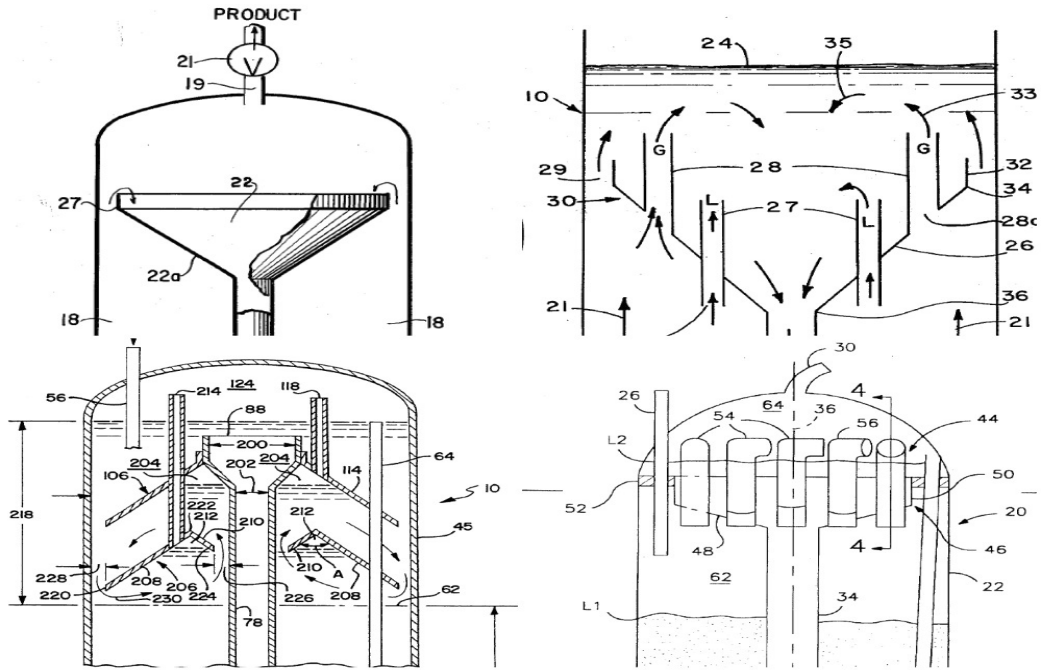

Figure 1.2: Examples of patented recycle cup designs

real operational conditions (high pressure and temperature), computational fluid dynamics (CFD) is rapidly drawing interest as a fast and an efficient tool to study the complex hydrodynamics within EBRs. The use of CFD to complement and enhance experimental studies could result in significant advances, but requires careful verification and validation. Rigorous validation requires close cooperation between modelers and the experimentalists and should be done across a wide range of operational parameters [67]. Rigorous validation of CFD studies in the case of co-current multiphase flows in the presence of internals such as recycle cups, are rare. In the majority of cases, CFD studies are validated only qualitatively and only against very limited experimental data.

1.2 Motivation

During the last few decades, the rate of world consumption of petroleum products has surpassed the rate of discovery of accessible high quality petroleum resources. As a result, the less desirable heavy oil and bitumen resources have attracted a lot of attention from oil and gas producers around the world. Although the cost of process and production of

such materials is high comparing to the desirable petroleum materials, these resources are abundant. Therefore, they have become significant as a secure future source of energy [68].

Canada has one of the largest bitumen reserves in the world, recently estimated at 173 billion barrels based on available commercial technology [68]. Canadian oil sands are found in three locations: the Athabasca, Peace River and Cold Lake areas in Alberta and Saskatchewan. Total oil sands production in Canada is reported as 2.3 million barrels per day. Currently, two methods are applied for recovery of bitumen, depending on the depth of the deposit. Mining techniques are used for the near-surface deposits, while the deeper deposits are recovered using in-situ techniques such as primary production, cyclic steam stimulation and steam assisted gravity drainage [1]. The recovered bitumen is highly viscous and requires upgrading to synthetic crude oil for conventional oil refining.

Currently, all bitumen recovered in Alberta is upgraded to synthetic crude oil in Shell, Suncore and Syncrude upgraders. These upgraders produce a wide range of synthetic products. The Shell upgrader, for example, produces intermediate refinery feedstock for the Shell Scotford refinery along with sweet and heavy crude oil [1]. Upgrading units can be located either close to the oil production or beside refineries. These common pathways are shown in Fig. 1.3. The efficient operation of the EBRs, which is crucial in terms of both economical and environmental aspects of the upgrading process, requires deep understanding of the system hydrodynamics. While it is agreed that the performance of the recycle cup plays a key role in efficient operation of the EBRs [31], very few studies have attempted to compare, let alone predict, the efficacy of these cups for gas/liquid disengagement under similar operating conditions. Progress in this direction has been further limited by the scarcity of pilot scale EBRs replicating the gas/liquid disengagement system of industrial scale units.

This study aims to fill existing knowledge gaps in the design and operation of recycle cups by constructing an experimental cold-flow pilot scale EBR with the flexibility to accommodate different cup designs. This enables comparisons of the performance of these designs with both foaming and non-foaming liquids, and improved understanding of the interaction between the hydrodynamics in the three-phase (particle bed) section and the recycle cup. At a more fundamental level, a systematic experimental investigation is enabled of the role of surface forces on bubble-bubble and bubble-particle interactions underpinning EBR hydrodynamics and foam formation. The acquisition of new experimental data prompts a quantitative re-evaluation of both empirical correlations and CFD simulation as means to predict the gas hold-up in EBR.

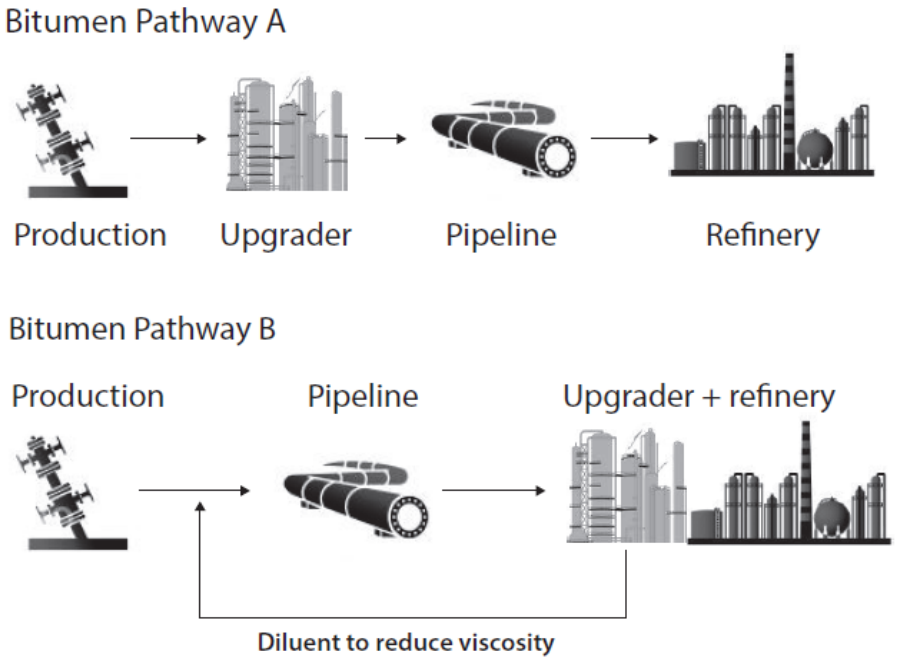

Figure 1.3: Common locations of upgraders [68]

1.3 Background

1.3.1 Gas-Liquid-Solid Fluidized Beds

As mentioned previously, EBRs are gas-liquid-solid fluidized beds employed for hydroprocessing of bitumen. Various aspects of three-phase fluidized beds have been studied extensively and key findings have been collected in several books and reviews [146, 51, 141, 53]. At this point, a distinction must be made between slurry bubble columns and three-phase fluidized beds. In a slurry bubble column, the size of solid particles is typically less than 100 µm and their volume fraction is less than 10%. In these systems, gas flows through a liquid containing suspended particles, while the liquid superficial velocity is kept low compared to gas. Considering the small particle size, fluidization occurs mainly due to bubble agitation. In the three-phase fluidized bed systems, however, particles are typically larger than 1 mm and their volume fraction is greater than 20% [141]. It is important to note that in slurry bubble columns, particles are usually carried in and out by the liquid stream. On the contrary, in fluidized beds addition or withdrawal of the particles is independent of the liquid stream. A three-phase fluidized bed consists of three main sections: the gas/liquid distributor (plenum chamber), the bulk fluidized bed and the freeboard region.

The plenum chamber is the area below the distributor grid where the gas and liquid enter and mix together. The bulk fluidized bed is the main part of the reactor where catalytic reactions take place and the freeboard region is the solid-free (gas-liquid) area above the fluidized section. Important hydrodynamic parameters for the design and development of three-phase fluidized bed reactors are flow regime transition, gas hold-up and minimum fluidization velocity [56].

Flow regime and morphology (bubble shape and size distribution) in the three-phase fluidized beds have been the topic of several studies. Muroyama and Fan [141] identified three flow regimes that can occur inside a three-phase fluidized bed consisting of air,water, and spherical particles; bubbling flow, slug flow and transitional flow. The bubbling flow is divided into two subcategories named dispersed bubble flow and coalesced bubble flow (see Fig. 1.4). Zhang et al. [229], also described seven distinct flow regimes observed in an air-water-glass beads system. A schematic of these flow regimes is shown in Fig. 1.5. The identified flow regimes are as follows [174]:

- Dispersed bubble flow: In this regime almost no bubble coalescence occurs. This causes small and uniform bubble sizes. Typically this regime predominates at high liquid velocities and low gas velocities.
- Discrete bubble flow: This regime is similar to the dispersed regime in term of size and uniformity of bubbles. However, the bubble frequency is lower.
- Coalesced bubble flow: Typically occurs at low liquid velocities and intermediate gas velocities. Bubbles tend to coalesce and show a wide size distribution.
- Slug flow: In small columns (diameters of less than 15 cm), large bubbles with lengths close to the column diameter, form at high gas and low or moderate liquid velocities. In industrial columns with large diameters slugging may not occur [135, 190].
- Churn flow: This regime is very similar to the slug flow, however, churn flow is much more chaotic. The regime is characterized by increase in downward liquid flow near the reactor wall. Both bubble size and bubble rise velocity demonstrate wide distribution.
- Bridging flow: In this regime liquid and solids form bridges across the reactors which continuously broken and re-formed.
- Annular flow: This regimes occurs at extreme gas velocities and it is characterized by a continuous gas phase at the core of the column surrounded by a liquid region at the wall.

Comparing the above mentioned classifications, it may be inferred that Zhang's dispersed bubble flow, discrete bubble flow and coalesced bubble flow may be also grouped as bubbling regime under Fan's classification. Churn, bridging and annular flow regimes can be considered as transitional regime in Fig. 1.4.

Knowledge of flow regime transition is essential for the design and operation of industrial reactors, as the flow regime can affect the reactors' performance significantly. Although several flow regimes have been identified in three-phase fluidized beds, the main interest lies in detecting the transition between the dispersed bubble flow (homogeneous flow regime) and the coalesced bubble flow (heterogeneous flow regime)[56, 58]. The term transition velocity describes the gas superficial velocity which, at a constant liquid velocity, marks the transition from homogeneous flow to heterogeneous flow. The transition velocity is known to depend on the physical properties of gas and liquid phases, solid characteristics, gas distributor design and the geometry of bed [135].

The particle size has a particularly significant effect on flow regime transition and morphology. Ostergaard [146] performed flow regime studies using glass particles with diameters of 1 mm and 6 mm and found that relatively small particles ($\leq$ 1 mm) were associated with large coalesced bubbles, whereas larger particles ($>$ 2.5 mm) were associated with small uniform bubbles. Darton [42] reported intense bubble coalescence in systems with glass bead particles $<$ 2.5 mm. It was observed in three-phase fluidized beds of small particles that large bubbles moved as a homogeneous fluid of high viscosity, while small bubbles within beds of large particles moved through the bed as in a pure liquid containing obstacles (the solid particles) around which they traveled. Zhang et al. [229] also observed a significant decrease in the region of the coalesced flow regime in beds with 4.5 mm glass bead particles compared to beds with 1.5 mm particles.

Studies on flow regime transition have been based mainly on visual observations. Although the flow pattern can be observed visually, determination of the transition point without quantitative measurements is troublesome [229]. Given the complex nature of the multiphase systems, more recent studies have focused on measurement of the time evolution of hydrodynamic variables either to identify a flow transition or to diagnose the underlying flow regime [99, 229, 27, 58].

1.3.2 Gas-Liquid Two-Phase Flows

The freeboard region above the reaction zone in the EBRs is a co-current gas-liquid flow system. Therefore, understanding the hydrodynamics of gas-liquid flows is relevant to the study of EBRs. Gas-liquid flows occur in several industrial applications including wastewater treatment, transportation of oil and nuclear reactors [223]. Among the two-phase flow

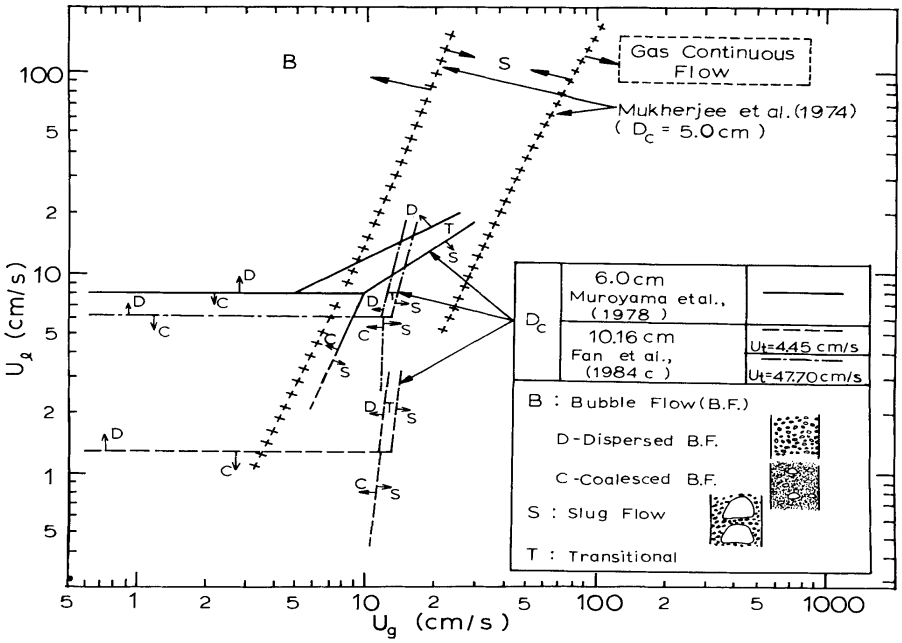

Figure 1.4: Flow regime diagram for the co-current gas-liquid-solid fluidized bed [141]

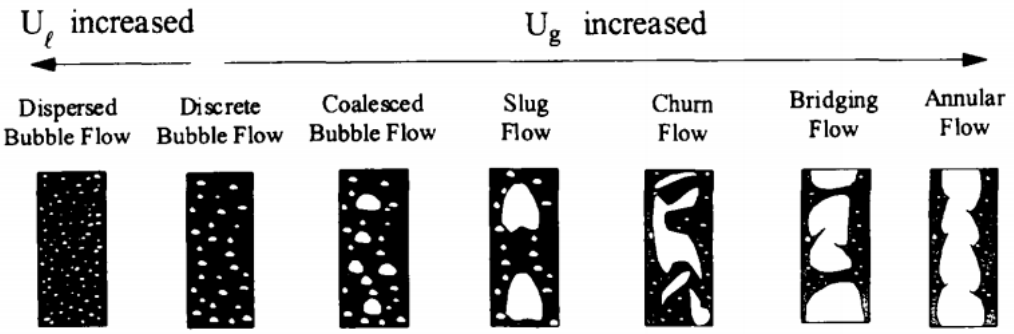

Figure 1.5: Schematic diagram of flow regimes [229]

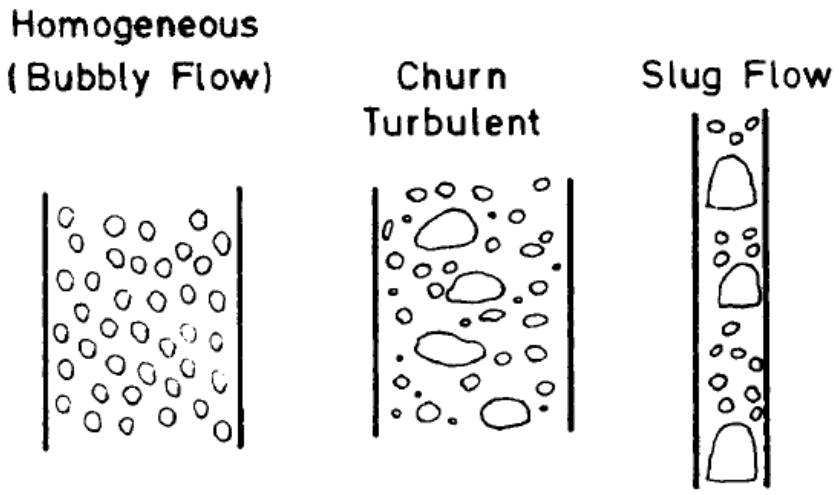

Figure 1.6: Common flow regimes in gas-liquid flows [189]

systems, gas-liquid flows are the most complex as they combine a deformable interface with the compressibility of the gas phase [76]. Due to the wide range of industrial applications, the hydrodynamics of gas-liquid flows have been studied extensively [94, 188, 20]. The bed of solid particles in EBRs acts as the distributor, where the gas and liquid phases mix together before entering the freeboard. Similar to the three-phase fluidized beds, two-phase gas-liquid flow also depends strongly on the prevailing two-fluid interfacial structure or flow regime. For co-current gas-liquid flow in a vertical column, three main flow regimes have been distinguished; dispersed or homogeneous, churn-turbulent or heterogeneous and slug flow regime (see Fig. 1.6).

The homogeneous flow is characterized by small bubble sizes and relatively uniform bubble size distribution over the cross section of the column. This flow regime generally occurs at low to moderate gas velocities or at very high liquid velocities [229, 120] and is associated with limited bubble interaction. The heterogeneous regime, which occurs at moderate to high gas velocities, is associated with unsteady flow patterns and broad bubble size distribution caused by recurrent bubble coalescence and break-up. Finally, at very high gas velocities and in small column diameters, slug flow regime prevails in the system [189, 94]. Understanding of flow regimes is of great importance in the design and scale-up of multiphase systems. The hydrodynamics of the homogeneous and heterogeneous flow regimes are completely different, giving rise to very different mixing, heat and mass transfer rates [190].

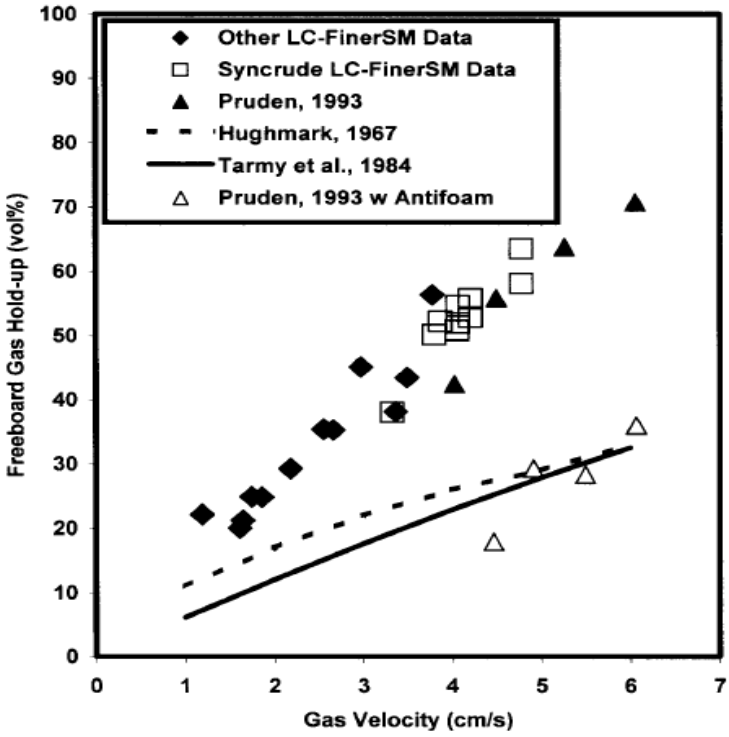

Figure 1.7: Gas hold-up in the freeboard region of commercial EBRs with recycle cup [134]

1.3.3 Previous fluid dynamics studies in EBRs

The majority of research studies concerned with EBRs have been conducted in air-water-glass beads systems under ambient conditions. These systems are considerably different from industrial hydroprocessors, which involve multicomponent liquids, non-spherical particles and higher gas densities. Measurements of gas hold-up and fluid physical properties in industrial hydroprocessors have shown that the EBRs operate with high gas hold-ups (more than 25%) and under dispersed flow regime [54, 134, 152]. The gas hold-up in the freeboard region is also reported to be over 50% (see Fig. 1.7). Simulating this hydrodynamic performance in systems with water as the liquid phase under ambient condition is difficult since generally such simple systems operate at lower gas hold-up values [53]. Several research studies have therefore tried to simulate high gas hold-up conditions in pilot scale systems using similar phase physical properties and operating conditions (elevated pressure and temperature) or by adjusting the bubble coalescence behavior by addition of solutes such as alcohols and surfactants [40, 152].

Application of liquids with surface tensions lower than water ($\sigma_{g,l}$ values of 0.025 to

0.03 N/m as opposed to 0.072 N/m), such as kerosene and gas oil, resulted in higher bed expansion and gas hold-up due to increased foaming [173]. Tarmy et al. [204] and Luo et al. [122] used n-pentane ($\sigma_{g,l} \approx 0.016$ N/m) and Paratherm NF heat transfer liquid ($\sigma_{g,l} \approx 0.025$ N/m) in pilot scale slurry bubble column reactors operating at high pressures (up to 17 MPa) and temperatures (up to 450 °C). They reported gas hold-ups as high as 50% and observed smaller bubble size and reduced bubble velocity at high pressures. Luo et al. [121] also studied the effect of elevated pressures (up to 15.6 MPa) on gas hold-up in a three-phase fluidized bed. They reported average bubble size reduction and narrower bubble size distribution at pressures up to 6 MPa which caused an increase in the gas transition velocity from dispersed to coalesced flow regime and increased gas hold-up. The effect of pressure was not significant above 6 MPa. Similar results were observed by Ruiz et al. [166, 165] while using diesel fuel and nitrogen to fluidize glass beads of 1.7 mm in a pilot scale EBR. Although pressures up to 15 MPa were employed, the increase in gas hold-up values was observed mainly at pressures up to 7.5 MPa. It should be mentioned that due to the low values of gas and liquid superficial velocities, high gas hold-up values were not observed.

Introducing surfactants is an alternative to the use of low surface tension liquids for achieving high gas hold-up behavior in the cold flow EBRs. However, their application increases the complexity of the multiphase system. Surfactants consist of a hydrophobic long tail and a hydrophilic head and tend to accumulate at the gas-liquid interface, thereby reducing the surface tension [184]. Addition of surfactants can affect the bubble dynamics in three ways. First, reduction of the surface tension facilitates the formation of small bubbles. Second, surfactants reduce the rate of coalescence of rising gas bubbles thereby preventing their growth [184]. Finally, as a result of the formation of surface tension gradients around the bubble surface, the drag force acting on the gas bubbles increases. The higher drag force reduces the bubble rise velocity, thereby increasing the gas hold-up [40, 189].

Both aqueous alcohol solutions and commercial surfactants have been used to provide gas hold-up higher than possible with water. Fan et al. [54] investigated the addition of 0.5 and 1 wt% n-butanol and t-pentanol to water in an annular fluidized bed at atmospheric pressure. Increased gas hold-ups were observed by comparison to distilled water systems due to bubble coalescence inhibition. Using t-pentanol solutions they were able to reproduce the data of Tarmy et al. [204] in a system of 1 mm glass beads. The effect of surfactant concentration has been reported as insignificant. Addition of t-pentanol to water in a cold flow EBR of 0.89 mm cylindrical aluminum particles also reproduced Tarmy's results [198]. Gorowara and Fan [66] studied the characteristics of solutions of 16 alcohol and commercial surfactants in water and categorized the liquids based on their surface

tension behavior and bubble rise velocity reduction into three groups of low, middle and high gas hold-up liquids. They also provide a correlation to predict gas hold-up for each group. According to their classification, gas hold-up in three-phase fluidized beds can be predicted without the knowledge of the type and the concentration of surfactants. Dargar and Macchi [41] examined this approach by measuring phase hold-ups in the systems of six surfactant solutions categorized according to the criteria proposed by Gorowara and Fan. They observed that gas hold-up was mainly affected by the system operating conditions rather than by the nature and surface tension of the surfactants. However, the type of surface active agent was found to affect the stability of the foam layer formed in the freeboard region of the EBR. In a recent study, Pjontek and Macchi [151] compared the hydrodynamics of three-phase fluidized beds in systems of water and 0.5wt% ethanol with particles of different shape. They observed similar gas hold-up values while using spherical glass beads and aluminum cylinders with equivalent volume/surface area ratios in the dispersed flow regime. Some discrepancies were observed in the presence of large coalescing bubbles. Although in almost all of the above mentioned studies foaming in the reactor was observed, no published study has hitherto examined experimentally the effects of foam generation and stability on gas-liquid disengagement and the performance of the recycle cup.

1.3.4 Foaming in EBRs

As mentioned in section 1.1, gas entrainment in the recycle cup increases the gas hold-up in the hydroprocessing unit and decreases bitumen conversion. Gas entrainment is also a cause of instability of industrial hydroprocessors. If the amount of gas in the recycle conduit becomes too high, a true liquid phase would not be available at the ebullating pump inlet. In severe cases, serious liquid flow fluctuations have been observed through the pump. These flow fluctuations are manifestation of foaming [201].

A foam is a dispersion of gas bubbles in a liquid. In non-foaming systems when two bubbles approach each other, the liquid film between them drains and ruptures rapidly, so the bubbles coalesce. When the system is operating with a foaming liquid (e.g. kerosene) or when a foaming agent (e.g. alcohol or surfactant) is present, the lifetime of the liquid film between the bubbles increases and bubble coalescence is slowed down or inhibited. The bubbles form clusters instead. The stability of a foam is mostly determined by the drainage and rupture of the thin films and it is determined by several factors including both bulk solution (e.g. viscosity) and interfacial properties [184]. In low viscosity fluids like aqueous alcohol solutions, foam coarsening caused by bubble coalescence and Ostwald ripening limits the stability of foam [12]. Bubble coalescence occurs when the liquid film separating

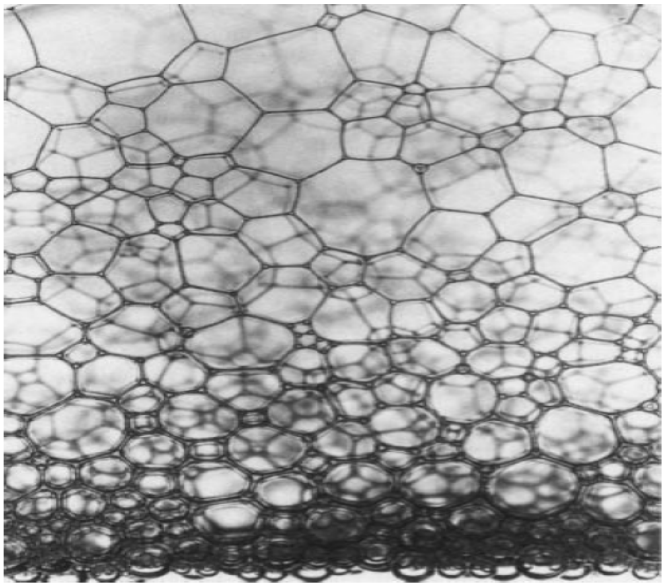

Figure 1.8: Photograph of a stable foam of an aqueous 5% SDS solution [177]

two bubbles becomes sufficiently thin and ruptures, causing the bubbles to merge. Ostwald ripening or inter-bubble gas diffusion, on the other hand, takes place when large bubbles consume adjacent smaller bubbles via solute diffusion driven by differences in pressure in the two bubbles [199]. Large bubbles are more buoyant, thus separated by thinner liquid films and more prone to coalescence. Ostwald ripening is more significant the greater the solubility and diffusion coefficient of the gas in the liquid phase [220]. The combination of bubble coalescence and Ostwald ripening causes foam coarsening (see Fig. 1.8). In high viscosity fluids, the rate of film drainage is slowed down, significantly limiting foam coarsening [150]. The process of foam generation, initially involves the accumulation at the macroscopic gas-liquid interface of bubbles surrounded by relatively thick liquid films. The foam grows at its largest rate as no bubbles burst at the top. As the foam height increases and liquid drainage takes place, adjacent bubbles are more likely to coalesce when the film separating them becomes sufficiently thin. This phenomenon is significant at the top of the foam where the oldest bubbles are present and the foam is relatively "dry". The foam reaches a steady-state height when the inlet flow of gas at the bottom of the foam equals the amount of gas released by bubbles bursting at the top [12]. Several theoretical and semi-empirical models exist in the literature to predict the steady state foam height by considering the foam growth and collapse kinetics. A list of these models can be found in the review of Wang et al. [215].

The foam produced in systems with low surface tension liquids like kerosene or aqueous alcohol solutions are generally not stable and disappears quickly after the gas injection is paused. The presence of surfactants is required for foam stability. Surfactants adsorb at the gas-liquid interface, such that their hydrophobic tail protrudes into the vapor phase leaving the hydrophilic head in contact with water. Such an arrangement reduces the surface tension and modifies the rheology of the interface [177]. For example, addition of a typical surfactant such as sodium dodecyl sulfate (SDS) up to a so-called critical micellar concentration (CMC), reduces the surface tension of water from 0.072 to 0.033 N/m. Above the CMC, the interface is saturated and the surface tension is independent of the concentration. One consequence of the reduced surface tension is that less mechanical energy is required to create great interfacial area, that is small bubbles. Additionally, bubble coalescence is resisted. Drainage of the liquid film between the bubbles occurs mainly due to gravity. If a surfactant-stabilized liquid film separating two bubbles goes through a sudden expansion due to the liquid drainage, the expanded section of the film will have a higher surface tension as the number of surfactant molecules per unit area decreases. This local surface tension gradient, induces liquid flow in the direction of higher surface tension (see Fig. 1.9). This phenomenon is called Marangoni flow and opposes film thinning due to gravity, preventing the neighboring bubbles from coalescing [184]. The Marangoni effect improves the elasticity of foam films, enabling them to resist deformations without rupturing.

The presence of fine solid particles in EBRs, which may be present in the feed or generated by catalyst attrition, may also lead to foam stabilization if these particles adsorb at the gas-liquid interface. Catalyst attrition is described as production of fines due to collisions among catalyst particles and the impact between catalyst particle and the reactor wall [127]. Attrition can vary from particle abrasion (production of fines from removal of asperities of particle surface) to complete fragmentation (breakage of mother particle into similarly size fragments). Unstable bed expansion and foam formation in the hydroprocessing reactors due to catalyst attrition has been reported in a few studies [93, 92]. Addition of finely divided solid particles has been reported as one of the most practical ways to improve foam stability [80, 95]. Adsorption of fine particles at the gas/liquid interface improves the film elasticity required for bubble coalescence prevention. Experiments on foam films stabilized by solid particles showed that the particles can bridge gas bubbles in close contact by formation of strong three phase contact lines pinned on the particle surface and inhibiting bubble coalescence [95].

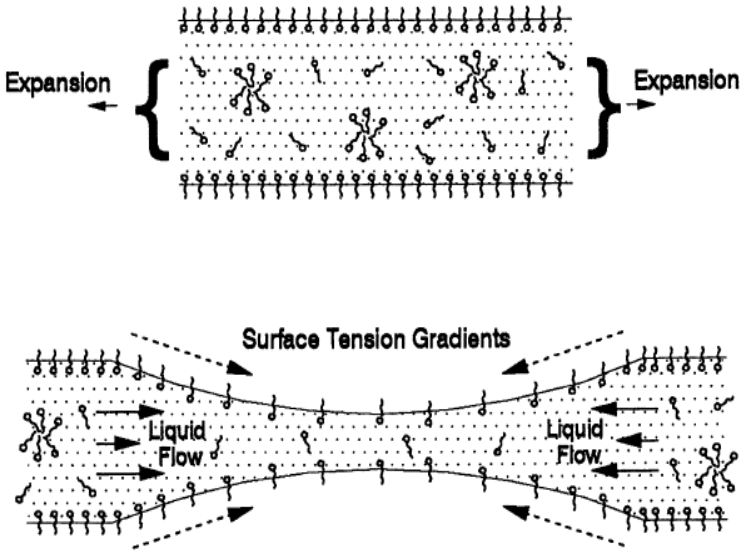

Figure 1.9: Induced liquid flow due to surface tension gradient (Marangoni effect) [184]

1.3.5 Design considerations in scale-down of pilot scale EBRs

Although significant effort has been focused on the hydrodynamics of EBRs, scaling-up the results from laboratory and pilot scale units to industrial scale ones remains an unmet challenge. The deviation among measurements in the experimental systems in the literature and those from industrial units are mainly due to significant differences in operating conditions, phase physical properties and column geometries [152]. To address these issues, scale-down approaches have been introduced by researchers. These approaches are based on the principles of dimensional similitude and the Buckingham Pi theorem [218].

Safoniuk et al. [175] proposed a scale-down approach based on matching a series of five dimensionless groups (Mo_l, Eo, Re_p, β_p and u_r, see Table 1.1) between separate systems. They validated their approach by comparing the average gas hold-up in two reactors of 0.0826 m and 0.91 m diameter with different gas, liquid and solid phases. In their method, gas density was only considered in the gas phase buoyancy term. Also the scaled particle diameter (d_r) was neglected due its minor effect in the cases where the column diameter is much larger than the particle diameter. Later, Macchi et al. [124] examined Safoniuk's approach to capture the coalescing behavior and concluded that the five dimensionless groups were not enough to characterize the hydrodynamics of three-phase fluidized beds. An attempt was also made by McKnight et al. [134] to examine this method by matching the five dimensionless groups between the larger cold-flow reactors used by Safoniuk and an

industrial scale LC-Finer. The gas hold-up value in the cold-flow reactor was half of those in the industrial column. This significant discrepancy could be due to following potential factors:

- Missing physical properties (or dimensionless groups) that are important on the bed hydrodynamics,
- Absence of the internal gas recycle in the cold-flow reactor,
- Inaccurate measurements of gas hold-up in either the cold-flow unit or the industrial unit

Recently, Pjontek et al. [152] found the first factor above as the main reason in the failure of dimensional similitude method. Therefore, by considering physical properties which were neglected in the work of Safoniuk (gas phase density and interfacial properties), they recommend $Re_l, Ar, \beta_g, \beta_p$ and u_r (see Table 1.1) as the dimensionless groups which should be matched between separate systems. In addition to the mentioned dimensionless groups, an equivalent bubble coalescence behavior is required for dynamic similarity. This implies that the systems with coalescing behavior (e.g. distilled water) can not be compared with the ones exhibiting coalescence inhibition (e.g. systems with surfactant).

Table 1.1: Dimensionless groups used in previous literature for scale-down of EBRs

Name	**Symbol**	**Expression**
Liquid-phase Morton number	Mo_l	$(g\mu_l^4)/(\rho_l\sigma_{g,l}^3)$
Eotvos number	Eo	$(g\Delta\rho D_c^2)/\sigma_{g,l}$
Solid-liquid density ratio	β_p	ρ_p/ρ_l
Gas-liquid velocity ratio	u_r	u_g/u_l
Particle Reynolds number	Re_p	$(\rho_l d_p u_l)/\mu_l$
Liquid-phase Reynolds number	Re_l	$(\rho_l D_c u_l)/\mu_l$
Gas-liquid density ratio	β_g	ρ_g/ρ_l
Archimedes number	Ar	$(d_p^3\rho_l(\rho_s-\rho_l)g)/\mu_l^2$
Scaled particle diameter	d_r	d_p/D_c

One of the factors pointed out above was the absence of internal recycle line in the cold-flow reactors. Besides the recycle line, and in order to make geometric similitude between the cold-flow reactors and industrial units, other important issues such as gas-liquid disengagement at the outlet of the EBRs, gas-liquid distribution into the bed section and wall effects due to the column diameter should also be considered [152].

As discussed before, a recycle cup connected to internal recycle line is used in the hydroprocessors to separate gas and liquid phases in the freeboard region. Liquid recycle stream which contains gas is returned to the bed section. This implies the interaction between the freeboard region (which contains the recycle cup) and the bed section in hydroprocessors. In the absence of recycle cup and the internal recycle line, this interaction does not exist. Almost all of the studies regarding the hydrodynamics of three-phase fluidized beds in the literature employed pilot scale systems which miss the cup and internal recycle line sections. Generally, in these systems disengagement occurs in an expended overflow section. It is argued that the impact of the gas entrainment in the recycle line may be simply accommodated by increasing the gas flow rate. Although gas entrainment in the recycle line is known to increase gas hold-up in the EBR, almost nothing is known about the reverse. That is to say, little is known about the effect of EBR hydrodynamics on gas-liquid disengagement in the recycle cup.

Industrial hydroprocessor are large-diameter columns and the wall effect on average gas hold-up is negligible. This not so in pilot scale systems. For bubble column reactors, Wilkinson et al. [219] stated that the gas hold-up is independent of the column dimension if the column diameter is larger than 15 cm and the column to height ratio is greater than five. Shah et al. [188] recommended column diameters of larger than 10-15 cm. Similar results were also reported by other researchers for both foaming and non-foaming bubble columns [94]. In three-phase fluidized bed systems, Fan [53] reported that in columns of larger than 15 cm slugging would not occur even at high gas flow rates. Considering presence of internal recycle line in the EBR, it has been also reported that the cross-sectional area of the recycle line should be between 1% to 10% of the column cross-sectional area of the reactor [38].

The role of gas-liquid distribution system should also be considered in scaling down the EBRs. In commercial LC-Finer reactors, the liquid feed and gas are introduced to the plenum chamber via a horse-shoe distributor and mixed with the recycled liquid before passing through the distributor grid plate [134]. Therefore, both fluids experience significant shearing which may cause bubble break up. The grid plate is used to properly distribute the flow through the bed section and typically contain several bubble caps [127]. In the pilot scale systems, the gas phase is generally introduced through a sparger and mixed with liquid phase before entering the distributed grid plate. The gas sparger and distributor plate in cold-flow systems should also be designed in a way to effect shearing between the gas and liquid phases. Design procedures for both sparger and distributor plates have been discussed in the literature especially for bubble column reactors [174, 104].

1.4 Thesis Scope and Structure

This dissertation ultimately seeks to tackle the following important challenges regarding the hydrodynamics of EBRs:

1 - Experimentally validate Eulerian models via the prediction of hydrodynamic behavior of a scaled down cold-flow EBR

2 - Assess the possibility of testing the performance of various recycle cups in gas/liquid separation in a scaled down cold-flow EBR

3 - Develop improved empirical correlations for the prediction of gas hold-up in EBRs

4 - Investigate the effect of solid surface properties on the fluidization and foam formation in the EBRs

To achieve these goals, a pilot scale cold-flow EBR was designed and constructed. The hydrodynamics of both the two-phase (freeboard) and three-phase (particle bed) regions inside the cold-flow EBR were investigated. A comprehensive set experiments were conducted over a wide range of operational parameters (gas and liquid velocities, gas/liquid surface tension, solid surface properties) mainly to determine a key parameter is the design and operation of multiphase flow systems, *i.e.*, the overall gas hold-up. The modular design of the pilot scale EBR in this study allowed the implementation of various recycle cup designs. Therefore, performance and efficiency of two patented cup designs in gas/liquid separation were examined and compared under similar operating conditions. In the two-phase flow (with and without the internal gas/liquid separator), the data collection was combined with CFD simulations performed using the `OpenFOAM` toolbox. These studies provided insight into the accuracy of two-fluid Eulerian models in predicting the hydrodynamic behavior of multiphase flow systems. An extensive classification of experimental data of gas hold-up data from the literature was also undertaken. This permitted the development of a set of empirical correlations which are able to predict the overall gas hold-up with higher accuracy than presently possible. Lastly, the effect of particle wettability on fluidization behavior of the EBRs, as well as on foam formation in the freeboard region was also studied and the results interpreted using available models.

This dissertation comprises 6 chapters organized as follows:

- *Chapter* 2 examines the accuracy of prediction of the overall gas hold-up for gas-liquid flows inside a simple vertical column using the two-fluid Eulerian model. Gas hold-ups were measured in two operation modes, namely bubble column (no liquid flow)

and the less-frequently studied co-current flow, and for both homogeneous and heterogeneous flow regimes. Bubble diameter, a key input to the Eulerian models, was measured by image analysis (where possible) or estimated using empirical correlations. The effect of addition of turbulence models as well as swarm correction factors on the ability of Eulerian models to predict the gas hold-up was also investigated.

- *Chapter* 3 examines the efficiency of two patented recycle cup designs (obtained through 3-D printing technology) in separation of gas and liquid phases in foaming and non-foaming two phase flow systems. Gas hold-up in the recycle line was measured using electrical conductivity probes. Also, following up on the findings of chapter 2, we explored the ability of two-fluid Eulerian models in prediction of the overall gas hold-up in the two-phase flow system and inside the recycle line.

- *Chapter* 4 presents a meta-analysis approach to develop statistically significant and accurate correlations for the prediction of the overall gas hold-up in systems involving spherical particles and water as the liquid phase. Experimental data published in numerous studies over the last 40 years were collected, classified and correlated for the first time.

- *Chapter* 5 reports on the role of particle wettability on the hydrodynamics of EBRs. The experiments were conducted inside the beds of hydrophilic and hydrophobic particles of the same size and the gas hold-up data in the bed and in the freeboard region were compared and discussed. The thickness of foam layer formed on the top of the freeboard region at various operating conditions were also measured and the results were compared with predictions of two semi-empirical models.

- *Chapter* 6 summarizes the main contributions of this PhD dissertation and provides recommendations for future work.

It should be noted that chapters 2 to 5 are presented in manuscript format. Consequently, some information will be repetitive, particularly in the introduction and the experimental procedure sections.

Chapter 2

On the Prediction of Gas Hold-up in Two-Phase Flow Systems Using an Euler-Euler Model

Amir Mowla, Mehrez Agnaou, Tanyakarn Treeratanaphitak, Hector M. Budman, Nasser M. Abukhdeir, Marios A. Ioannidis

The contents of this chapter have been submitted for publication in *AIChE*.

2.1 Synopsis

We quantify the ability of the two-fluid Euler-Euler model to predict the overall gas hold-up during two-phase flow in vertical columns using a combination of experiments and simulations. Gas hold-up in a bubble column and gas hold-up in the less-frequently studied co-current flow, are investigated. For homogeneous flow characterized by nearly uniform bubble size, Euler-Euler model predictions are within 10% of the experimental values for both modes of operation, provided that the bubble diameter supplied as input to the model is the average bubble diameter in the physical system. This also holds true for heterogeneous flow in bubble columns despite the presence of a broad distribution of bubble sizes, provided that turbulence and bubble swarm effects on momentum exchange between phases are properly accounted for. Swarm corrections adequate for bubble columns, are less successful for co-current heterogeneous flow, for which gas hold-up predictions are least accurate (average error of 22%).

2.2 Introduction

Gas-liquid flow is encountered very frequently in industrial-scale reaction and separation systems associated with wastewater treatment, coal liquefaction, cooling, and food processing, to name a few [225]. The performance of these systems depends strongly on the prevailing two-fluid interfacial structure or flow regime. For vertical two-phase flow, three distinct flow regimes have been described: dispersed or bubbly flow (homogeneous regime), churn-turbulent flow (heterogeneous regime) and slug flow. Bubbly flow is characterized by small bubble sizes and relatively uniform bubble distribution over the cross section of the column. The heterogeneous regime, on the other hand, is associated with unsteady flow patterns and broad bubble size distribution caused by recurrent bubble coalescence and breakup [94]. Slug flow, described by large bubbles with lengths close to the column diameter, has been observed only in small diameter columns (less than 15 cm) at high gas flow rates [190]. Whatever the flow regime, the most fundamental parameter in the design and scale-up of gas-liquid flow systems is the average volume fraction of gas phase or overall gas hold-up [179]. Knowledge of the gas hold-up enables the determination of the gas residence time in the gas-liquid mixture and, in combination with knowledge of the average bubble diameter or bubble size distribution, it informs the gas-liquid interfacial area associated with inter-phase mass and heat transfer. The gas hold-up is a key indicator of the flow structure inside the column, the turbulent characteristics of the phases and the energy dissipation rates [106, 147, 59].

The overall gas hold-up in flowing gas-liquid systems is measurable experimentally and may be estimated from empirical correlations [227, 229, 156, 18]. The latter have been the focus of a large number of studies seeking to summarize experimental observations of gas hold-up in terms of measurable operating parameters (e.g. gas and liquid superficial velocities, liquid physical properties, *etc.*) and geometric characteristics of the studied system (e.g. column diameter). A list of these correlations can be found in the reviews of Shah et al. [188] and Gandhi et al. [59]. To date, no single correlation has succeeded in representing all experimental data. An additional limitation of empirical correlations is that they have been mainly developed using data from cold-flow systems and for specific ranges of operational parameters and working fluids, not always found in industrial applications. For these reasons, they generally fail to predict gas hold-up in high pressure/temperature systems or in systems different from those used to develop the empirical correlations [188, 195, 140].

Considering the above mentioned challenges, simulation methods – specifically, computational fluid dynamics (CFD) [214, 83] – have been used to study two-phase flow systems for the purpose of determining the gas hold-up, as well as other flow characteristics

[85, 97, 91, 84]. A key aspect of the CFD approaches to modeling multiphase flows is model selection. In this respect, the Eulerian two-fluid (Euler-Euler) model offers significant advantages for dispersed gas-liquid flow systems [33, 172]. The Euler-Euler model treats the phases as inter-dispersed continua and is stated in terms of momentum conservation equations derived for each phase through either spatial or time averaging [83]. Phase fractions indicate the amount of each phase that is present at a particular location and time. The momentum conservation equations of the phases are coupled together via closure models for inter-phase momentum transfer terms, which contain the bubble size (assumed uniform) as a key input parameter. Closure models generally consider the drag force, lift force, virtual mass force and turbulence [112, 155], and must be chosen judiciously [162, 202]. Simulation at industrially-relevant scales is possible at a reasonable computational cost with Euler-Euler models, but is prohibitively costly with models for which the computational cost scales with the number of bubbles/interfaces [197, 64, 123]. Thus, the potential exists for validation of Euler-Euler models against experimental data from large systems [62]. Validation is defined here as "the process of determining the degree to which a model is an accurate representation of the real world from the perspective of the intended uses of the model" [67]. This means that if the primary objective of CFD simulation with an Euler-Euler model is to predict the overall gas hold-up, then validation must be carried out against experimental measurements of this quantity.

In recent years, a number of computational studies have assessed different inter-phase closure relations by means of qualitative comparison of model predictions of local gas hold-up and velocity profile against limited experimental data [196, 35, 126, 73, 216, 223, 114, 24, 21, 170, 148]. While the aforementioned studies have provided significant insight into the sensitivity of Euler-Euler model results to closure relations, they have not provided a definitive test of the ability of this model to predict the overall gas hold-up. Rather, as recently noted [170], tuning of empirical parameters in order to match selected experimental data has most frequently been the case. Despite its fundamental significance for process design [122], the overall gas hold-up has not received particular attention in these studies, which have instead focused on qualitative comparisons with local parameters such as the radial gas hold-up and axial liquid velocity. A notable exception is the recent work of Gemello et al. [62]. These authors compared predictions of overall gas hold up by an Euler-Euler model against experimental data from bubble column reactors of different diameter over a wide range of operating conditions relevant to industrial application, emphasizing high gas hold-up in the heterogeneous flow regime. Gemello et al. [62] concluded that a modification to the swarm factor proposed by Simonnet et al. [193], is necessary for accurate predictions of gas hold-up. Their work supports the use of Euler-Euler model with uniform bubble size under conditions of heterogeneous flow, but has been limited to bubble columns in which the net liquid velocity is zero.

Extending the work of Gemello et al. [62], the present paper seeks to delimit the predictive capabilities of the Euler-Euler two-fluid model, especially concerning the overall gas hold-up. Using a pilot scale air-water flow reactor we acquire new experimental data on the overall gas hold-up and the average bubble size over a wide range of operational conditions. We then simulate the system using the `multiphaseEulerFoam` solver of the open-source CFD toolbox `OpenFOAM` and directly confront simulation with experiment. The paper is structured as follows: First, the experimental setup and the measurement techniques used are described in Section 2.3. Then, the Euler-Euler model, the momentum exchange closure relation and the specific simulation conditions are detailed in Section 2.4. The experimental measurements are compared to simulation results and discussed in Section 2.5, and conclusions are summarized in Section 2.6.

2.3 Experimental Setup and Procedure

2.3.1 Experimental Setup

The gas-liquid flow system used in this study is depicted in Fig. 2.1. It consists of two sections: the gas-liquid distributor (plenum chamber) and the test section. The column is a 15.2 cm inner diameter (ID) clear PVC pipe, 1.7 m in total height. The use of clear PVC allows observation of the interior of the pipe. The plenum chamber section, of the same diameter as the column, is 20 cm in height. A perforated plate containing 3 mm circular holes is sandwiched between the test section and the plenum chamber. The plate is designed to evenly distribute gas and liquid within the column.

Air and distilled water were used as the working fluids. In some cases, a 0.5wt.% aqueous solution of ethanol was used instead of distilled water. According to the literature, the addition of such small amount of ethanol to water decreases the surface tension while leaving other physical properties unchanged [41, 65]. Air was introduced to the system through two gas spargers with openings of 100 µm installed symmetrically in the plenum chamber. The liquid was pumped from a plastic tank using a centrifugal pump (Goulds pump, model 2ST1E4F4) to the bottom of the plenum chamber at specified flow rates. The gas and liquid flow rates were measured by two rotameters (Blue-White, models F-43040LNS and F-55376-GP, respectively). The range of operating parameters was selected such that either dispersed or churn-turbulent flow prevailed inside the column. Prevalence of one or the other regime depends mainly on the superficial velocities of the gas and liquid phases, as well as on the column diameter. If the liquid velocity is higher than 0.4 m/s, dispersed flow regime is established for almost all values of gas velocity [229, 120]. On

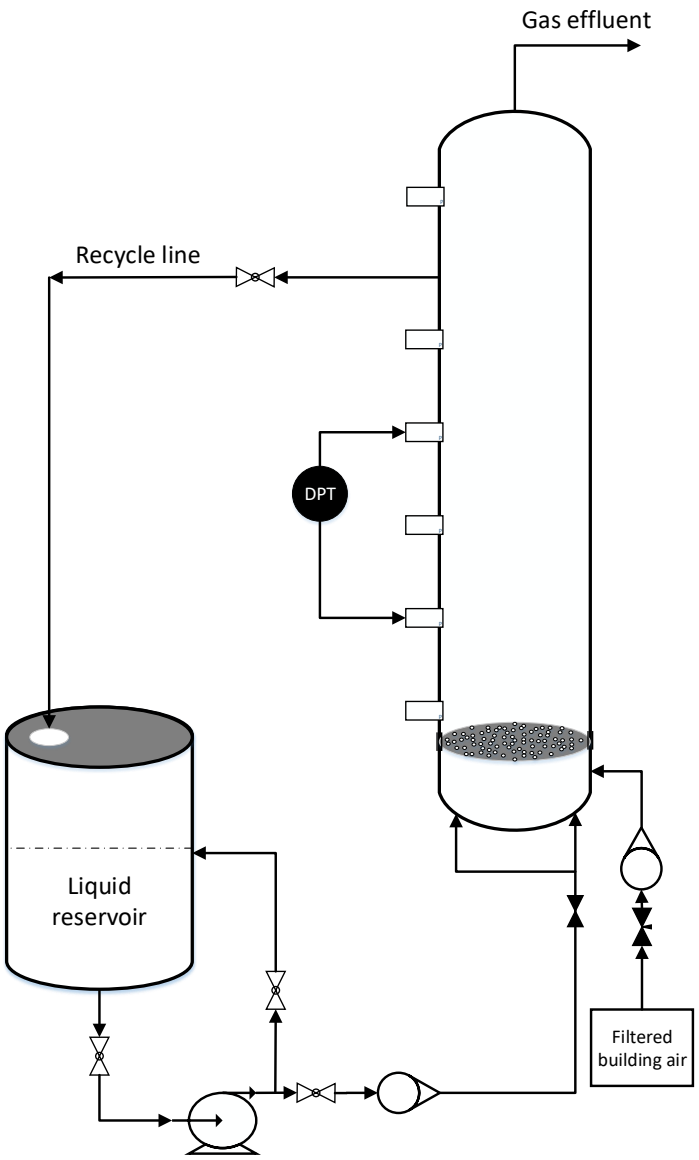

Figure 2.1: Schematics of the experimental set-up

the other hand, for liquid velocities less than 0.1 m/s, dispersed flow takes place for gas superficial velocities less than 0.04 m/s [52, 185, 43, 229, 82]. At higher gas flow rates the system switches to the churn-turbulent regime. To cover both flow regimes, three gas superficial velocities in the range 0.01 to 0.03 m/s and six gas superficial velocities in the range 0.05 to 0.19 m/s were selected for data collection. To investigate the effect of liquid flow rate, experiments were conducted in bubble column mode (without liquid injection), and in co-current flow mode with liquid injected at superficial velocity of 0.06 m/s.

2.3.2 Overall Gas Hold-up Measurement

The overall gas hold-up in the column was measured using a differential pressure transducer (Rosemount, model 3051CD2A22A1AM5C6Q4) connected to a data acquisition system. Six pressure ports were installed along the column height. The ports were located in 25 cm intervals, beginning at 10 cm above the distributor plate. Assuming negligible frictional drag, the dynamic pressure drop between any two arbitrary pressure ports can be related to the gas volume fraction (ϵ_g), as follows:

$$\epsilon_g = \frac{\frac{\Delta P}{g\Delta z}}{\rho_l - \rho_g} \tag{2.1}$$

where ΔP is the pressure difference, Δz is the elevation difference between the two pressure ports and ρ_l and ρ_g are the density of the liquid and gas phases, respectively. As there are only gas and liquid phases in the system, we have:

$$\epsilon_g + \epsilon_l = 1 \tag{2.2}$$

Using above equation, the liquid hold-up can also be calculated.

2.3.3 Bubble Size Measurement

Quantification of momentum exchange between the gas and liquid phases in the context of an Euler-Euler model is impossible without specification of a bubble diameter. This is considered essential for accurate prediction of the hydrodynamics of multiphase flows [154]. Both intrusive (e.g. optical probes) and non-intrusive (e.g. image analysis) techniques have been employed to measure the bubble size inside the multiphase systems [5, 107, 156, 221, 71, 110, 17, 159]. When applicable, non-intrusive methods are preferred as they do not disturb the flow inside the system. Compared to optical probes, imaging approaches have the additional advantages of lower cost and ease of implementation. Aloufi

[6] investigated the difference between bubble diameter measurements made from images and by optical probes, concluding that the imaging technique is reliable in the case of dispersed flow regime. Hibiki et al. [77] and Besgani et al. [17] also compared bubble diameter measurements in gas-liquid flow systems made by the two methods and observed less than 7% discrepancy between the measured mean bubble diameter values.

An image analysis approach similar to the procedure described in the studies of Bouaifi et al. [25] and Besgani and Inzoli [18] was adopted here. A Cannon EOS 550D (f/4; 1/1000 s; ISO 3200) digital camera focused at the center of the column was used to take images in the developed region of the two-phase flow (1.2 m above the distributor plate). A light source was placed behind the test section to remove light reflections. Images of size 5184x3456 pixels at a resolution of 21 pixel/mm were taken. A ruler attached to the column was used for calibration purposes. To minimize optical errors, only those bubbles situated in the central region of the column (at the same focal distance as the ruler) were selected for measurement.

For each pair of gas and liquid velocity investigated, about 100 bubbles were measured using two photographs. Each bubble was approximated as an ellipse by manually selecting six points on the bubble edge. Afterwards, the major axis (2a) and the minor axis (2b) of the ellipse were measured (see Fig. 2.2), from which the bubble equivalent diameter, d_b, was obtained as follows [6]:

$$d_b = 2\sqrt[3]{a^2 b} \tag{2.3}$$

Lage and Esposito [107] also approximated bubbles with ellipses and reported about 6% error in the axis measurement of an ellipse using photographs. Considering the optical error and the inaccuracy of the ellipsoidal bubble hypothesis, they estimated 10 to 15% error in equivalent bubble diameter measurement using this procedure, relative to measurements by an optical probe. A sample of bubble diameter measurements using image analysis in this study is shown in Appendix B.

At higher gas velocities (see Fig. 2.3b), the presence of vortices, the short residence time of larger bubbles, and the high rate of bubble coalescence and break-up, render the image analysis method quite inaccurate [6]. For this reason, the bubble size in the churn-turbulent regime was instead estimated from empirical correlations developed by Yu and Kim [227]. The correlations are based on extensive bubble chord length measurements using a U-shaped optical fiber probe in an air-water flow system (0.25 m diameter) for gas and liquid superficial velocities within the range used in this study. According to Yu and Kim [227], the local mean bubble chord length $l_v(r)$ can be estimated as,

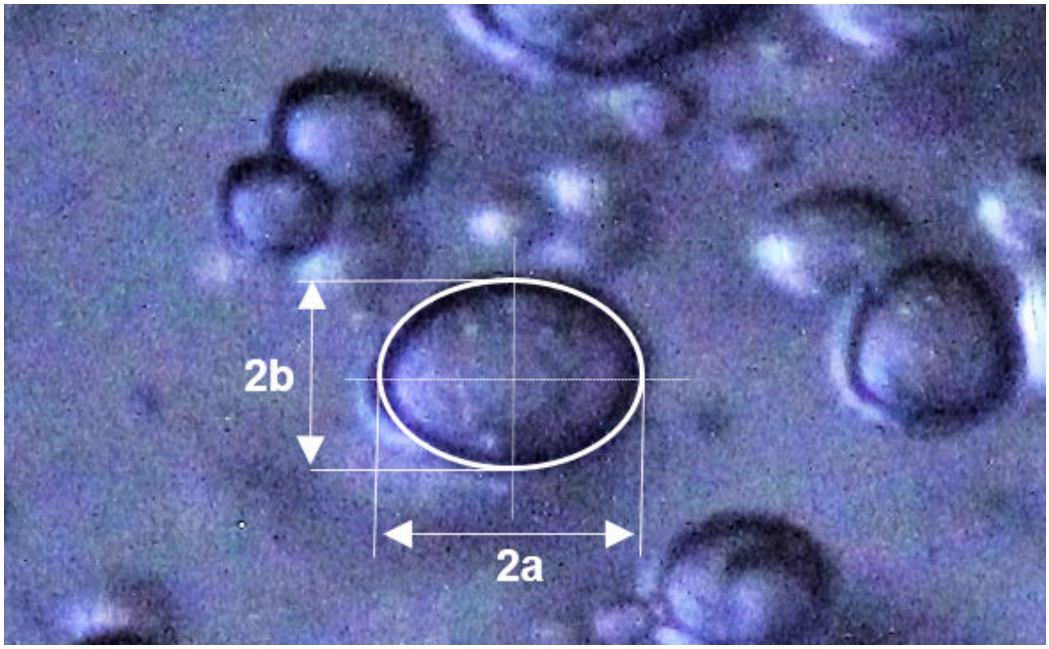

Figure 2.2: Axes of an ellipsoidal bubble.

$$l_v(r) = l_{vc} - (l_{vc} - l_{vw})(\frac{r}{R})^{2.02}, \tag{2.4}$$

where l_{vc} and l_{vw} are the time-smoothed bubble chord lengths at the center (r = 0) and wall (r = R). The values of l_{vc} and l_{vw} are correlated as follows,

$$l_{vc} = 0.023\ u_{sg}^{0.32}(1 - 24.82\ u_{sl}^{2.36}), \tag{2.5}$$

$$l_{vw} = 6.85 \times 10^{-3}\ u_{sg}^{0.11} \tag{2.6}$$

Given the superficial velocities of the working fluids, the mean bubble chord length can be obtained as follows,

$$\langle l_v \rangle = \frac{l_{vc}}{2} + \frac{l_{vw}}{2} \tag{2.7}$$

Finally, the mean bubble chord length is related to the mean bubble size as [227]

$$d_b = 1.43\ \langle l_v \rangle \tag{2.8}$$

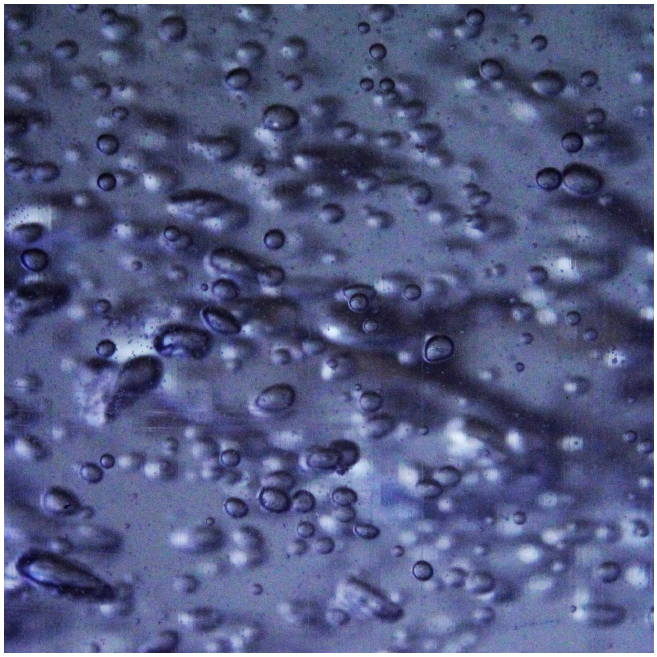

(a)

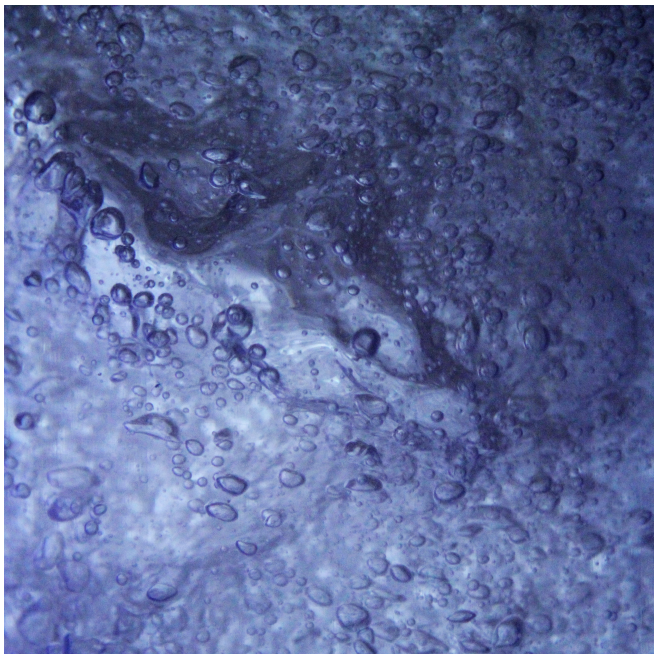

(b)

Figure 2.3: Observed flow regimes in the gas-liquid flow, 1.2 m above the distributor plate; a) $u_{sl} = 0, u_{sg} = 0.02$ m/s and b) $u_{sl} = 0, u_{sg} = 0.07$ m/s.

2.4 Model Description

2.4.1 Euler-Euler Model

The two-fluid or Euler-Euler model [83] does not resolve individual bubbles, treating instead the phases as inter-penetrating continua where the volume of one phase can not be occupied by the other and the presence of each phase is described by a phase volume fraction. Defining the phase velocity and time by $\boldsymbol{u}_q$ and t, respectively, the phase averaged mass and momentum conservation equations are given as follows,

$$\frac{\partial(\alpha_q\rho_q)}{\partial t} + \boldsymbol{\nabla}.(\alpha_q\rho_q\boldsymbol{u}_q) = 0, \qquad \text{in} \quad V, \tag{2.9a}$$

$$\frac{\partial(\alpha_q\rho_q\boldsymbol{u}_q)}{\partial t} + \boldsymbol{\nabla}.(\alpha_q\rho_q\boldsymbol{u}_q\boldsymbol{u}_q) = \boldsymbol{\nabla}.(\alpha_q\boldsymbol{\tau}_q + \alpha_q\boldsymbol{R}_q) + (\alpha_q\rho_q\boldsymbol{g}) + \boldsymbol{M}_q, \qquad \text{in} \quad V, \tag{2.9b}$$

where V is the volume of the computational domain, the subscript $q = g, l$ denotes the phase, α_q is the phase volume fraction and ρ_q the phase density. In the momentum conservation equation (Eq.2.9b), $\boldsymbol{\tau}_q$ is the phase laminar stress tensor which is defined, for Newtonian fluids, by

$$\boldsymbol{\tau}_q = -\rho_q\nu_q(\boldsymbol{\nabla}\boldsymbol{u}_q + \boldsymbol{\nabla}^T\boldsymbol{u}_q) + \frac{2}{3}\rho_q\nu_q\boldsymbol{\nabla}.(\boldsymbol{u}_q)\mathbf{I}, \quad q = g, l, \tag{2.10}$$

The other terms on the right hand side of Eq.2.9b are $\boldsymbol{R}_q$, which is the phase Reynolds (turbulent) stress tensor that will be discussed later in section 2.4.2, $\boldsymbol{g} = -g\boldsymbol{e}_z$ which is the gravitational acceleration, and $\boldsymbol{M}_q$ which is the inter-phase momentum transfer term. The term $\boldsymbol{M}_q$ can be decomposed into different terms depending on their origin as follows [50, 217],

$$\boldsymbol{M}_q = \boldsymbol{F}_{drag} + \boldsymbol{F}_{lift} + \boldsymbol{F}_{vm}, \quad q = g, l, \tag{2.11}$$

where $\boldsymbol{F}_{drag}$, $\boldsymbol{F}_{lift}$ and $\boldsymbol{F}_{vm}$ represent the drag, lift and virtual mass contributions to the momentum transfer term, respectively.

The drag force contribution in Eq.2.11 is the result of the form and skin drag forces which occurs due to the imbalance of pressure and shear forces at the interface, respectively [83]. Drag acts in the opposite direction of the relative motion of the bubble/particle. The drag term has the most important effect on the inter-phase momentum transfer term [217], hence, the choice of the drag model has a significant impact on simulation results [202, 228, 47]. The drag effect is modeled by means of a mixture model that is assumed to

be valid for the whole range of volume fractions in the two-phase system as follows [217],

$$\boldsymbol{F}_{drag} = \frac{3}{4}\alpha_a\alpha_b\left[\left(\alpha_a\frac{C_{d,a}\rho_b}{d_a}\right)+\left(\alpha_b\frac{C_{d,b}\rho_a}{d_b}\right)\right]\|\boldsymbol{u}_r\|\boldsymbol{u}_r, \quad a,b=g,l, \qquad a\neq b, \tag{2.12}$$

where $C_{d,a}$ and $C_{d,b}$ are the drag coefficients of phases a and b, respectively, and $\boldsymbol{u}_r = \boldsymbol{u}_b - \boldsymbol{u}_a$ is the relative velocity. Terms d_a and d_b are the diameter of the particles of phases (*i.e.*, gas bubbles and liquid droplets). The Tomiyama empirical correlation for an isolated bubble in pure gas-liquid systems was employed for the drag coefficients [207] and is given as follows,

$$\begin{aligned} C_{do,a} &= \max\left\{\min\left[\frac{16}{Re_a}(1+0.15Re_a^{0.687}), \frac{48}{Re_a}\right], \left[\frac{8}{3}\frac{Eo_a}{Eo_a+4}\right]\right\}, \\ Eo_a &= \frac{g(\rho_b-\rho_a)d_a^2}{\sigma_{g,l}}, \qquad\qquad a,b=g,l, \\ Re_a &= \frac{d_a\|\boldsymbol{u}_r\|}{\nu_b}, \qquad\qquad a\neq b, \end{aligned} \tag{2.13}$$

where $\sigma_{g,l}$ is the gas-liquid interface surface tension, Eo_a is the Eötvös number of phase a and represents the ratio of buoyancy to surface tension force, ν_b is the kinematic viscosity of phase b and Re_a is the Reynolds number. Bubble diameter values used as input in the simulations are reported in Table 2.1. Other parameters are collected in Table 2.2. Hydrodynamic interactions between bubbles become significant as the gas hold-up increases. To account for such interactions, Eq.2.13 which is valid for isolated bubbles is modified by a so-called swarm factor, h, defined as C_d/C_{do} , where C_d represents the drag force acting on a bubble under actual operating conditions. Following Gemello et al. [62], we take h to be equal to:

$$h = max\left[(1-\alpha_g)\ \left\{(1-\alpha_g)^{25}+(4.8\ \frac{\alpha_g}{1-\alpha_g})^{25}\right\}^{-\frac{2}{25}},\ h_{min}\right] \tag{2.14}$$

where h_{min} depends on column diameter [62] and is set equal to 0.12 for the column used in this work. The swarm factor calculated using this approach (see Fig. 2.4) is independent of bubble size and empirical in nature.

The lift contribution to the momentum transfer term, $\boldsymbol{F}_{lift}$, is given by [217]

$$\boldsymbol{F}_{lift} = \alpha_a\alpha_b(\alpha_b C_{l,a}\rho_b + \alpha_a C_{l,b}\rho_a)\boldsymbol{u}_r \times \boldsymbol{\nabla} \times (\alpha_a\boldsymbol{u}_a + \alpha_b\boldsymbol{u}_b), \quad a,b=g,l, \qquad a\neq b, \tag{2.15}$$

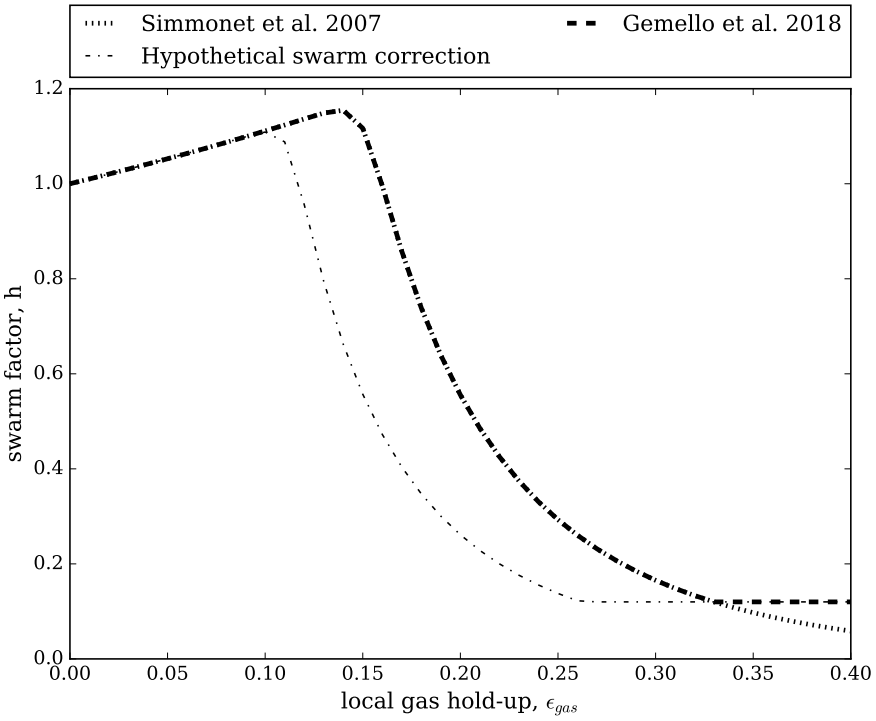

Figure 2.4: Swarm factor dependence on local gas hold-up

Table 2.1: Average bubble diameter in (a) air-water and (b) air-0.5wt.% ethanol solution systems used in the simulations

u_{sl}(m/s)	u_{sg}(m/s)	d_b(mm)
0,0.06	$\leq$ 0.03	2.7 $\pm$0.5 [1,a], 1.9 $\pm$0.2 [1,b]
0	0.05	9.7 [2,a]
0	0.07	10.6 [2,a]
0	0.09	11.4 [2,a]
0	0.12	12.2 [2,a]
0	0.14	12.7 [2,a]
0	0.19	13.7 [2,a]
0.06	0.05	9.6 [2,a]
0.06	0.07	10.4 [2,a]
0.06	0.09	11.2 [2,a]
0.06	0.12	12 [2,a]
0.06	0.14	12.4 [2,a]
0.06	0.19	13.4 [2,a]

[1] From image analysis
[2] From the correlation of Yu and Kim [227].

where $C_{l,a}$ and $C_{l,b}$ are the lift coefficients for phases a and b, respectively. Few studies have attempted to quantify the lift coefficient and in several works the lift force is either neglected or a constant value for the lift coefficient is assumed [158, 90]. We note that the lift force governs the transverse movement of the dispersed phase in a fluid, acting perpendicularly to the flow direction. Lift is a consequence of the shear forces as well as the asymmetric pressure distribution around the dispersed particle/bubble [46, 208, 196]. In the flow configurations under consideration here, the transverse movement of the fluids is negligible compared to the main flow, yielding a minor lift contribution to the inter-phase momentum transfer term. While inclusion of the lift force may be needed in order to account for variations of the gas hold-up with radial distance, neglect of the lift force has no significant effect on the radially-averaged gas hold-up. This was shown by Agnaou et al. [4] in recent work on comparable flow configurations and is also verified here.

The virtual mass force that occurs when one phase accelerates with respect to the other one. When the dispersed phase accelerates in the continuous phase, it replaces the surrounding fluid and consequently it increases the inertia [46]. The virtual mass force is modeled here in the same way as the drag contribution. Accordingly, the virtual mass

Table 2.2: Studied operating parameters and fluid physical properties.

Parameter	Symbol	Values	Unit
Superficial liquid velocity	u_{sl}	0, 0.06	m/s
Superficial gas velocity	u_{sg}	0.01 to 0.19	m/s
Liquid kinematic viscosity	ν_l	1.004×10^{-6}	m^2/s
Gas kinematic viscosity	ν_g	15.11×10^{-6}	m^2/s
Gas-liquid surface tension (water)	$\sigma_{g,l}$	0.072	N/m
Gas-liquid surface tension (0.5 wt.% aqueous ethanol solution)	$\sigma_{g,l}$	0.0685	N/m
Liquid density	ρ_l	998.3	kg/m^3
Gas density	ρ_g	1.205	kg/m^3
Droplet diameter[1]	d_d	0.001	m

[1] Simulation input (*viz.* Eq.2.12)

force is given by;

$$\boldsymbol{F}_{vm} = \alpha_a \alpha_b (\alpha_b C_{vm,a} \rho_b + \alpha_a C_{vm,b} \rho_a) \left[\left(\frac{\partial \boldsymbol{u}_b}{\partial t} + \boldsymbol{u}_b \cdot \boldsymbol{\nabla} \boldsymbol{u}_b \right) - \left(\frac{\partial \boldsymbol{u}_a}{\partial t} + \boldsymbol{u}_a \cdot \boldsymbol{\nabla} \boldsymbol{u}_a \right) \right], \quad a, b = g, l, \quad a \neq b, \tag{2.16}$$

where $C_{vm,a}$ and $C_{vm,b}$ are the virtual mass coefficients for phases a and b. Similar to the lift coefficients, $C_{vm,a}$ and $C_{vm,b}$ are often assumed to be 0.5 [196].

2.4.2 Turbulence Modeling

Several turbulence closure models have been analyzed and tested in the literature in the context of two-phase flows. The large eddy simulation (LES) model and the Reynolds averaged models, such as the k-ε and the Reynolds stress models (RSM) have been extensively used [155, 24, 213, 98, 148]. It was shown that the LES and the k-ε models predict comparable transient flow structures [228]. Furthermore, Tabib et al. [202] reported that all three of LES, RSM, and the k-ε models, predict comparable average flow characteristics, with the latter model being less computationally expensive for simulations of a dispersed bubble column. In the present work, turbulence was modeled using the k-ε model.

The classical k-ε model was originally derived for single phase flow [111, 49]. Two main approaches have been employed to extend the use of this turbulence model into two-phase flow problems. The first one consists of using a mixture k-ε model in which only one set of k and ε equations is considered for the mixture of the continuous and dispersed phases

[15, 167, 16]. This approach is recommended for systems with high phase fraction of the dispersed phase [16]. The main assumption of the mixture model is that both phases fluctuate in the same manner. This assumption was supported by experimental studies for phase fractions no less than 6% [60]. In the second approach, the k-ε transport equations are only solved for the continuous phase and the dispersed phase induced turbulence is taken into account by including extra source terms [167, 194].

Since the flows investigated in this work involve gas phase volume fractions in the range 5% to 20%, the turbulent kinetic energy, k, and the turbulence dissipation rate, ε, were computed from transport equations of the k-ε turbulence model for the gas-liquid mixture. The solution of this model allowed the closure of the mass and momentum conservation equations system (Eqs.2.9) by providing the Reynolds stress tensor, $\boldsymbol{R}_q$, defined by

$$\boldsymbol{R}_q = -\rho_q \nu_t (\boldsymbol{\nabla} \boldsymbol{u}_q + \boldsymbol{\nabla}^T \boldsymbol{u}_q) + \frac{2}{3}\rho_q \nu_t \boldsymbol{\nabla}.(\boldsymbol{u}_q)\mathbf{I} + \frac{2}{3}\rho_q k \mathbf{I}, \tag{2.17}$$

where ν_t is the turbulent viscosity,

$$\nu_t = C_\mu \frac{k^2}{\varepsilon}, \tag{2.18}$$

and $C_\mu = 0.09$ [202].

2.4.3 Initial Boundary Value Problem

The multiphase process considered in this study is the two-phase incompressible flow of two immiscible, Newtonian fluids in a vertical cylindrical pipe of height of $H = 1.5$ m and diameter $D = 0.15$ m under isothermal conditions ($T = 293.15$ K). As with experiments, two flow configurations are considered; bubble column and two-phase co-current flow. The lower, upper and lateral boundaries are referred to as inlet, outlet and wall, respectively (Fig. 2.5). The physical properties of gas and liquid phases (See Table 2.2) are assumed constant.

The initial and boundary conditions associated with the mass and momentum conservation equations (Eqs.2.9) and, when appropriate, with the turbulent kinetic energy and the turbulence dissipation rate transport equations of the k-ε model, are presented in this

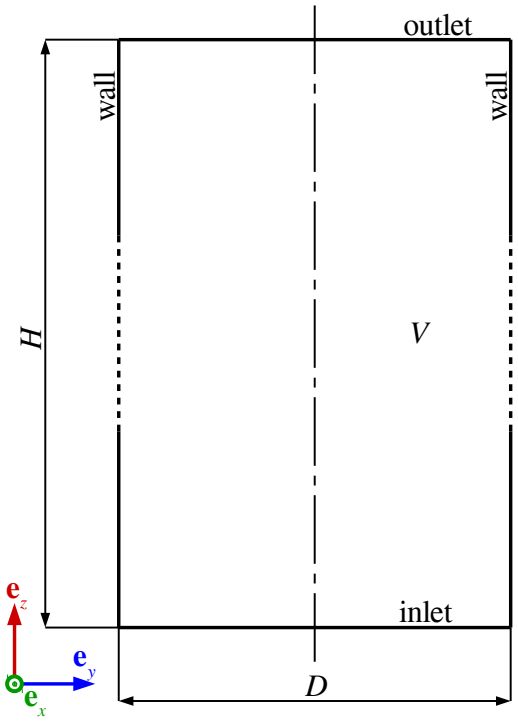

Figure 2.5: Schematic of the longitudinal section of the three-dimensional simulation domain, a pipe of height $H = 1.5$ m, diameter $D = 15$ cm and volume V.

section. The initial conditions are stated below

$$\boldsymbol{u}_q(\boldsymbol{x},0)=\boldsymbol{0}, \qquad q=g,\, l, \tag{2.19a}$$

$$p(\boldsymbol{x},0)=0, \tag{2.19b}$$

$$\alpha_g(\boldsymbol{x},0)=0.15, \qquad \alpha_l(\boldsymbol{x},0)=1-\alpha_g, \tag{2.19c}$$

$$k(\boldsymbol{x},0)=0, \tag{2.19d}$$

$$\varepsilon(\boldsymbol{x},0)=0, \tag{2.19e}$$

where the two phases are initially static (Eqs.2.19a-2.19b), forming a dispersion of 15% gas (Eq.2.19c), and the turbulent kinetic energy and dissipation rate are initially zero (Eqs.2.19d-2.19e).

At the wall boundary, the following conditions were imposed,

$$\boldsymbol{u}_q(\boldsymbol{x},t)=\boldsymbol{0}, \qquad \text{on wall}, \qquad q=g,\, l, \tag{2.20a}$$

$$\begin{aligned}&\boldsymbol{\nabla}_{\boldsymbol{n}} p(\boldsymbol{x},t)=\boldsymbol{0},\\ &\boldsymbol{\nabla}_{\boldsymbol{n}} \alpha_q(\boldsymbol{x},t)=\boldsymbol{0},\end{aligned} \qquad \text{on wall}, \qquad q=g,\, l, \tag{2.20b}$$

$$\nu_t(\boldsymbol{x},t)=f_\mu C_\mu k^2/\varepsilon, \qquad \text{on wall}, \tag{2.20c}$$

$$k(\boldsymbol{x},t)=\boldsymbol{u}^{*2}/\sqrt{C_\mu}, \qquad \text{on wall}, \tag{2.20d}$$

$$\varepsilon(\boldsymbol{x},t)=C_\mu^{3/4}k_N^{3/2}/Ky_N, \qquad \text{on wall}, \tag{2.20e}$$

such that a no-slip velocity boundary condition (Eq.2.20a) was considered for both phases in addition to the Neumann zero normal gradient boundary condition for both the pressure and phase fractions (Eqs.2.20b), where $\boldsymbol{n}$ is the unit outward normal to the surface. Moreover, Eqs.2.20c, 2.20d, and 2.20e represent the k-ε turbulence model wall functions [26, 2]. In these equations, f_μ (Eq.2.20c) is a damping function, $\boldsymbol{u}^*$ (Eq.2.20d) is the friction velocity, K (Eq.2.20e) is the von Karman constant, y_N the distance from the wall to the first interior node N, and k_N the turbulent kinetic energy at N.

At the outlet boundary, the conditions imposed are

$$p(\boldsymbol{x},t)=p^{outlet}, \qquad \text{on outlet}, \tag{2.21a}$$

$$\begin{aligned}&\boldsymbol{\nabla}_{\boldsymbol{n}} \boldsymbol{u}_q(\boldsymbol{x},t)=\boldsymbol{0},\\ &\boldsymbol{\nabla}_{\boldsymbol{n}} \alpha_q(\boldsymbol{x},t)=\boldsymbol{0},\\ &\boldsymbol{\nabla}_{\boldsymbol{n}} k(\boldsymbol{x},t)=\boldsymbol{0},\\ &\boldsymbol{\nabla}_{\boldsymbol{n}} \varepsilon(\boldsymbol{x},t)=\boldsymbol{0},\end{aligned} \qquad \text{on outlet}, \qquad q=g,\, l, \tag{2.21b}$$

where a uniform Dirichlet pressure boundary condition was considered (Eq. 2.21a) and the Neumann zero normal gradient condition was imposed for the velocity and phase fractions of both phases and for the turbulent kinetic energy and dissipation rate (Eqs. 2.21b). In Eq. 2.21a, the pressure is atmospheric, $p^{outlet} = 101325\,\mathrm{Pa}$.

Finally, at the inlet boundary, the boundary conditions used in this study are given as follows,

$$\boldsymbol{\nabla}_{\boldsymbol{n}}\boldsymbol{u}_q(\boldsymbol{x},t) = \mathbf{0}, \qquad \text{on inlet,} \qquad q = g,\, l, \tag{2.22a}$$

$$\begin{aligned} p &= p^{inlet}, \\ \alpha_q &= \alpha_q^{inlet}, \end{aligned} \qquad \text{on inlet,} \qquad q = g,\, l, \tag{2.22b}$$

$$\begin{aligned} k &= k^{inlet}, \\ \varepsilon &= \varepsilon^{inlet}, \end{aligned} \qquad \text{on inlet,} \tag{2.22c}$$

where the Neumann zero normal gradient condition was imposed for the velocity (Eqs.2.22a). Dirichlet boundary conditions (Eqs.2.22b) were adopted for both the pressure and phase fractions. An inlet Dirichlet pressure boundary condition, as opposed to the commonly used uniform velocity boundary condition, is physically consistent because a gas-liquid slip velocity at the inlet is present and the non-slip velocity condition at the wall is not violated. Additionally, it allows for the development of non-uniform flow profiles at the inlet consistent with the model governing equations [4]. The boundary conditions given by Eqs.2.22b were imposed by means of a multi-variable control procedure that sets values of p^{inlet} and α_q^{inlet} according to the target superficial velocities. Details of the implementation are given by Agnaou et al. [4]. For configurations yielding non-dispersed flow regimes, the control strategy fails to adjust the inlet pressure corresponding to the target flow rate. This may be explained by the fast local velocity fluctuations, which require a control strategy more advanced than the one currently available. For flow configurations where the controller cannot be used, *i.e.*, in the non-dispersed regime, the pressure Dirichlet boundary condition of Eqs.2.22b was replaced by a uniform Dirichlet velocity boundary condition. Whereas the impact of the inlet boundary condition on the flow structure is important [4], it is found here, at least for the dispersed regime, that its impact on the overall gas hold-up is negligible for either bubble column or two-phase flow configurations.

Dirichlet uniform boundary conditions were also used for the turbulence quantities k and ε at the inlet (see Eqs. 2.22c). Because turbulence at the inlet is not precisely known, the literature of two-phase dispersed flows tends to tacitly assume that the effect of k^{inlet} and ε^{inlet} is insignificant. In this work, these values were instead estimated using empirical relations derived for turbulent single-phase upward flows in a pipe, as relations for two-

phase flows are not available. These estimations made use of gas volume fractions, ϵ_g, obtained experimentally and are explained below.

The average turbulence intensity over the pipe cross-sectional area was first estimated as [168]

$$I = 0.14 Re^{-0.079}, \tag{2.23}$$

where Re is the pipe's Reynods number defined as follows,

$$Re = \boldsymbol{u}_m D/\nu_m, \tag{2.24}$$

where $\boldsymbol{u}_m$ is the mixture velocity, D is the diameter of the pipe, and ν_m is the mixture kinematic viscosity that is determined from the viscosities of the two phases, ν_g and ν_l, and the experimental volume fraction ϵ_g as follows,

$$\nu_m = \epsilon_g \nu_g + (1 - \epsilon_g)\, \nu_l, \tag{2.25}$$

In a second step, k^{inlet} and ε^{inlet} were estimated assuming isotropic turbulence, with $\boldsymbol{u}_m$ as a reference velocity, and a turbulent length-scale corresponding to the diameter of the pipe, D. The turbulent kinetic energy and dissipation rate at the inlet boundary are then given by,

$$\begin{aligned} k^{inlet} &= 3/2\, (\boldsymbol{u}_m I)^2\,, \\ \varepsilon^{inlet} &= C_\mu k^{3/2}/D. \end{aligned} \tag{2.26}$$

2.4.4 Numerical considerations

The partial differential equation system under consideration consists of Eqs.2.9, the k-ε turbulence model, and the associated initial and boundary conditions, Eqs.2.19 through 2.22. The two-phase flow problem was solved numerically using the `multiphaseEulerFoam` solver of the open-source CFD toolbox `OpenFOAM 4.0` [3]. The experimental conditions were reproduced to assess the accuracy of the Eulerian model. Bubble column and two-phase co-current flow simulations were performed for a range of gas and liquid superficial velocities. Simulations were also ran with and without turbulence modeling to investigate its impact on simulation results.

The computational domain (Fig. 2.5) was meshed using hexahedral elements and mesh-independent (converged) numerical solutions where determined through a sensitivity analysis of the solution to the number of elements (Fig. 2.6). This analysis was carried out using the bubble column and co-current flow configurations with the highest superficial

velocities, as the sensitivity of the numerical solution to the mesh size increases with flow velocity.

The CFD gas hold-up ϵ_g^{CFD} was used as the basis for comparison. This quantity corresponds to the time-average over the fully-developed flow interval (FDFI) of the volume-averaged gas volume fraction α_g and is given by

$$\epsilon_g^{CFD} = \frac{\int_{FDFI} \langle \alpha_g \rangle^V \, \mathrm{d}t}{\int_{FDFI} \mathrm{d}t}, \tag{2.27}$$

where the volume averaged gas volume fraction is

$$\langle \alpha_g \rangle^V = \frac{\int_V \alpha_g \mathrm{d}v}{\int_V \mathrm{d}v}, \tag{2.28}$$

and $\mathrm{d}v$ is an elementary volume. Fig. 2.6 plots the normalized gas hold-up $\epsilon_{g,n}^{CFD}$ against the number of mesh elements. The normalization was performed with respect to the result obtained with the mesh with highest number of elements. It is evident in this figure that mesh-independence is achieved after 50000 elements for bubble column and after 85000 elements for co-current flow configurations. Increasing the number of grid blocks around 5 and 8 times leads to a relative error of less than 2.8% and 3.4% on the gas hold-up for the bubble column and co-current flow configurations, respectively. The mesh adopted in this work comprises of 137592 elements - a trade-off between acceptable accuracy and computation time.

2.5 Results and Discussion

2.5.1 Gas Hold-up in Gas-Liquid Flow System

Fig. 2.7 represents the overall gas hold-up data obtained in this study. The results of our study agree with measurements of previous studies to within 10% of the reported gas hold-up values [5, 78, 41]. As can be seen from Fig. 2.7 the overall gas hold-up depends mainly on gas superficial velocity. The increase in the hold-up with respect to gas superficial

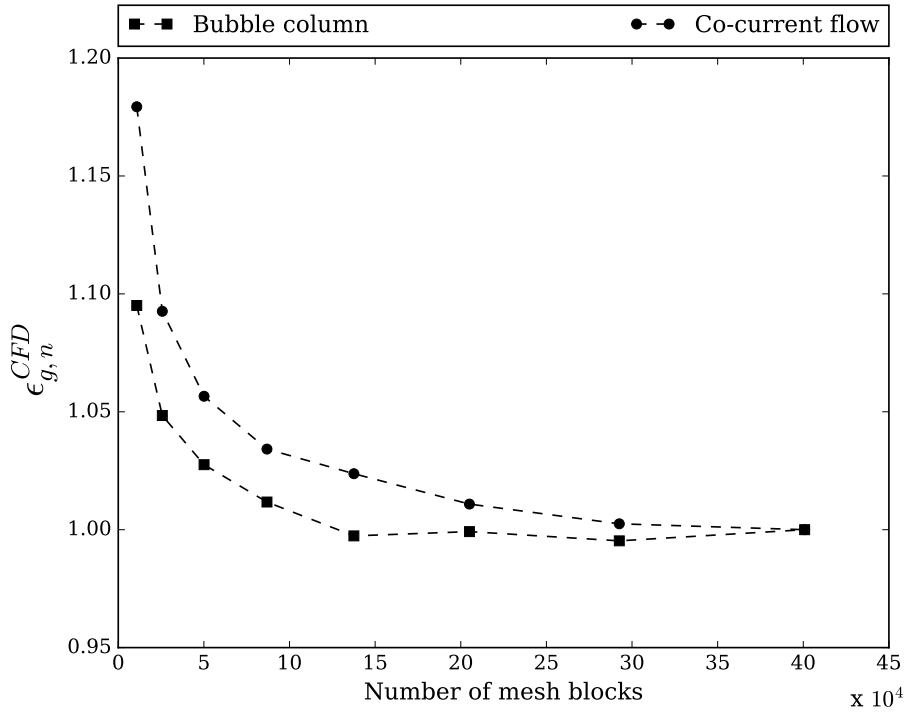

Figure 2.6: Normalized gas hold-up $\epsilon_{g,n}^{CFD}$ versus number of mesh elements. Overall gas hold-up computed using Eq.2.27 and normalized with respect to the result obtained from the mesh with the highest number of elements. Bubble column; $u_{sl} = 0$ and $u_{sg} = 0.09$ m/s. Co-current flow; $u_{sl} = 0.06$ m/s and $u_{sg} = 0.09$ m/s.

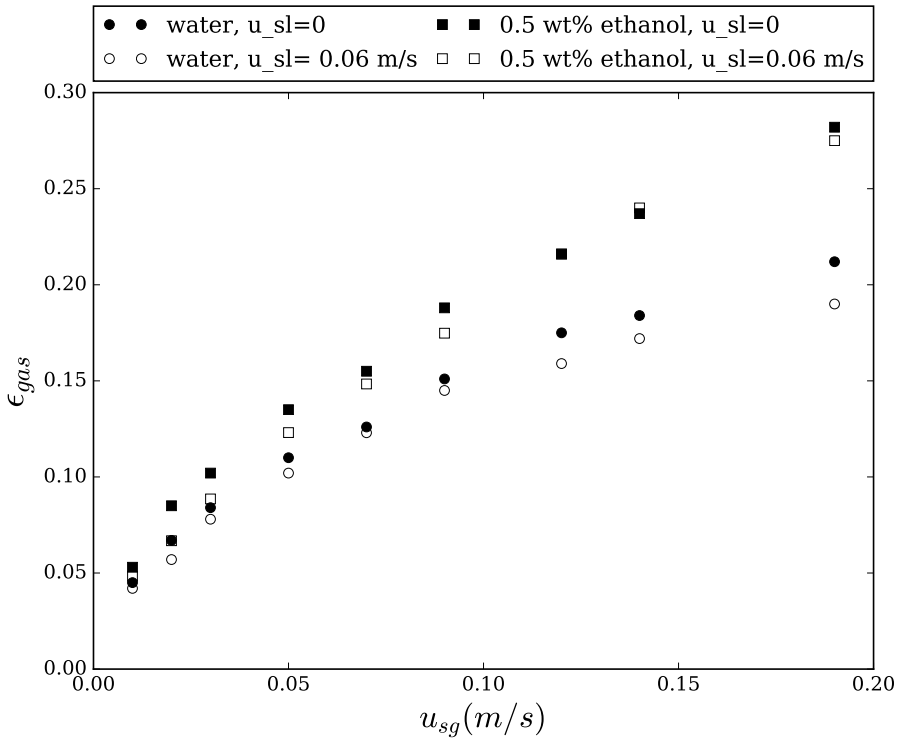

Figure 2.7: Overall gas hold-up data in gas-liquid two phase flow system.

velocity is more pronounced in the dispersed regime than in the churn-turbulent regime. A similar trend has been observed previously [94]. Increasing the liquid superficial velocity from 0 to 0.06 m/s decreases the hold-up by an average of at most 8% for either distilled water or aqueous ethanol solution. This may be attributed to an increase in bubble rise velocity and the concomitant reduction of the gas phase residence time [105].

Another observation from Fig. 2.7, is the generally higher gas hold-up values for the system containing 0.5wt.% ethanol solution as compared to distilled water. Addition of ethanol to water reduces the surface tension and is expected to suppress bubble coalescence, thereby reducing bubble size [189, 41, 193]. This causes an increase in the bubble interfacial area as well as a decrease in bubble rise velocity, both of which lead to higher values of the gas hold-up.

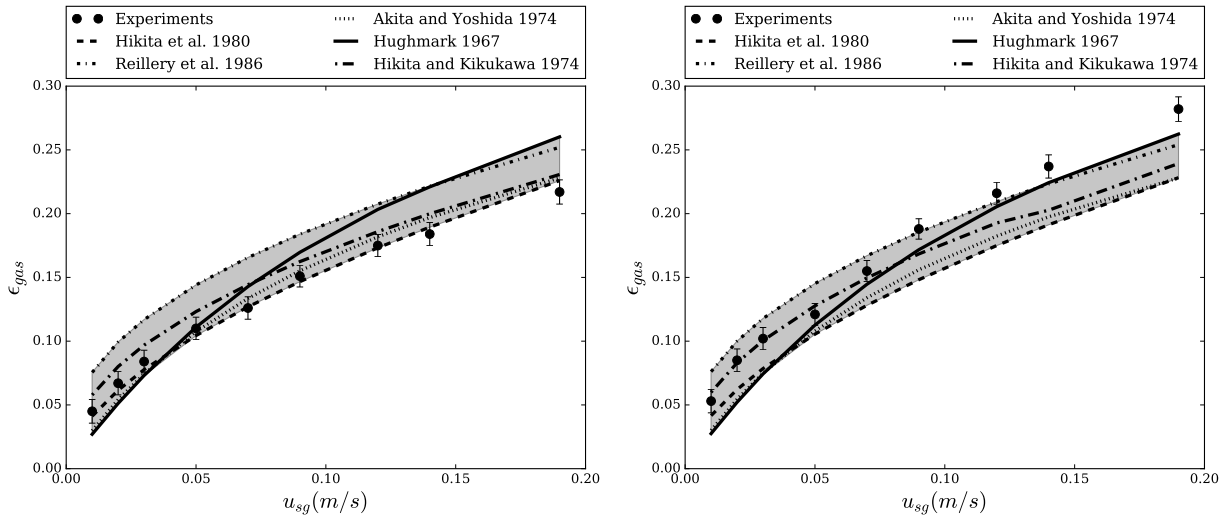

(a) (b)

Figure 2.8: Comparison of experimental overall gas hold-up data to the predictions of empirical correlations, $u_{sl} = 0$, (a) air-water system and (b) air-0.5wt.% ethanol solution system.

2.5.2 Prediction of Overall Gas Hold-up with Empirical Correlations

How accurately available empirical correlations can predict the experimental data of this study is examined in Figs. 2.8 and 2.9. For the air-water system, the average gas hold-up for both flow configurations (bubble column and co-current two-phase flow) is predicted to within experimental error only by the correlations of Akita and Yoshida [5] and Hikita et al. [78], and only for $\epsilon_{gas} \leq 0.15$ in the case of co-current flow. However, when only a small amount of alcohol is added to the system (resulting in a surface tension reduction from 0.072 N/m to 0.0685 N/m), this is no longer true. In this case, a different correlation (Hikita and Kikukawa [79]) predicts the gas hold-up to within experimental error, but only for $\epsilon_{gas} \leq 0.15$. Other correlations are in error by up to 50%. This is despite the fact that all correlations are supposed to account for surface tension. Clearly, a priori prediction of the gas hold-up by empirical correlations is subject to uncertainty that is much greater than implied by the comparison of any specific correlation with any specific set of experimental data.

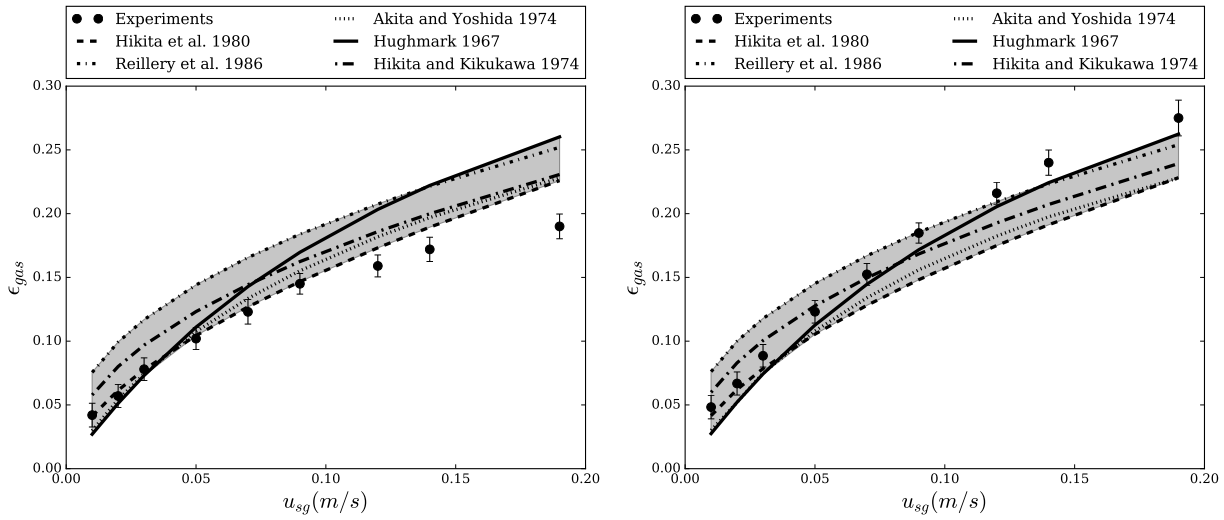

(a) (b)

Figure 2.9: Comparison of experimental overall gas hold-up data to the predictions of empirical correlations, $u_{sl} = 0.06$ m/s, (a) air-water system and (b) air-0.5wt.% ethanol solution system.

2.5.3 Results of Bubble Size Measurement

Using the image analysis technique described above, we found average bubble diameters of 2.7 ± 0.5 mm and 1.9 ± 0.2 mm for the air-water and air-0.5wt.% ethanol aqueous solution systems, respectively, in the dispersed flow regime ($u_{sg} \leq 0.03$ m/s). For air-water dispersed flow systems, bubble diameters between 2.3 mm to 5 mm have been reported in the literature, depending on the column diameter and gas sparger design [78, 29, 222, 178, 77, 182]. For air-0.5wt.% ethanol aqueous solution, Keitel and Onken [96] have reported a Sauter mean diameter of about 1.7 mm in a dispersed bubble column. We also observed that the bubble diameter was almost independent of gas velocity in the dispersed regime. A similar trend has also been reported in the literature [5, 178]. Schafer et al. [182] and Gemello et al. [63] have investigated the effect of sparger material and design on bubble size distribution inside bubble column systems. They found that the mean bubble size varies significantly with changes in gas sparger design. For example, in a dispersed air-water system the stable (far from the sparger) mean bubble diameter varied between 2.1 and 3.3 mm for the same operating parameters. This implies that the features of the experimental setup can affect the bubble size measurement. Therefore, any attempt to correlate mean bubble diameter should consider sparger characteristics, such as the orifice

diameter [94, 8]. Our results also demonstrate the sensitivity of bubble size to changes in the gas-liquid surface tension, since only a 5% decrease in surface tension causes a 30% decrease in mean bubble diameter. For air-0.5wt.% ethanol solution, in a study with gas sparger, Sauter bubble diameters of 2.4 mm have been reported for a bubble column operating at 0.021 m/s gas superficial velocity [115].

In the churn-turbulent (heterogeneous) regime image analysis is unreliable and the correlations of Yu and Kim [227] were applied instead to obtain the results shown in Table 2.1. The average bubble diameter values slightly decreased in the two-phase flow system compared to the bubble column. The predictions of the correlations of Yu and Kim [227] agree with measurements of Sarrafi et al. [178] to within 8%. It should be noted that the correlations of Yu and Kim [227] are only applicable to air-water systems.

It is instructive at this point to consider a simple prediction of the overall gas hold-up based on a balance between buoyancy and drag forces. The steady state mass balance for an incompressible and non-reacting gas phase in a vertical bubble column yields [169] :

$$\epsilon_g = \frac{u_{sg}}{u_g} \tag{2.29}$$

where u_g is the mean bubble velocity. The latter is given by :

$$u_g = u_o f(\epsilon_g) \tag{2.30}$$

where u_o is the terminal velocity of an isolated bubble and $h = f(\epsilon_g)$ is a swarm correction factor (*viz.* Eq.2.14). The bubble terminal velocity is related to the drag coefficient as follows:

$$u_o \propto C_{do}^{-0.5} \tag{2.31}$$

Considering Eqs.2.30 and 2.31, we can write:

$$\frac{u_o}{u_g} = (\frac{C_d}{C_{do}})^{0.5} = h^{0.5} \tag{2.32}$$

and combining Eq.2.29 with Eq.2.32 we obtain the following result:

$$\epsilon_g = \frac{u_{sg}}{u_o}\ h^{0.5} \tag{2.33}$$

Eq.2.33 may be solved for ϵ_g given the gas superficial velocity (u_{sg}) and the bubble diameter (d_b), where the latter provides u_o via the drag model (Eq.2.13). Using this procedure we estimated the overall gas hold-up for bubble columns studied here and in Gemello et al. [62]. The results shown in Fig. 2.10 reveal significant departure of these estimates from the experimental observations ($\sim$ 30-40% error). Clearly, consideration of the local hydrodynamic conditions is necessary for accurate prediction of the overall gas hold-up.

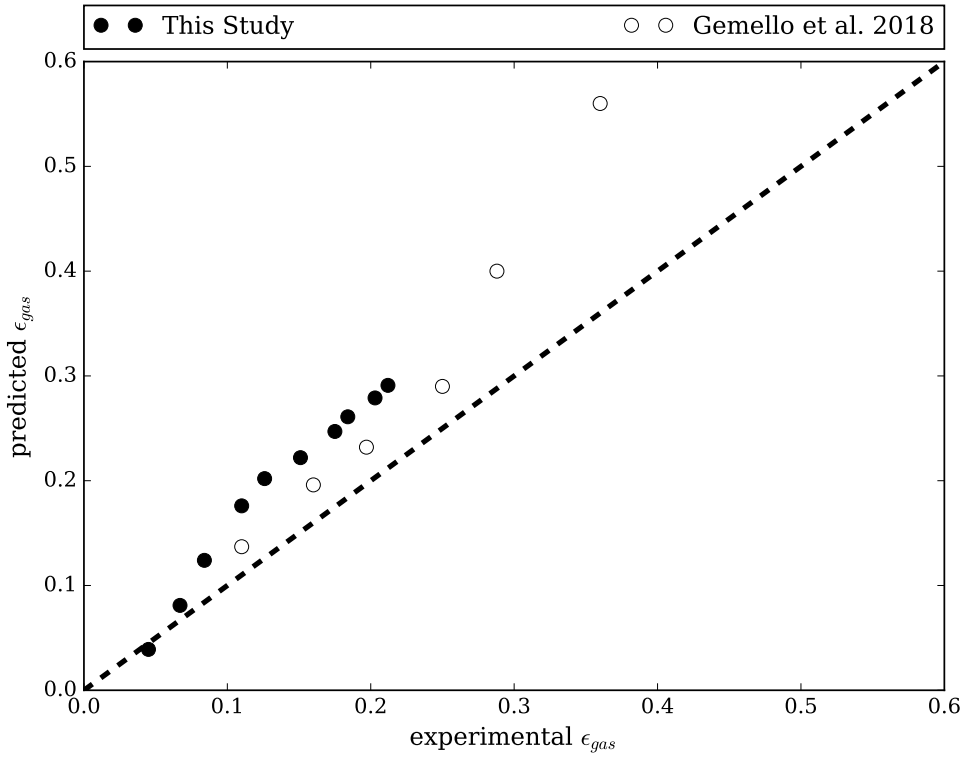

Figure 2.10: Comparison of the experimental overall gas hold-up data with the prediction of the model proposed by Ruzicka [169]

Table 2.3: Effect of lift force [206] on prediction of an experimental overall gas hold-up from the study of Gemello et al. [62] with the Eulerian model used in this study ($D_c = 0.4$ m, $u_{sg} = 0.09$ m/s, $d_b = 0.007$ m)

Reference	$\epsilon_{gas,exp.}(\%)$	$\epsilon_{gas,CFD}^{no\ swarm,no\ lift}$	$\epsilon_{gas,CFD}^{with\ swarm,no\ lift}$	$\epsilon_{gas,CFD}^{with\ swarm,with\ lift}$
Gemello et al. [62]	19.7	33.6	19.8	–
This study	–	29.7	20.9	20.5

2.5.4 Prediction of Overall Gas Hold-up with Two-Phase Eulerian Models

Before using the Eulerian model described above to predict the overall gas hold-up in the experiments reported here, the model was verified against computations reported by Gemello et al. [62]. A representative comparison is detailed in Table 2.3. As expected, inclusion of the lift force has a negligible effect on the prediction of the overall gas hold-up and there is no more than a few percent difference between the prediction of Gemello et al. [62], the prediction of the present model and the experimentally observed value.

The results obtained in this study for the air-water system can be seen in Fig. 2.11, in which the shaded region represents a range of gas superficial velocities for the transition from dispersed to churn-turbulent flow regime [188, 82, 94]. For the air-ethanol aqueous solution system, simulations were limited to the dispersed flow regime and the results are shown in Fig. 2.12.

In the dispersed flow regime, the Euler-Euler model computed the overall gas hold-up within the range of experimental error for both flow configurations (bubble column and co-current gas-liquid flow), using the experimentally-determined values of the average bubble diameter as input (see Table 2.1). Since the dispersed flow regime is indeed characterized by narrow bubble size distributions and low degree of interaction between bubbles, this result confirms the validity of the Euler-Euler model in this regime.

It can be seen in Fig. 2.11, that inclusion of a turbulence model has no significant effect on the prediction of gas hold-up in the dispersed flow regime. The performance of different turbulence models has been examined by several researchers in recent years. For example, Ekambara and Dhotre [48] compared the k-ε, LES and RSM turbulence models in a fully dispersed bubble column and observed no significant difference in the prediction of radial gas hold-up in the developed region of system. In a recent study, Lote at al. [119] also observed minor differences in radial gas hold-up prediction between k-ε and RSM within a dispersed two-phase flow system. A similar observation was reported by Tabib et al. [202] and by Gupta and Roy [73] regarding the prediction of axial liquid velocity. Rzehak

and Krepper [171] investigated the inclusion of different bubble-induced source terms for the dispersed phase to the k-ε model. Except for minor qualitative differences in terms of radial gas hold-up, the overall hold-up values were very similar. Colombo and Fairweather [39] also applied the RSM and k-ε models combined with bubble-induced source terms to predict the hold-up reported in previous experimental works. They concluded that the performance of different turbulence models was in fact comparable, and that best agreement between simulation and experiment was observed when experimentally-determined values of the bubble diameter were used as input.

The results of the present study lend additional support to the conclusion that consideration of turbulence is not required for the prediction of the average gas hold-up in the dispersed (homogeneous) flow regime using an Euler-Euler model. Rather, accurate specification of the bubble size appears to be condition *sine qua non*, as evidenced in Fig. 2.12. To this point, Table 2.4 lists previous studies in which Eulerian models were used to predict the gas hold-up observed in experiments. In all studies listed, the bubble diameter used as input to the model was determined experimentally. The average gas hold-up observed experimentally in the dispersed flow regime, is indeed reproduced with absolute average relative error (AARE) of less than 10% using a simple Euler-Euler model (see also Table 2.5 for a summary), provided that the bubble diameter is accurately specified. As shown in this work, a reduction of the average bubble size from 2.7 mm to 1.9 mm is brought about by a 5% reduction of the gas-liquid surface tension. This effect, which is difficult to predict, needs to be taken into account in the Euler-Euler model in order to achieve accurate prediction of the average gas hold-up in the dispersed regime. Considering that the bubble size is additionally influenced by the characteristics of the sparger [182] and the fluid viscosity [19], the requirement for accurate specification of the bubble size may be very difficult to meet without experimentation. This limits the predictive potential of Euler-Euler models in the dispersed flow regime.

In the churn-turbulent (heterogeneous) flow regime, omission of turbulence modeling coincides with significant disagreement between simulated and measured gas hold-up (see Fig. 2.11). Inclusion of turbulence modeling in this regime does not, however, consistently improve the agreement between simulation and experiment. When the average bubble size estimated using the correlations of Yu and Kim [227] (see Table 2.1) is used as input in the Euler-Euler model, consideration of turbulence is associated with significant improvement of gas hold-up predictions in the bubble column. For co-current two-phase flow, the addition of turbulence modeling does not result in improvement of the predicted average gas hold-up. When, in addition to turbulence, the swarm correction (*viz.* Eq.2.14) is applied, the agreement with experiment is improved for the highest values of gas superficial velocity. This is true for both bubble column and co-current flow configurations with the

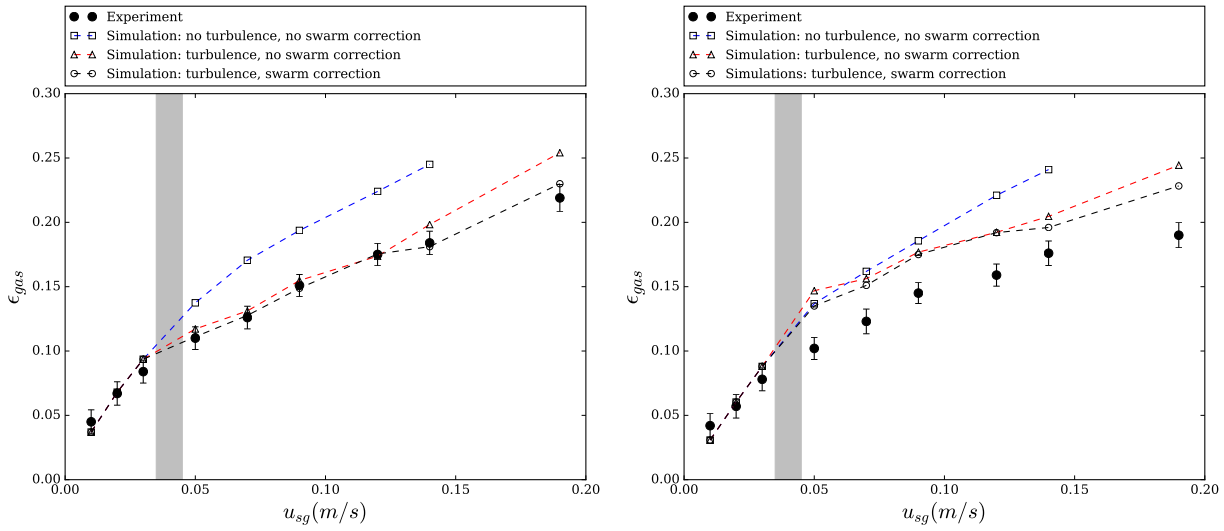

Figure 2.11: Comparison of overall gas hold-up data measured through experiments with predictions of Eulerian models in air-water system (a) $u_{sl} = 0$ and (b) $u_{sl} = 0.06$m/s. (Note: dashed lines are a guide to the eye.)

following difference. For bubble column, excellent agreement between experiment and simulation is observed throughout the range of gas superficial velocities tested (see Table 2.4). For co-current flow, the Euler-Euler model consistently over predicts gas hold-up in the heterogeneous flow regime (see Table 2.4). These observations are discussed below within the context of previous attempts to predict the average gas hold-up under conditions of churn-turbulent (heterogeneous) flow, almost exclusively focused on bubble columns (see Table 2.4).

Silva et al. [192] applied Eulerian models in the ANSYS CFX package to predict radial gas hold-up in a bubble column. Their simulations failed to predict the gas hold-up using a single bubble diameter (and the k-ε turbulence model), but use of the multiple size group (MUSIG) model with three bubble size groups improved the results significantly. Using the LES model instead of the k-ε model resulted in minor improvement. McClure et al. [132] and Fletcher et al. [57] also used ANSYS with single bubble size (measured experimentally) and predicted the overall gas hold-up in a churn-turbulent bubble column with about 15% error. They further showed that addition of a bubble-induced turbulence model for the dispersed phase improved the gas hold-up prediction only slightly. In a recent study, Huang et al. [81] investigated the effect of various bubble size models in CFD simulation of

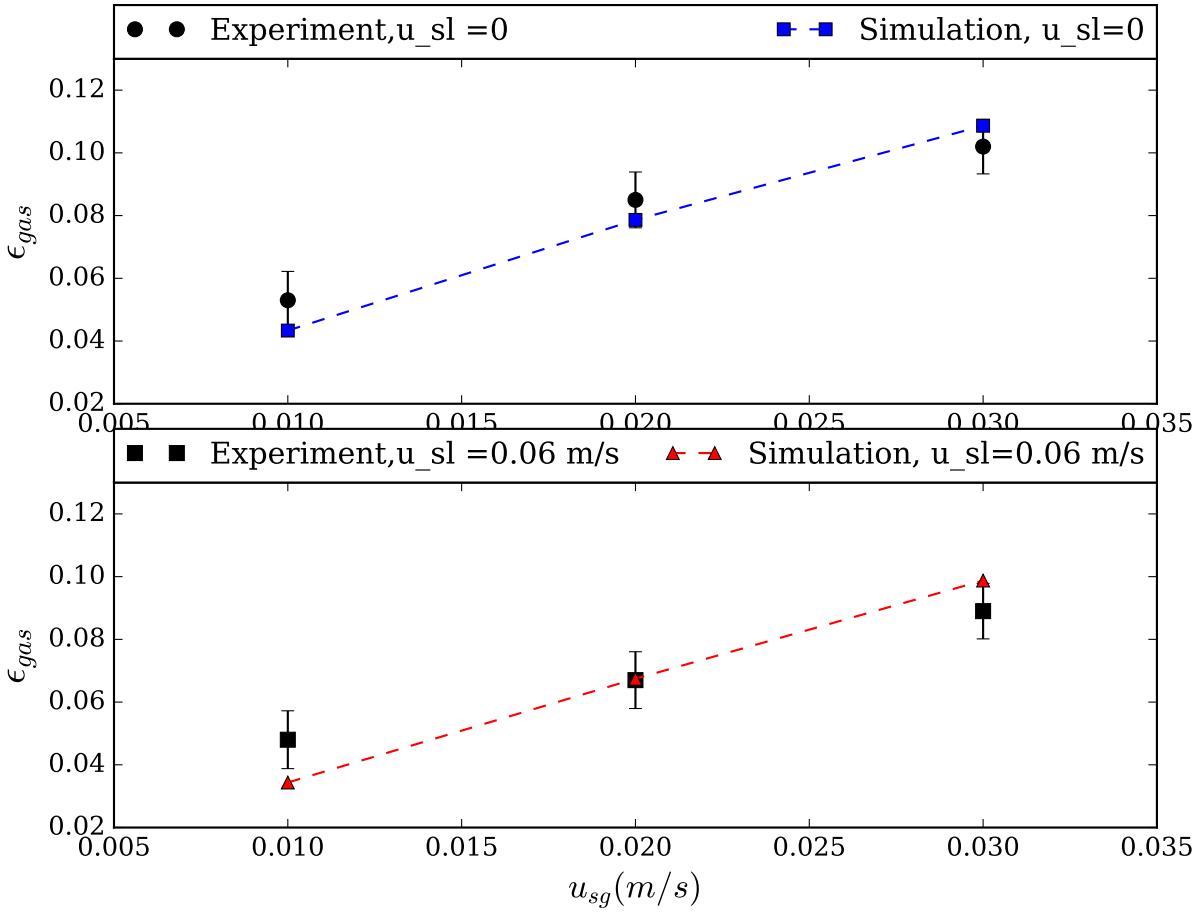

Figure 2.12: Comparison of overall gas hold-up data measured through experiments with predictions of Eulerian model (without turbulence or swarm correction) for the air-0.5wt.% ethanol solution system. (Note: dashed lines are a guide to the eye.)

heterogeneous bubble column systems. The bubble size models assessed were the constant single bubble size, the variable single bubble size and the MUSIG models. Their results demonstrated that the single bubble size approach provided the best agreement between experiments and CFD predictions, while the MUSIG model over-predicted the gas hold-up. In contrast to bubble columns, satisfactory prediction of co-current two-phase flow systems in the heterogeneous regime is challenging (average error of about 30%), even when a population balance model is used [85] (see Table 2.5).

Clearly, prediction of the average gas hold-up by an Euler-Euler model is as accurate as the account of momentum exchange between the gas and liquid phases. The sensitivity of the latter to bubble size is demonstrated in the results shown in Fig. 2.11 and Fig. 2.12 for dispersed (homogeneous) flows characterized by narrowly-distributed bubble size (see Table 2.1). This fact is accentuated in heterogeneous flow, which is characterized by broad bubble size distributions. Our results for bubble columns as well as those of Gemello et al. [62] support the conclusion that accurate prediction of the overall gas holdup is possible in this regime using a single bubble size under two conditions. Firstly, that hydrodynamic interactions between bubbles be appropriately accounted for (*i.e.* swarm correction). Secondly, that the bubble size be appropriately chosen. In the study of Gemello et al. [62], the bubble size used was the mean Sauter diameter measured experimentally using a method based on cross correlation between the signals from two optical probes [63]. In the present study the bubble size used is the mean diameter estimated from the correlation of Yu and Kim [227], itself based on experimental measurements using an optical fiber probe. At this point, it is instructive to consider the sensitivity of predicted overall gas hold-up on uncertainty in the value of bubble size. To this end, we simulated co-current flow with u_{sl} of 0.06 m/s and u_{sg} of 0.14 m/s using d_b = 14.9 mm - a value 20% greater than the one obtained from the correlation of Yu and Kim listed in Table 2.1. The prediction of the overall gas hold-up decreased by less than 2%. The prediction of the overall gas hold-up during heterogeneous co-current flow is much more sensitive to the swarm correction. Changing the constant in Eq.2.14 from 4.8 to 7 (see Fig. 2.4) results in $\epsilon_{g_{sim.}} = 0.182$ with bubble size as listed in Table 2.1 - a result that is accurate to within experimental error. It is important to recall that Eq.2.14 is an empirical fit to experimental data obtained from a bubble column [193] and it is not obvious that it applies to co-current two-phase flow without modification. Prediction of the overall gas hold-up is least accurate under conditions of co-current heterogeneous flow (see Table 2.5), suggesting that further work is needed to improve the account of hydrodynamic interactions between bubbles under such conditions.

Table 2.4: Accuracy of Eulerian models in prediction of gas hold-up

Reference	u_{sl}(m/s)	u_{sg}(m/s)	d_b(mm)	$\epsilon_{g_{exp}}$ (%)	$\epsilon_{g_{sim.}}$ (%)	Error (%)
Homogeneous Flow Regime						
Selma et al. [187]	0	0.0073	5	1.9	1.7	12
This study	0	0.01	2.7	4.5	3.8	15
This study	0	0.02	2.7	6.7	6.8	1.5
Silva et al. [192]	0	0.02	2.12	9.2	9.5	3.5
Simonnet et al. [194]	0	0.02	4	7.6	7.4	2.6
This study	0	0.03	2.7	8.4	9.3	10
Guedon et al. [70]	0	0.033	4.2, 7.2 [1]	9.75	10.33	5.93
Rzehak and Kriebitzsch [172]	0.0405	0.0235	4.5	5.3	5.2	1.8
This study	0.06	0.01	2.7	4.1	3.1	19
This study	0.06	0.02	2.7	5.7	6	5.5
This study	0.06	0.03	2.7	7.8	8.8	10
Wang and Yao [216]	0.405	0.011	4.5	1.89	1.62	16.3
Wang and Yao [216]	0.491	0.0556	2.5	7.8	6.7	10.6
Colombo and Fairweather [39]	0.5	0.12	2.94	15.2	14.5	4.5
Colombo and Fairweather [39]	1	0.036	3.66	3.3	2.8	15.5
Yamoah et al. [223]	1	0.05	3.41	5	5.3	6
Rzehak and Kriebitzsch [172]	1	0.14	3.03	10.6	10.2	3.8
Yamoah et al. [223]	1	0.3	3.68	22	23.6	7.5
Wang and Yao [216]	2.6	1.275	9.3	25.7	29.8	16.1
Heterogeneous Flow Regime						
This study	0	0.05	9.7	11.1	11.1	0
This study	0	0.07	10.6	12.6	12.8	1.8
Silva et al. [192]	0	0.08	1-5 [1]	23	20.8	10
This study	0	0.09	11.4	15.1	14.8	2
This study	0	0.12	12.2	17.5	17.5	0
This study	0	0.14	12.7	18.4	18.1	1.6
Fletcher et al. [57]	0	0.16	6	22.8	20.1	3.5
Gemello et al. [62]	0	0.16	7	25	25.7	2.8
This study	0	0.19	13.7	21.9	23.1	8
Gemello et al. [62]	0	0.25	8	28.8	29.2	1.5
McClure et al. [132]	0	0.25	8	26.2	30.4	16.2
Jakobsen [85]	0.01	0.08	3.8-12 [2]	25.7	18	29.5
This study	0.06	0.05	9.6	10.2	12.7	24.5
This study	0.06	0.07	10.4	12.3	15.1	22.7
This study	0.06	0.09	11.2	14.5	17.5	20.1
This study	0.06	0.12	12	15.9	19.2	22
This study	0.06	0.14	12.4	17.6	19.6	11.2
This study	0.06	0.19	13.4	19	23.5	23.8

[1] Multiple size group model.
[2] Population balance model.

Table 2.5: Average relative error for the cases listed in Table 2.4

	Homogeneous flow regime	Heterogeneous flow regime
Bubble column	7 %	4.5 %
Co-current flow	10 %	22 %

2.6 Conclusion

Motivated by a growing interest in CFD as a tool for design and scale up of industrial-scale systems involving gas-liquid flows, and considering the overall gas hold-up as the most fundamental parameter related to system performance, we sought to validate an Euler-Euler model against experimental measurements of this quantity for dispersed (homogeneous) and churn-turbulent (heterogeneous) air-water flow in a vertical column.

For operation either as a bubble column or in co-current flow, with and without the addition of a small amount (0.5wt.%) of ethanol in the aqueous phase, we found agreement to within 10% of the experimentally determined values of average gas hold-up in the dispersed flow regime, provided the bubble size supplied as input to the Euler-Euler model was the average bubble size measured experimentally. The considerable sensitivity of this, otherwise narrowly distributed, bubble size to changes in surface tension (and possibly other factors), is identified as the main limitation to the predictive ability of the model in the homogeneous regime. In the heterogeneous regime, the main limitation to the predictive ability of the model stems from uncertainty in accounting for the hydrodynamic interactions between bubbles (swarm correction). A model proposed by Simonnet et al. [193] leads to agreement to within 10% of the experimentally determined values of overall gas hold-up in bubble columns. Much greater errors (22% on average) are, however, observed for co-current flow. Since in neither flow regime can the appropriate bubble size be known a priori, Euler-Euler models are likely to require quantitative calibration in simple systems, such as the one investigated here, before they can be used to investigate industrial systems of greater geometric complexity (e.g., [134, 108]).

Acknowledgements

This research was supported by the Natural Sciences and Engineering Research Council (NSERC) of Canada, and Compute Canada.

Chapter 3

Gas Separation in a Pilot-Scale Ebullated Bed: Experimental and Numerical Investigation

3.1 Synopsis

Gas hold-up reduction inside hydroprocessors is critical to improve the efficiency of bitumen conversion. Installation of internal gas/liquid separators (recycle cup) has been studied in the last 50 years. In this study, we designed and fabricated two recycle cups, employing 3-D printing technology, and investigated their performance in a pilot scale cold-flow ebullated bed reactor. The recycle cups made based on the designs proposed in published patents. Air-water and air-5wt.% ethanol aqueous solution were used as working fluids. Addition of ethanol helped creating high gas hold-up and foaming conditions frequently observed in commercial hydroprocessors. It was observed that in the foaming systems performance of the recycle cups deteriorated. Also, increasing the inlet liquid flow rate and/or recycle liquid flow diminished the separation efficiency. The ability of two-fluid Euler-Euler model in prediction of gas hold-up in the pilot scale system as well as inside the recycle line was also investigated. In the homogeneous flow regime, given the proper bubble size, the model estimated the gas hold-up in the column with less than 5% error. However, unlike the experimental observations, the model did not predict any gas in the recycle line. Such findings are assumed to be the result of small computational mesh grids (smaller than a single bubble) or due to the changes in the average bubble size inside the recycle line.

3.2 Introduction

Upgrading is the term given to a process which converts bitumen, heavy oil or vacuum residue to an improved quality synthetic crude oil [68]. Bitumen is upgraded by hydrogen addition (hydroprocessing) or carbon rejection (fluid bed coking) processes into a product that is lighter, less viscous and relatively free of contaminants (particularly sulfur). Compared to coking, hydroprocessing offers higher liquid yields, better distillate qualities and lower emission levels of sulfur dioxide [68].

Hydroprocessing of bitumen is carried out primarily in ebullated bed reactors (EBRs), which are three-phase (gas-liquid-solid) fluidized bed reactors with an internal recycle line (downcomer) (see Fig. 3.1). Bitumen and hydrogen enter the EBR at the bottom of the column (plenum chamber), are mixed and introduced into the bed of solid particles. The recycle line in the EBRs is connected to an ebullating pump which returns the liquid to the reactor. EBRs generally consist of a three-phase section in which catalyst particles are kept in a fluidized state by the upward flow of the liquid (feed and the recycle) and gas (hydrogen and vapor products), and a catalyst-free section (freeboard region) above three-phase zone. The height of the expanded bed of catalysts is controlled by the rate of the recycled liquid flow [201, 186]. Hydrocracking reactions take place in the three-phase section of the reactor. The hydrogen and vapor products along with the hydrogenated bitumen then enter the freeboard region. Part of the liquid is withdrawn as product and the rest is recycled to the bottom of the reactor [201]. Ideally, gas and vapor products rise to the top of the reactor and removed as effluent.

Although the presence of a minimum amount of gas phase is required in order to sustain the catalytic reactions in the three-phase zone, excessively high gas hold-up values (more than 25%), have been observed in industrial scale EBRs [54, 134]. The excess hydrogen and vapor products decrease the effective volume and bitumen residence time in the reactor. As the level of catalyst bed expansion is controlled by recycled liquid flow, the presence of gas or vapors in the recycle stream decreases the efficiency of the recycle pump and destabilizes the ebullated bed [34]. Entrainment of gas in the recycle line is a major cause of excessively high gas hold-up values, which are detrimental to bitumen conversion. Foam formation in the EBRs and its extension into the recycle line exacerbates gas entrainment [201, 134], spurring interest in the development of techniques to reduce the amount of circulating gas. Previous studies on gas hold-up reduction led to the addition of an internal gas/liquid separator, known as recycle cup, in the freeboard region of the reactor. Implementation of the recycle cup is an effort to improve the gas/liquid disengagement in the freeboard region, such that a smaller amount of gas is entrained in the recycle line [108]. The optimization of recycle cup design has been an ongoing challenge, as numerous cup designs have been

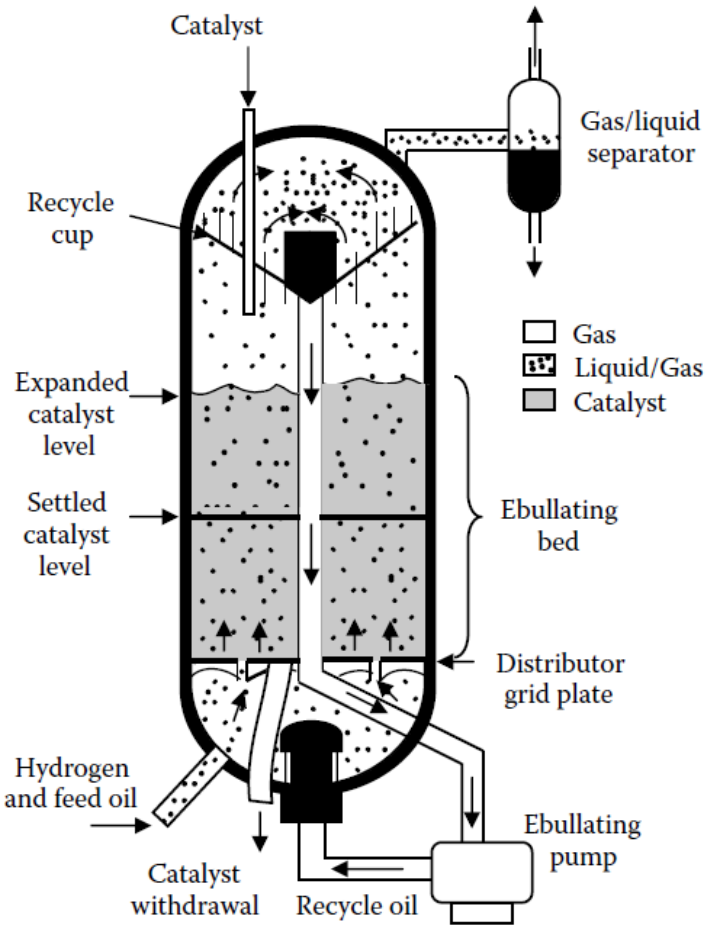

Figure 3.1: Schematics of EBRs used for hydroprocessing of bitumen [10]

developed and patented over the past 50 years [74, 130, 69, 38, 32, 181, 201, 34, 31, 45, 28, 61]. These designs have focused on geometric modification of the recycle cup to improve separation efficiency, the latter determined by measuring the gas hold-up in the internal recycle line of the EBR.

Almost all experimental studies of EBR hydrodynamics published to date have employed pilot scale systems lacking the recycle cup and internal recycle line sections [54, 151, 152]. Generally, in these pilot scale systems gas/liquid disengagement occurs in an expanded overflow section. Fluid dynamic studies in cold-flow pilot scale EBRs with disengagement systems similar to the industrial hydroprocessors are scarce. Only a few reports (mainly in patents) exist that measure and compare the efficiency of recycle cups [31, 45]. The information that can be drawn from these studies is very limited. Aiming to close this gap, this study reports on the design, construction and use of a pilot scale cold-flow system which is equipped with an internal recycle line. The modular structure of the system affords the flexibility to install various recycle cup designs and examine their efficiency in a systematic study. In the first part of this study we demonstrate the use of this system by testing the efficiency of two patented recycle cup designs for gas/liquid separation. By carefully reviewing the design features, two patented recycle cup are reproduced using 3D-printing technology and implemented in the system. The effect of operating parameters, such as the inlet gas and liquid flow rates and recycle ratio (ratio of recycled liquid flow rate to inlet liquid flow rate) are investigated. The system is operated with gas and liquid phases only (without solids), as only the performance of the recycle cups is of interest. In the second part of the study, computational fluid dynamic (CFD) simulations are used to study the ability of an Eulerian two-fluid (Euler-Euler) model to predict of gas hold-up in the pilot scale column and inside the recycle line.

The high cost and practical difficulties of conducting experiments in EBRs at real operating conditions (high pressure and temperature), makes CFD studies an attractive alternative in studies of the hydrodynamics of such complex systems [214, 83]. The Euler-Euler model treats the phases as inter-dispersed continua and is stated in terms of momentum conservation equations derived for each phase through either spatial or time averaging [83]. Phase fractions indicate the amount of each phase that is present at a particular location and time. Simulation at industrially-relevant scales is possible at a reasonable computational cost with Euler-Euler models, whereas it is prohibitively costly with models for which the computational cost scales with the number of bubbles/interfaces [197, 64, 123]. For Euler-Euler models to serve design purposes, rigorous validation of model results against experimental measurements is imperative [67]. Yet, CFD studies to predict the hydrodynamics of EBRs with internal recycle are rather scarce. McKnight et al. [134] used an Eulerian model in the CFX-FLOW3D toolbox to simulate the freeboard region of a

cold-flow EBR (ID of 1.2 m) operating with kerosene and nitrogen and equipped with the recycle cup designed by Buttke and Frey [32]. Only qualitative CFD results were reported in that study. In a recent study, Lane et al. [108] simulated the system described in the study of McKnight et al. [134] using an Eulerian framework within the `OpenFOAM` toolbox. The effect of several parameters, such as the average velocity of the phases, bubble diameter and recycle ratio on gas entrainment inside the recycle line was investigated, but the results were not compared to experimental measurements. Such a comparison is a key objective of this study, which seeks to quantify the ability of two-fluid Euler model to predict the average gas hold-up both in the EBR freeboard and in the recycle line.

The paper is structured as follows: First, the experimental setup and the applied measurement techniques are described in section 3.3. Then, the Euler-Euler model, the momentum exchange closure relations and the specific simulation conditions are presented in section 3.4. The experimental results as well as a discussion of the performance of recycle cups and the effect of various operational parameters on separation efficiency are presented in section 3.5. The Eulerian model predictions are presented and compared with the experimental data in section 3.5.3 and conclusions are summarized in section 3.6.

3.3 Experimental Setup and Procedure

3.3.1 Experimental Setup

The cold-flow pilot scale system used in this study is shown in Fig. 3.2. The column is made of clear PVC with an ID of 15.2 cm and a height of 220 cm. It consists of the gas/liquid distributor section (*i.e.* plenum chamber, 20 cm in height), the test section which contains the recycle cup, and the freeboard region above the recycle cup. The plenum chamber and the section devoted to the recycle cup are connected to the other parts via knob and flange connections. This gives the flexibility to implement various recycle cup designs in the system. A perforated plate containing 3 mm circular holes is fitted between the plenum chamber and the test section. The plate is designed to evenly distribute the gas and liquid phases within the column. The internal recycle line (downcomer) is a 2.54 cm ID acrylic pipe, one end of which is attached to the recycle cup and the other connected to an external gas/liquid separator which receives the recycled liquid and entrained gas. Flow in the recycle line is driven by gravity and controlled by a valve. Gas is completely removed in the separator and the liquid is returned to the storage tank. This external separator enables accurate measurement of the recycled liquid flow. A product line is also installed at the junction of the cup and the internal recycle line. The product flow rate is controlled by

a valve which maintains a desired level of the gas/liquid mixture in the column. Gas/liquid mixture from the product line is also returned to the storage tank. It should be noted that the experimental system lacks the recycle pump of industrial hydrocrackers. This poses certain limitations on the range of recycle flow rates that can be explored.

Distilled water and a 5wt.% ethanol aqueous solution were used as the liquid phase. The liquid was stored in a plastic tank and was pumped through a centrifugal pump (Goulds pump, model 2ST1E4F4) to the bottom of the plenum chamber. The flow rates of the inlet and the recycled liquid streams were measured by two rotameters (Blue-White, models F-43040LNS and F-41017LN-16, respectively). Air was used as the gas phase and it was sparged to the plenum chamber through two symmetrically-installed gas spargers with openings of 100 µm in diameter. Another rotameter (Blue-White, model F-55376-GP) was used to measure the flow rate of injected air. Air flow leaving from the top of the system was also measured by a flow meter (Dwyer, model VFA-26).

To observe the effect of inlet liquid flow rate on gas/liquid separation, two flow rates of 20 and 30 L/min were used which correspond to inlet liquid superficial velocities of 0.019 and 0.028 m/s, respectively. Also, the recycled liquid flow rate was set to obtain recycle ratios in the range 0.33 to 0.7. The recycle ratio (R_r) is defined as:

$$R_r = \frac{Q_l^{recycle}}{Q_l^{inlet}} \tag{3.1}$$

The flow rate of injected air was varied to obtain gas superficial velocities of up to 0.1 m/s. Such wide range has allowed the observation of both dispersed (homogeneous) and churn-turbulent (heterogeneous) flow regimes in the system. According to the literature, for distiled water as the liquid phase and liquid superficial velocities below 0.1 m/s, dispersed flow occurs for gas superficial velocities less than 0.04 m/s [185, 43, 229, 82]. At higher gas velocities, the system switches to the heterogeneous regime. The values of operating parameters are summarized in Table 3.1.

3.3.2 Development of Recycle Cups

The modular structure of the pilot scale system allows implementation of various designs of recycle cups. In this study we fabricated two patented recycle cups and compared their gas/liquid separation efficiency over a wide range of operational conditions. The recycle cups were obtained using a desktop 3-D printer and 3 mm acrylonitrile butadiene styrene (ABS) filaments.

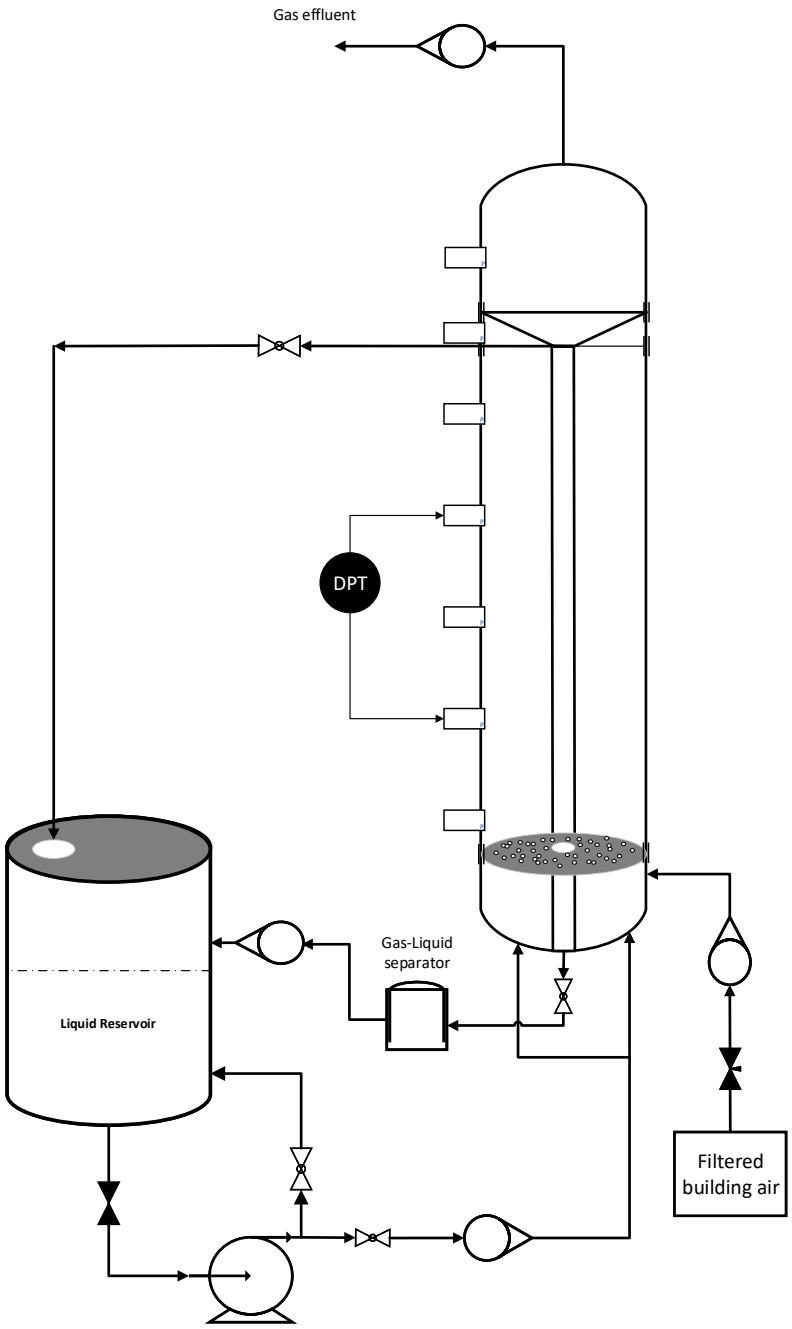

Figure 3.2: Schematics of the experimental setup used in this study

Table 3.1: Studied operating condition and phase physical properties.

Parameter	Symbol	Values	Unit
Superficial liquid velocity	u_{sl}	0.019, 0.028	m/s
Recycle ratio	R_r	0.33 to 0.7	
Superficial gas velocity	u_{sg}	0.01 to 0.1	m/s
Liquid kinematic viscosity	ν_l	1.004×10^{-6}	m^2/s
Gas kinematic viscosity	ν_g	15.11×10^{-6}	m^2/s
Gas-liquid surface tension (water)	$\sigma_{g,l}$	0.072	N/m
Gas-liquid surface tension (5wt.% aqueous ethanol solution)	$\sigma_{g,l}$	0.055	N/m
Liquid density (water)	ρ_l	998.3	kg/m^3
Liquid density (5wt.% aqueous ethanol solution)	ρ_l	989	kg/m^3
Gas density	ρ_g	1.205	kg/m^3
Liquid droplet[1]	d_d	0.001	m

[1] Simulation input

The design of recycle cups for the experimental system was based on geometric similitude with patented designs. The 3D-printed cups and associated patent drawings are shown in Figs. 3.3b and 3.4b. The first cup (see Fig. 3.3b), hereafter referred to as the "simple cup", was developed based on a design proposed in U.S. patent No. 3124518 [74]. This patent is one of the first inventions addressing the separation of gas from the recycled liquid in hydrocracking reactors. The proposed gas/liquid separator apparatus is a simple funnel-shaped (frustoconical) cup with a vertically upward extending upper lip. According to the patent, the cross-sectional area of the recycle line should be between 1% to 10% of the column cross-sectional area. Too small of a downcomer limits the rate of liquid recycled. Too large of a downcomer decreases the effective volume available for hydrogenation reactions inside the reactor. The area of the enlarged section of the cup is also recommended to be between 20% to 50% of the column cross-sectional area. This is in order to reduce the liquid velocity relative to gas velocity such that the entrained gas has an opportunity to separate from the liquid and rise to the top outlet [38]. For the simple cup developed in this study, the ratios of the areas of recycle line and enlarged section of the cup to the area of the column are 3% and 45%, respectively. The angle of the funnel was also set to 45° [31]. During the experiments, the level of gas/liquid mixture was maintained close to the lip of recycle cup as recommended in the patent [74] by adjusting the valve on the product line.

The second recycle cup (see Fig. 3.4b), which is called "cup with risers" in this study, was developed based on the designs disclosed in Patent No. 4221653 [38]. The patent recommended installation of two or more vertical conduits in the funnel-shaped cup for passage of the gas/liquid mixture. These conduits are called risers and they allow fluid communication. The diameter of these cylindrical conduits should be greater that 1.27 cm

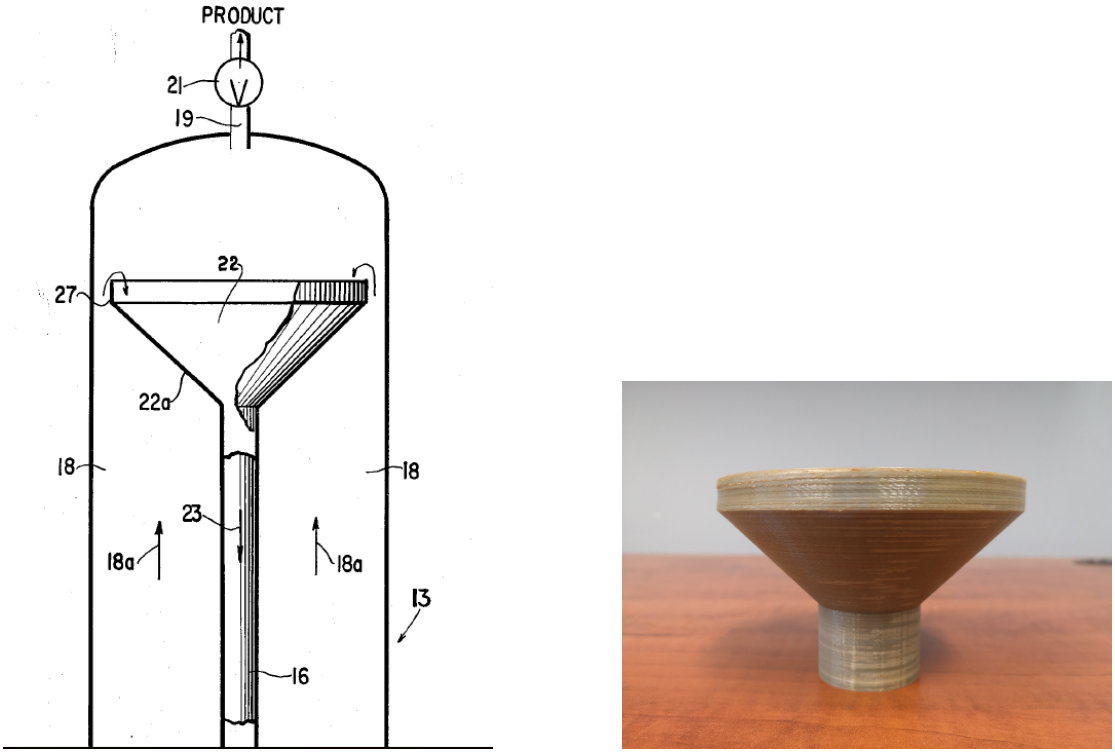

(a) (b)

Figure 3.3: (a) Schematics of recycle cup design from U.S. patent No. 3124518 and (b) Fabricated recycle cup

(0.5 inch) to prevent plugging. In order to improve separation efficiency, specific positioning for the risers has been recommended. A group of risers should have lower inlet ends extended into the gas/liquid mixture. These risers are called liquid-rich. The other risers should intersect the surface of the funnel shape cup, but they should not extent into the gas/liquid mixture. These risers are called gas-rich, as they receive a fluid which is richer in gas. The total cross-sectional area of the risers should be between 10% to 50% of the column cross-sectional area [38]. The cup with risers designed in this study contains two liquid-rich and two gas-rich risers with ID of 3.81 cm (1.5 inches). The liquid-rich risers extended about 5 cm below the funnel surface and into the gas/liquid mixture. The cup was not extended to the wall of the column and an annular space of 0.25 inches was available for the passage of the fluid. The total cross sectional area of the risers was about 45% of the column area and the funnel angle was kept at 45°.

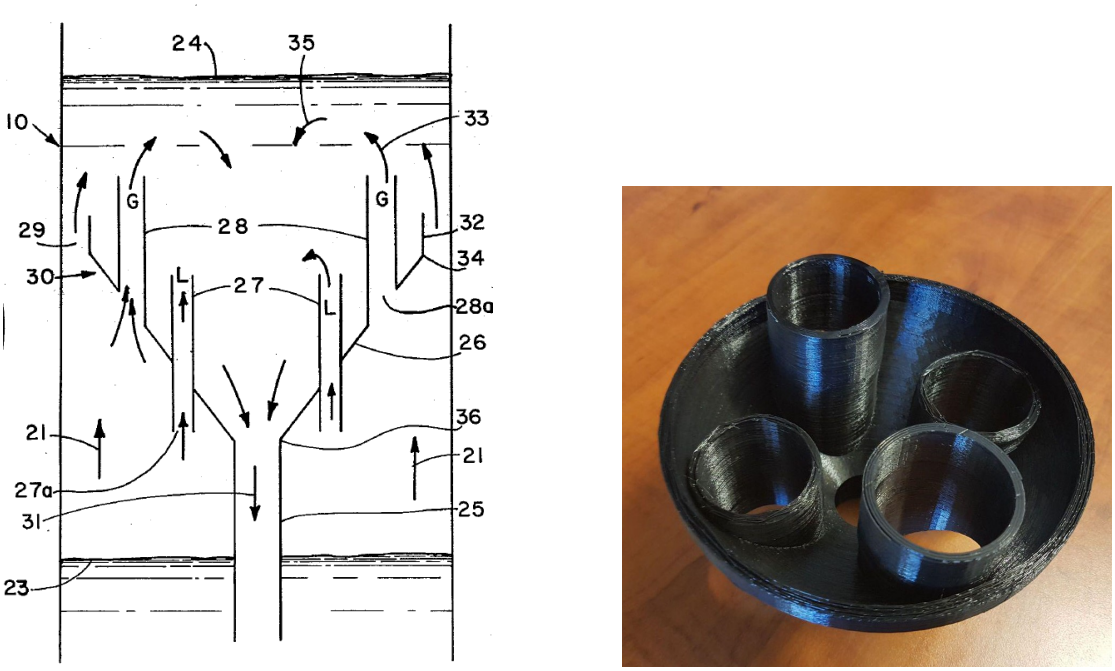

(a) (b)

Figure 3.4: (a) Schematics of recycle cup design from U.S. patent No. 4221653 and (b) Fabricated recycle cup

3.3.3 Gas Hold-up Measurement inside the Column

Gas hold-up in the column was obtained using a differential pressure transducer (Rosemount, model 3051CD2A22A1AM5C6Q4). Seven pressure ports were installed along the column height. The ports were located in 25 cm intervals, starting at 10 cm above the distributor plate. Assuming negligible frictional drag, the dynamic pressure drop between any two arbitrary pressure ports can be related to the gas volume fraction (ϵ_g), as follows:

$$\epsilon_g = \frac{\frac{\Delta P}{g\Delta z}}{\rho_l - \rho_g} \tag{3.2}$$

where P is the pressure, Δz is height difference between the two pressure ports and ρ_l and ρ_g are the densities of the liquid and gas phase, respectively. As there are only gas and liquid phases in the system, we have:

$$\epsilon_g + \epsilon_l = 1 \tag{3.3}$$

Using the above equation, the liquid hold-up can also be calculated.

3.3.4 Gas Hold-up Measurement inside the Recycle Line

In order to measure gas hold-up in the recycle line a method based on the difference in electrical conductivity of gas and liquid phases was used [212, 142, 7]. Specifically, gas hold-up was determined by measuring the electrical impedance of a two-phase system by properly introducing metallic electrodes in the flow. The instrument used in this study was a precision LCR meter (Quadtech, model 1920). Gas hold-up in the recycle line was measured at 2 kHz AC, using two pairs of electrical conductivity cells made of stainless steel plates (2.5 cm $\times$ 1.5 cm) and mounted facing each other on opposite sides of the inner surface of the recycle line (see Fig. 3.5). Conductance readings were made by connecting the LCR meter to the stainless steel plates using a pair of Kelvin leads. The vertical distance between the two pairs of cells was 90 cm. In order to increase the sensitivity of conductance measurements, a small amount of sodium chloride (0.5 g/L) was added to the liquid phase. Enough time was given for the system to reach steady state prior to reading conductance values. Then, conductance readings from one pair of electrical cells were collected for three minutes. The same procedure was repeated for the second pair of cells. The average of readings from both pair of cells was used for further calculations. A sample of LCR meter readings used for gas hold-up calculation in the recycle line is shown in Appendix C.

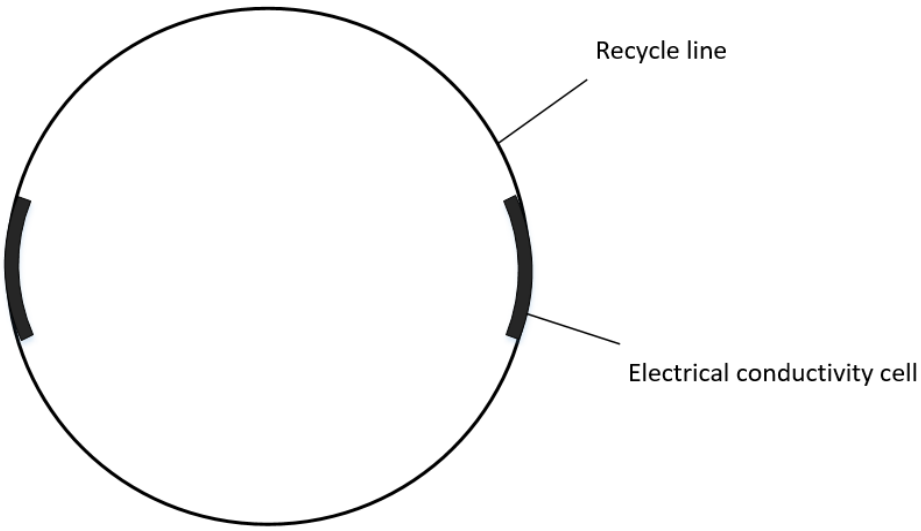

Figure 3.5: Top view schematics of the electrical conductivity cells mounted on the recycle line surface.

Several expressions are proposed in the literature to relate the conductance of a gas/liquid mixture to the conductance of liquid phase and the gas hold-up. Among those, the theoretical expression proposed by Maxwell [131] has been tested and validated in several studies especially for hold-up values of less than 20% (see Fig. 3.6) [125, 212, 7]:

$$G_m = G_l \, \frac{1 - \epsilon_g}{1 + 0.5 \, \epsilon_g} \tag{3.4}$$

where G_m and G_l are the conductance values of the gas/liquid mixture and the liquid, respectively. It should be mentioned that a few studies have reported poor reliability of this expression and recommended obtaining an empirical correlation between dispersion conductivity and gas hold-up instead.

In order to test the accuracy of Eq.3.4, a pair of electrical cells was installed in a 100 cm long acrylic pipe similar to the recycle line (2.54 cm ID). One end of the pipe was closed and the pipe was filled with water. Air was introduced through the pipe using a gas sparger with openings of 100 µm. The cells were installed 50 cm above the gas sparger in the developed region of two-phase flow. The gas hold-up in the pipe was measured experimentally, using the difference between the height of aerated (H) and unaerated (H_0) liquid [230](Eq.3.5) and also determined from conductance measurements using Maxwell's

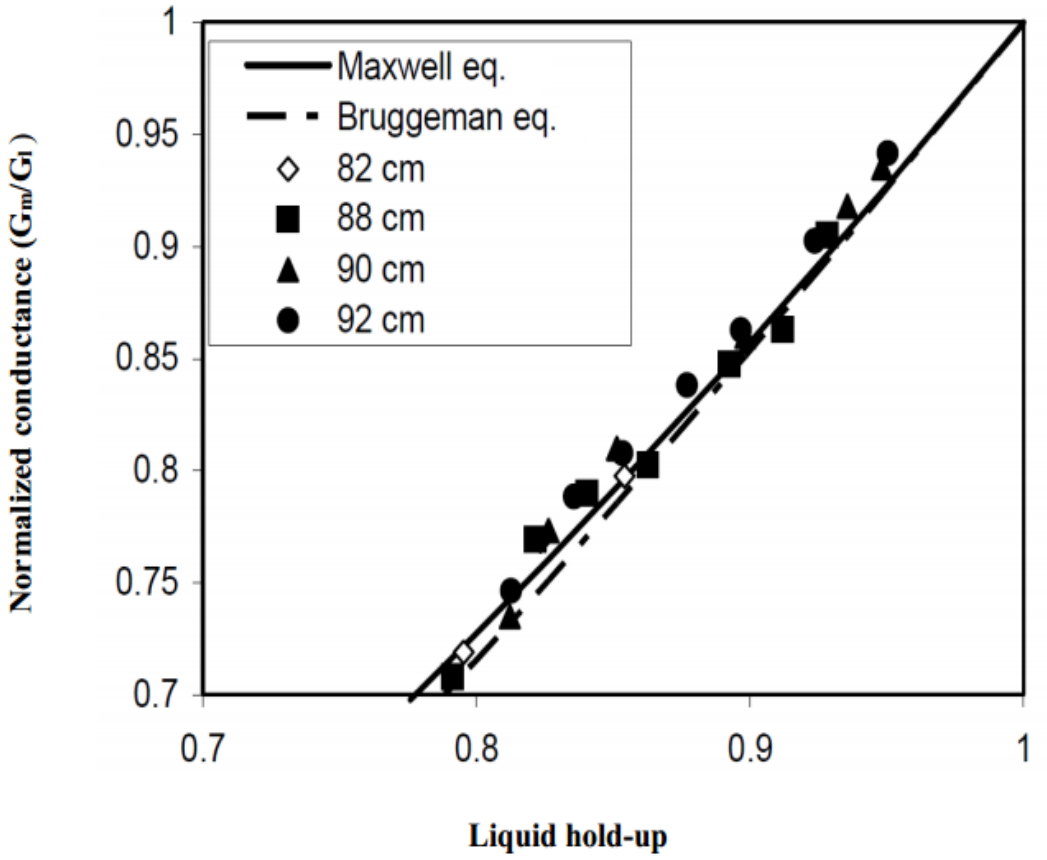

Figure 3.6: Measured and predicted dimensionless conductance as a function of liquid hold-up [7]. (The numbers are the height of electrical conductivity cells in the reactor.)

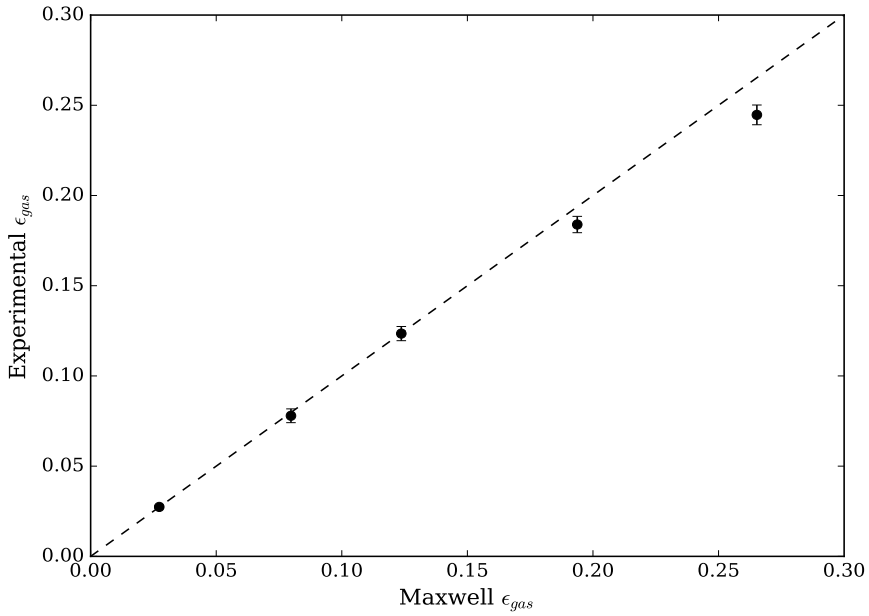

Figure 3.7: Accuracy of Maxwell equation in prediction of gas hold-up data in a 2.54 cm ID acrylic pipe

equation. The results are compared in Fig. 3.7.

$$\epsilon_g = 1 - \frac{H_0}{H} \tag{3.5}$$

It can be seen from Fig. 3.7 that the Maxwell equation predicts accurately gas hold-up values of up to about 20%. Since gas hold-up in the recycle line is expected to be less than 20%, employing the Maxwell equation to obtain the gas hold-up from conductance measurements is justified.

3.4 Model Description

3.4.1 Euler-Euler Model

The multiphase process of interest here is the two-phase incompressible flow of two immiscible, Newtonian fluids under isothermal conditions ($T = 293.15$ K) in the system shown

on Fig. 3.8. A two-fluid or Euler-Euler model [83], similar to the one described in Chapter 2, was used to model two-phase flow in this system. This model treats the phases as inter-penetrating continua where the volume of one phase can not be occupied by the other and the presence of each phase q is described by a phase volume fraction α_q.

3.4.2 Turbulence Modeling

The flows investigated in the present study involve gas phase (air) volume fractions in the range 5% to 20%. For this reason, the mixture k-ε turbulence model was used to compute the Reynolds stress tensor. The complete description of the turbulence model employed can be found in Chapter 2.

3.4.3 Initial Boundary Value Problem

The operating conditions prevailing in the experiments were reproduced with CFD simulations by enforcing specific initial and boundary conditions, as described next. The boundaries over which conditions on the pressure, velocity, phase volume fractions, and turbulence quantities were specified are, as shown on Fig. 3.8, *walls*, *inlet*, *top*, *bottom*, and *lateral*. It must be highlighted here that only the upper portion of the real system, shown on Fig. 3.2, was considered for modeling (see Fig. 3.8). This portion corresponds to a total height of 0.74 m. This was done in order to reduced computational costs and is justified because the variation of flow profiles in the ommitted bottom portion is negligible. The physical properties of the gas and liquid phases (see Table 3.1) were assumed to be constant.

The initial conditions associated with the mass and momentum conservation equations (Euler-Euler) and with the turbulent kinetic energy and turbulence dissipation rate conservation equations of the k-ε model are stated below,

$$\boldsymbol{u}_q(\boldsymbol{x}, 0) = \mathbf{0}, \qquad q = g,\, l, \tag{3.6a}$$

$$p(\boldsymbol{x}, 0) = 0, \tag{3.6b}$$

$$\begin{aligned} &\alpha_g(\boldsymbol{x}, 0) = 0, \quad \text{for } z < 0.43\,\text{m}, \\ &\alpha_g(\boldsymbol{x}, 0) = 1, \quad \text{for } z \geq 0.43\,\text{m}, \end{aligned} \qquad \alpha_l(\boldsymbol{x}, 0) = 1 - \alpha_g, \tag{3.6c}$$

$$\nu_t(\boldsymbol{x}, t) = 0, \tag{3.6d}$$

$$k(\boldsymbol{x}, 0) = 0, \tag{3.6e}$$

$$\varepsilon(\boldsymbol{x}, 0) = 0, \tag{3.6f}$$

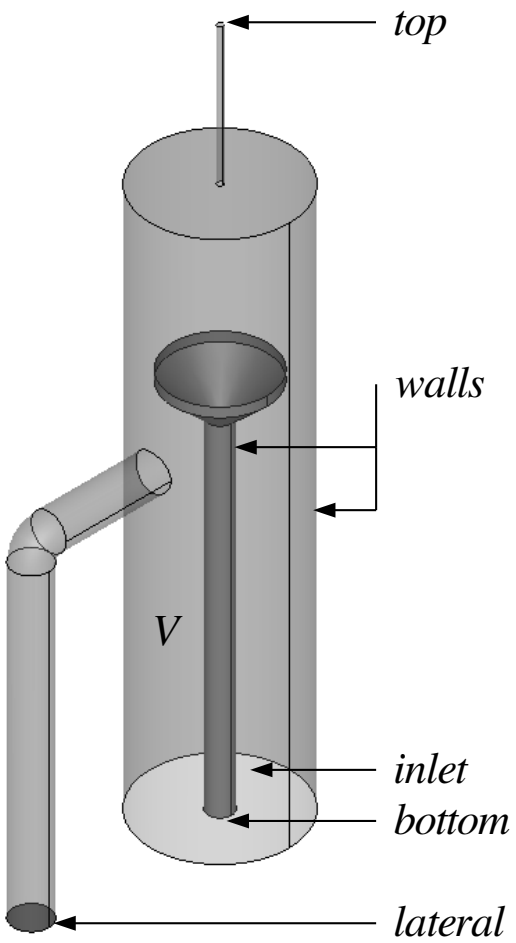

Figure 3.8: Three dimensional view of the computational domain V used to model the real system. configuration with the simple cup geometry. Boundaries are defined and used to enforce the desired operating conditions in CFD simulations.

where the two phases are initially static (Eqs.3.6a-3.6b). The system is full of liquid at $t = 0\,\mathrm{s}$ up to a level slightly above the cup, where $0 \leq z \leq 0.43\,\mathrm{m}$ (Eqs.3.6c). Above this level, $0.43 \leq z \leq 0.74\,\mathrm{m}$, only gas (air) is present. The turbulent viscosity, kinetic energy, and dissipation rate are initially zero (Eqs.3.6d, 3.6e and 3.6f, respectively). It should be mentioned here that starting with this phase distribution allows for a faster convergence to permanent flow and reduces the amount of corrections needed by the control strategy, discussed in what follows, to set the target operating conditions.

At the *walls* boundary, the following conditions were imposed,

$$\boldsymbol{u}_q(\boldsymbol{x},t) = \boldsymbol{0}, \qquad \text{on } walls, \qquad q = g,\, l, \tag{3.7a}$$

$$\boldsymbol{\nabla}_{\boldsymbol{n}} p(\boldsymbol{x},t) = \boldsymbol{0}, \qquad \text{on } walls, \tag{3.7b}$$

$$\boldsymbol{\nabla}_{\boldsymbol{n}} \alpha_q(\boldsymbol{x},t) = \boldsymbol{0}, \qquad \text{on } walls, \qquad q = g,\, l, \tag{3.7c}$$

$$\nu_t(\boldsymbol{x},t) = f_\mu C_\mu k^2/\varepsilon, \qquad \text{on } walls, \tag{3.7d}$$

$$k(\boldsymbol{x},t) = \boldsymbol{u}^{*2}/\sqrt{C_\mu}, \qquad \text{on } walls, \tag{3.7e}$$

$$\varepsilon(\boldsymbol{x},t) = C_\mu^{3/4} k_N^{3/2}/K y_N, \qquad \text{on } walls, \tag{3.7f}$$

where a no-slip velocity condition is adopted for the gas and liquid phases (Eq.3.7a), and a Neumann zero normal gradient condition for both the pressure and phase fractions (Eqs.3.7b and 3.7c) such that $\boldsymbol{n}$ is the unit outward normal to the surface. In addition, the k-ε turbulence model wall functions [26, 2] were used in Eqs. 3.7d, 3.7e, and 3.7f. The parameter f_μ in Eq.3.7d is a damping function whereas $\boldsymbol{u}^*$ (Eq.3.7e) is the friction velocity, K (Eq.3.7f) is the von Karman constant, y_N the distance from the wall to the first interior node N, and k_N the turbulent kinetic energy at N.

The boundary conditions enforced at the *inlet* are given as follows,

$$\boldsymbol{u}_q = (0,\, 0,\, u_{sq}^{inlet}/\alpha_q^{inlet}), \qquad \text{on } inlet, \qquad q = g,\, l, \tag{3.8a}$$

$$\boldsymbol{\nabla}_{\boldsymbol{n}} p(\boldsymbol{x},t) = \boldsymbol{0}, \qquad \text{on } inlet, \tag{3.8b}$$

$$\begin{aligned} &\alpha_q = \alpha_q^{inlet}, \\ &\alpha_q^{inlet} = u_{sq}^{inlet}/(u_{sg}^{inlet} + u_{sl}^{inlet}), \end{aligned} \qquad \text{on } inlet, \qquad q = g,\, l, \tag{3.8c}$$

$$\nu_t = \nu_t^{inlet}, \qquad \text{on } inlet, \tag{3.8d}$$

$$k = k^{inlet}, \qquad \text{on } inlet, \tag{3.8e}$$

$$\varepsilon = \varepsilon^{inlet}, \qquad \text{on } inlet, \tag{3.8f}$$

where the Dirichlet uniform velocity conditions (Eq.3.8a) were imposed for both phases such that u_{sq}^{inlet} is the phase q superficial velocity and α_q^{inlet} the phase volume fraction at the *inlet*. The velocity vectors $\boldsymbol{u}_q$ at the entrance of the system are normal to the *inlet* boundary and point inwards. The Neumann zero normal gradient condition was considered for the pressure (Eq.3.8b). Dirichlet boundary conditions (Eq.3.8c) were adopted for phase fraction of both phases. Dirichlet uniform boundary conditions were also used for the turbulence quantities ν_t, k, and ε at the *inlet* (see Eqs.3.8d through 3.8f). Since the exact values of these turbulent quantities at the *inlet* are unknown, it is generally assumed in the literature of two-phase dispersed flows that the effect of these *inlet* values is insignificant. In the previous chapter, the turbulence quantities at the entrance of the system were estimated from empirical relations derived for turbulent single-phase upward flows in a pipe [168], as relations for two-phase flows are not available. These estimations were made using the gas volume fractions which was obtained experimentally. The approach described in Chapter 2 was also adopted here.

It should be mentioned here that a Dirichlet pressure boundary condition at the inlet boundary was argued to be more appropriate than the commonly used uniform velocity boundary condition [4], because it (i) allows for the development of a gas-liquid slip velocity at the inlet and (ii) avoids violation of the non-slip velocity condition at the wall. In addition, it yields non-uniform flow profiles at the inlet consistent with the model governing equations [4]. Implementation of the inlet Dirichlet pressure boundary condition, however, requires adopting a multi-variable control strategy to set values of p^{inlet} and α_q^{inlet}, which are unknown *a priori*, such that target superficial velocities are met [4]. Here, in order to simplify the flow problem and improve numerical stability, since other control strategies were required on the *bottom* and *lateral* boundaries as discussed below, a Dirichlet velocity boundary condition was used instead of the pressure one. It is expected that the impact of this simplification on the solutions is insignificant, as it was found in Chapter 2. That is, although the type of inlet boundary conditions strongly affects the flow profiles, its impact on the overall gas hold-up is negligible for either bubble column or two-phase upward flow configurations.

The conditions imposed at every outlet boundary (*top*, *bottom*, and *lateral*) are presented below. Two distinct approaches, referred to as configurations A and B, were considered and both were implemented. The outlet boundary conditions, which are the same

for both configurations, are as follows,

$$p(\boldsymbol{x},t) = p^{top}, \qquad \text{on } top, \tag{3.9a}$$

$$\boldsymbol{\nabla_n}\alpha_q(\boldsymbol{x},t) = \boldsymbol{0}, \qquad \text{on } bottom \text{ and } lateral, \qquad q = g,\, l, \tag{3.9b}$$

$$\boldsymbol{\nabla_n}\nu_t(\boldsymbol{x},t) = \boldsymbol{0}, \qquad \text{on } bottom \text{ and } lateral, \qquad q = g,\, l, \tag{3.9c}$$

$$\boldsymbol{\nabla_n}k(\boldsymbol{x},t) = \boldsymbol{0}, \qquad \text{on } bottom \text{ and } lateral, \qquad q = g,\, l, \tag{3.9d}$$

$$\boldsymbol{\nabla_n}\varepsilon(\boldsymbol{x},t) = \boldsymbol{0}, \qquad \text{on } bottom \text{ and } lateral, \qquad q = g,\, l, \tag{3.9e}$$

where a uniform Dirichlet pressure boundary condition was considered (Eq.3.9a) at the *top* boundary such that p^{top} corresponds to the atmospheric pressure, $p^{top} = 101325\,\text{Pa}$. At the *bottom* and *lateral* outlets, the Neumann zero normal gradient condition was imposed for the phase fractions of both phases and for the turbulent viscosity, kinetic energy and dissipation rate as stated on Eqs.3.9b through 3.9e, respectively.

For configuration A, outlet boundary conditions are,

$$\boldsymbol{\nabla_n}\boldsymbol{u}_q(\boldsymbol{x},t) = \boldsymbol{0}, \qquad \text{on } bottom \text{ and } lateral, \qquad q = g,\, l, \tag{3.10a}$$

$$p(\boldsymbol{x},t) = p^{bottom}, \qquad \text{on } bottom, \tag{3.10b}$$

$$p(\boldsymbol{x},t) = p^{lateral}, \qquad \text{on } lateral, \tag{3.10c}$$

such that a Neumann zero normal gradient condition is enforced to the velocity of both phases (Eq.3.10a), while Dirichlet uniform pressure conditions are imposed on the *bottom* and *lateral* boundaries (Eqs.3.10b and 3.10c, respectively). Since the pressure values p^{bottom} and $p^{lateral}$ corresponding to the target liquid superficial velocities u_{sl}^{bottom} and $u_{sl}^{lateral}$, respectively, are not known, a proportional integral (PI) controller is used on each of these outlets. Implementation of the PI control is described elsewhere [4].

Simulations carried-out using configuration A are not constrained by the level of the gas/liquid mixture in the column, showing that multiple combinations of p^{bottom} and $p^{lateral}$ can satisfy the target liquid superficial velocities u_{sl}^{bottom} and $u_{sl}^{lateral}$ at steady state (each corresponding with a different level of the gas/liquid mixture within the column). This suggests that additional constraints need to be introduced into the numerical model in order to ensure uniqueness of the solution. Therefore, configuration B, with the following

boundary conditions was adopted.

$$\boldsymbol{u}_l(\boldsymbol{x},t) = \boldsymbol{u}_l^{bottom}, \qquad \text{on } bottom, \tag{3.11a}$$

$$\boldsymbol{u}_l(\boldsymbol{x},t) = \boldsymbol{u}_l^{lateral}, \qquad \text{on } lateral, \tag{3.11b}$$

$$\boldsymbol{\nabla_n} \boldsymbol{u}_g(\boldsymbol{x},t) = \boldsymbol{0}, \qquad \text{on } bottom \text{ and } lateral, \tag{3.11c}$$

$$\boldsymbol{\nabla_n} p(\boldsymbol{x},t) = \boldsymbol{0}, \qquad \text{on } bottom \text{ and } lateral, \tag{3.11d}$$

In this configuration, Dirichlet liquid velocity boundary conditions were used on *bottom* and *lateral* boundaries (Eqs.3.11a and 3.11b) to set the target liquid superficial velocities. It must be emphasized that $\boldsymbol{u}_l^{bottom}$ and $\boldsymbol{u}_l^{lateral}$ require a continuous adjustment as a function of the gas volume fractions at both outlets, α_g^{bottom} and $\alpha_g^{lateral}$, to maintain the liquid superficial velocities at their target values. On the other hand, the Neumann zero normal gradient condition is enforced for the gas velocity and the pressure (Eqs.3.11c and 3.11d). This configuration allowed for a faster convergence to the fully developed flow, compared to configuration A, since generally the PI controller require a certain time period to reach the target values. In addition, in configuration B, the one way valves present in the experimental setup were modeled by suppressing back flow at all the outlet boundaries (*top*, *lateral*, *bottom*). It should be mentioned that suppressing back flow in configuration A led to numerical instability due to the action of the PI controllers.

3.5 Results and Discussion

3.5.1 Gas Hold-up in the Gas-Liquid System

The overall gas hold-up in the column was obtained from pressure readings as described in section 3.3.3. The results are shown in Fig. 3.9. It can be seen that gas hold-up mainly depends on gas velocity. Liquid velocity has a minor effect on the gas hold-up in the air-water system. Increasing the liquid velocity from 0.019 to 0.028 m/s, reduced the gas hold-up in the ethanol solution system by an average of 7%. As expected, the gas hold-up values are higher in the presence of ethanol in the system. Addition of ethanol reduced the surface tension from 0.072 to 0.055 N/m, thereby limiting bubble coalescence and reducing the bubble size. Consequently, bubble rise velocity decreased and this resulted in an increase in the gas hold-up values [189, 41, 62]. For the distilled water system, gas hold-up changes significantly with gas superficial velocities of up to 0.03 m/s. For higher values the dependence of gas hold-up on gas velocity is not as strong, which implies transition

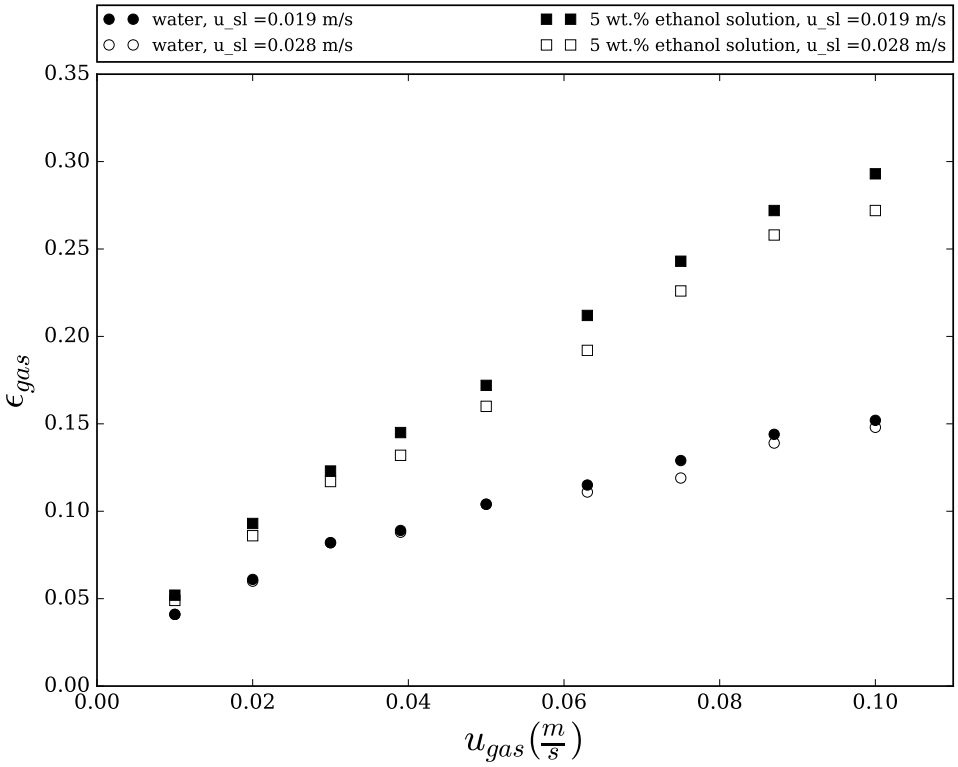

Figure 3.9: Overall gas hold-up in the column

to the heterogeneous flow regime. Addition of ethanol delayed this transition up to a gas velocity of about 0.05 m/s. Similar trends have been observed in previous studies [41].

As described before, gas hold-up values of up to 25% and higher, as well as foaming, have been observed in the freeboard region of hydrocracking reactors [201, 134]. In order to simulate high gas hold-up conditions in cold-flow systems, researchers have sought to limit bubble coalescence by introducing surface-active components into the liquid phase. Both aqueous alcohol solutions [53, 198] and commercial surfactants have been used [204]. A 5wt.% ethanol solution was used in this study in order to test the efficiency of recycle cups under gas-hold up conditions resembling industrial operation. It can be seen from Fig. 3.9 that hold-up values of about 30% was obtained while using gas velocities of up to 0.1 m/s. A similar range of gas hold-up values was reported in the freeboard region of the AMOCO cold-flow EBRs (ID of 1.2 m) using kerosene and nitrogen [31, 45, 134]. Also, significant foaming was observed in the system when operating with ethanol solutions especially at gas velocities of over 0.05 m/s. It should be noted that changing the recycle ratio (R_r), did not have an effect on the gas hold-up in the column. Therefore, the data shown in Fig. 3.9 are valid for all the recycle ratios tested in this study.

3.5.2 Gas Hold-up in the Recycle Line

Gas hold-up data in the recycle line was measured and used to establish the efficiency of the recycle cups in gas/liquid disengagement. Fig. 3.10 shows the gas hold-up in the recycle line for both simple cup and cup with risers operating with u_{sl} of 0.019 m/s and recycle ratio of 0.5. For the simple cup, gas entrainment in the recycle line was observed even for the smallest gas superficial velocity. As a result of foaming and higher gas hold-up in the column operating with the ethanol solution, more gas was entrained in the recycle line. As the gas velocity increased to more than 0.03 m/s, the gas hold-up values in the recycle line became higher than the hold-up values in the column, corresponding to complete failure of the cup to separate gas from liquid. Uncertainty measurement is seen to increase as a result of unsteady flow patterns in the recycle line at higher gas hold-ups. The cup with risers demonstrates superior performance in gas/liquid disengagement. For the system of distilled water, over the entire range of gas velocities, gas hold-up in the recycle line remained below 1.5%. When ethanol was added to the system, especially for gas velocities of over 0.05 m/s, gas entrainment started to increase. As discussed before, a thick layer of foam was observed in the column for gas velocities of 0.05 m/s or higher. These data confirm that foaming can negatively affect the performance of recycle cups. The cup with risers did not fail even at very high gas velocities and the gas hold-up in the recycle line remained below 10%. The presence of conduits with inlet ends within the gas/liquid

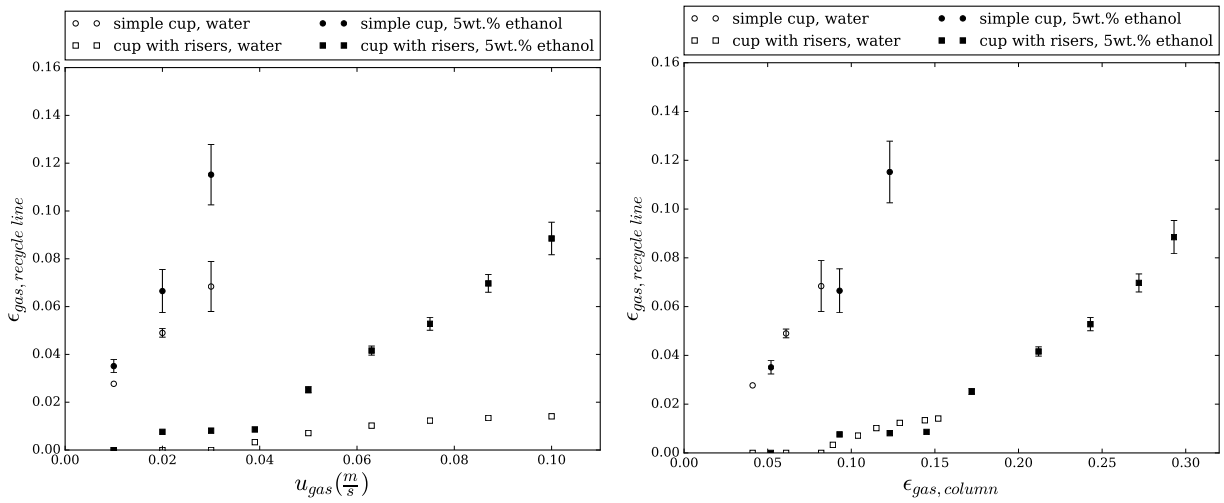

(a) (b)

Figure 3.10: Gas hold-up in the recycle line for $u_{sl} = 0.019$ m/s and $R_r = 0.5$

mixture and outlet ends at different levels made a vapor rich stream to pass through the conduits which terminate at a higher level (gas-rich conduits). The gas discharged in the region above the lip of the cup and left from the top outlet. Consequently, the liquid rich stream, entered the conduits that end inside the funnel, therefore, collected and discharged lower than the lip of the cup [38].

The effect of the inlet liquid velocity on the gas entrainment was also studied. For the ethanol solution system, the entrained gas hold-up in the recycle line of cup with risers is shown in Fig. 3.11 for the two liquid velocities of 0.019 and 0.028 m/s and for recycle ratios of 0.33 and 0.7. It can be seen from the figure that at the higher liquid velocity, gas has less time to escape from liquid and therefore the recycle line gas hold-up is generally higher. The effect becomes more notable as the gas velocity increases. Similar behavior was also reported by Devanathan et al. [45] in the AMOCO cold-flow unit. They observed that the gas hold-up in the recycle line doubled while increasing the inlet liquid velocity from 0.026 to 0.037 m/s.

In an industrial hydrocracking system a certain fraction of the liquid phase is being recycled using an ebullating pump to control the expansion and motion of catalyst particles in the three-phase section. The fraction of liquid being recycled or the recycle ratio can affect the amount of the entrained gas in the recycle line and consequently the gas hold-up in the reactor [134, 108]. To investigate the effect of recycle ratio on the gas/liquid separation in this study, three different ratios for each inlet liquid velocity were tested.

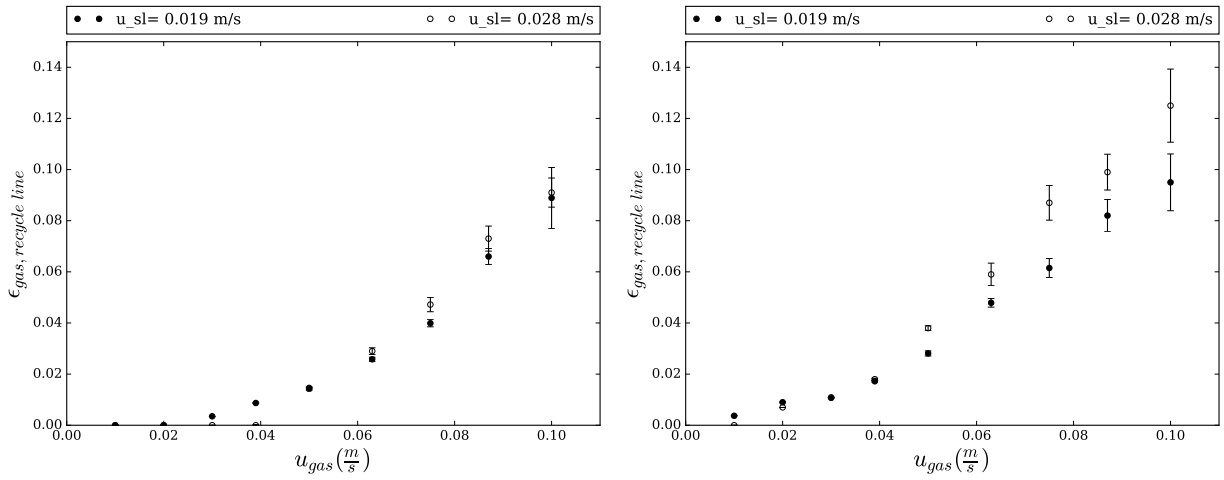

(a) (b)

Figure 3.11: Gas hold-up in the recycle line of the cup with risers for 5wt.% ethanol solution system and for (a)$R_r = 0.33$ and (b)$R_r = 0.7$

The results for the ethanol solution system and for u_{sl} of 0.019 m/s are presented in Fig. 3.12. It is apparent from the figure that gas entrainment increases with increasing recycle ratio. The greater velocity of liquid in the recycle line traps more bubbles into the recycle stream. The effect of recycle ratio is more prominent in the simple cup as compared to the cup with risers, in which gas hold-up changes only slightly as the recycle ratio increases from 0.5 to 0.7. This relative insensitivity is advantageous since the system is able to operate at higher recycle ratio without adverse effects on conversion.

3.5.3 Prediction of Gas Hold-up with the Eulerian Model

The Eulerian model described in section 3.4 was used to predict the gas hold-up in the column and in the recycle line of the system with the simple cup. We simulated both air-water and air-5wt.% ethanol systems operating with $u_{sl} = 0.019$ m/s ($Q_l^{inlet} = 20$ L/min), $u_{sg} = 0.03$ m/s ($Q_g^{inlet} = 29.3$ L/min) and for $R_r = 0.33$ ($Q_l^{recycle} = 6$ L/min). The cases simulated are shown in Table 3.2. For the air-water system, the bubble diameter of 2.7$\pm$ 0.5 mm found in the dispersed flow regime through image analysis (see Chapter 2) was taken as the base case. Similar measurements were not made in the system with 5wt.% aqueous ethanol solution, since the presence of ethanol rendered image analysis very inaccurate. Using electrical conductivity and optical probes, several literature studies have measured the bubble size distribution in gas-liquid flows with various concentrations of ethanol in

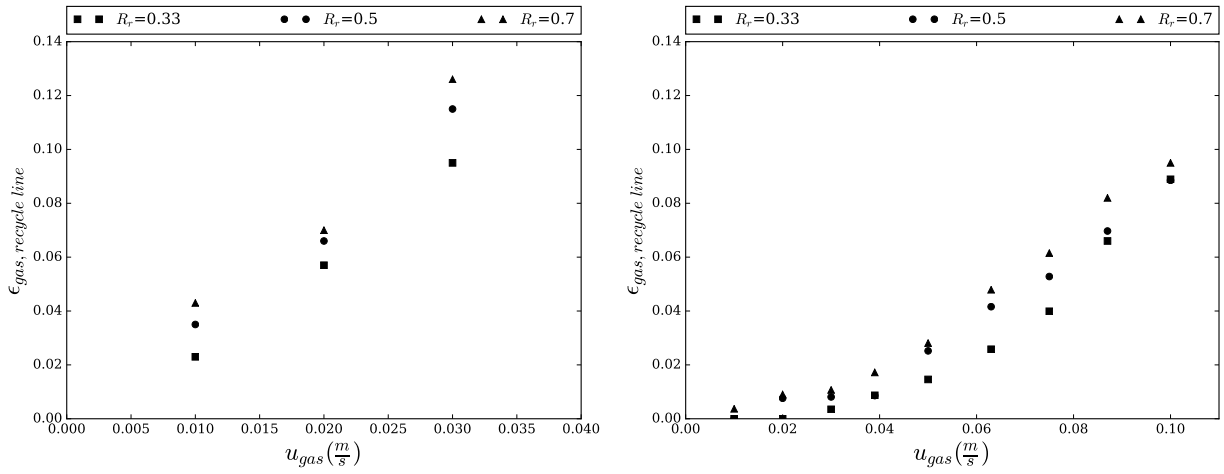

Figure 3.12: Gas hold-up in the recycle line for 5wt.% ethanol solution system at u_{sl} = 0.019 m/s for (a) simple cup and (b) cup with risers

water [189, 153]. Considering the findings of these studies, the average bubble size was estimated to be between 1 and 1.5 mm for dispersed flow in the air-5wt.% ethanol system.

First, we simulated the air-water system with the Eulerian model using the pressure boundary condition at both lateral and bottom outlets (configuration A) and the average bubble diameter obtained experimentally (2.7 mm). Fig. 3.13 illustrates convergence of the simulation using the PI controller. In this case (case no. I in Table 3.2), the model predicts the gas hold-up in the column with high accuracy (3.5% error), but fails to predict any gas hold-up in the recycle line. The simulation predicts instead complete separation of the gas and liquid phases at the top of the cup with no gas entering the recycle line. As noted previously, prescribing the boundary conditions of configuration A leads to multiple steady state solutions, each corresponding with a different level of the gas/liquid mixture in the column. Here, the correct level of gas/liquid mixture was obtained by trial and error and the results are shown in Figs. 3.14 and 3.15. It can be seen from the figures that due to the sudden changes in the cross sectional area around the cup, a recirculation occurs above the cup and the velocity streamlines became larger and took toroidal shape. Such recirculation enhances gas/liquid segregation above the cup. Also all the gas entered the column left from the top outlet only.

The air-water system was subsequently modeled using the velocity boundary condition at th bottom and lateral outlets (configuration B). This choice resulted in much faster convergence of the simulations compared to configuration A. Using an average bubble size

Table 3.2: Various cases simulated using the Eulerian model in this study, $Q_l^{inlet} = 20$ L/min, $Q_g^{inlet} = 29.3$ L/min, $Q_l^{recycle} = 6$ L/min. (B.C. refers the boundary condition at the bottom and lateral outlets according to Fig. 3.8)

Case No.	**System**	d_b (mm)	**B.C.**	$\epsilon_{g,exp.}^{column}$	$\epsilon_{g,sim.}^{column}$	$\epsilon_{g,exp.}^{recycle}$	$\epsilon_{g,sim.}^{recycle}$	$Q_{g,exp.}^{top}$ (L/min)	$Q_{g,sim.}^{top}$ (L/min)
I	air-water	2.7	config. A	0.085	0.088	0.061	0	27±1	29.3
II	air-water	2.7	config. B	0.085	0.088	0.061	0	27±1	26
III	air-water	2	config. B	0.085	0.097	0.061	0	27±1	26.1
IV	air-5wt.% ethanol	1.5	config. B	0.123	0.104	0.094	0	26±1	25.6
V	air-5wt.% ethanol	1	config. B	0.123	0.116	0.094	0	26±1	25.6

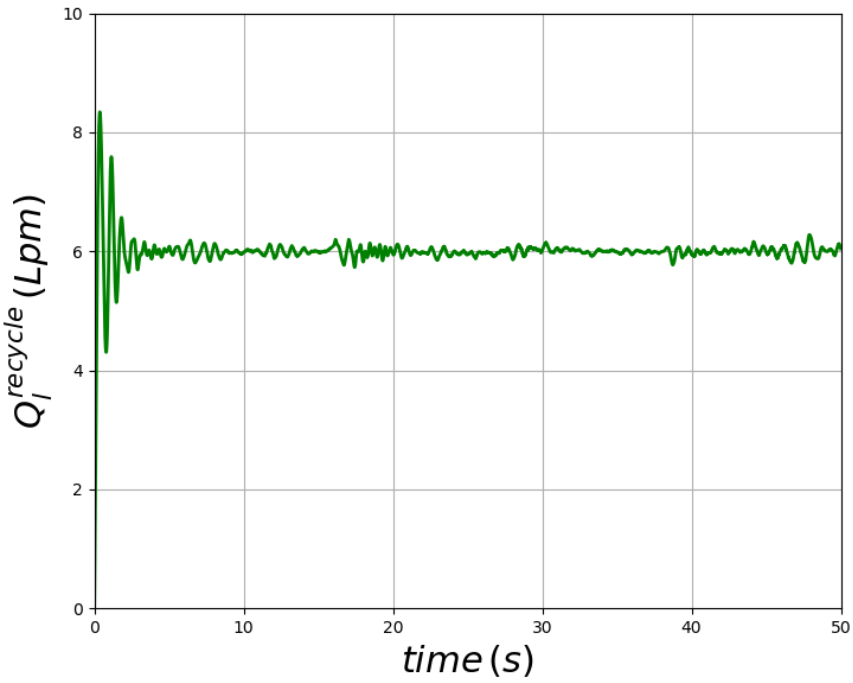

Figure 3.13: Convergence of the simulation with pressure boundary condition (configuration A), $u_{sl} = 0.019$ m/s, $u_{sg} = 0.03$ m/s, $R_r = 0.33$, $d_b = 2.7$ mm.

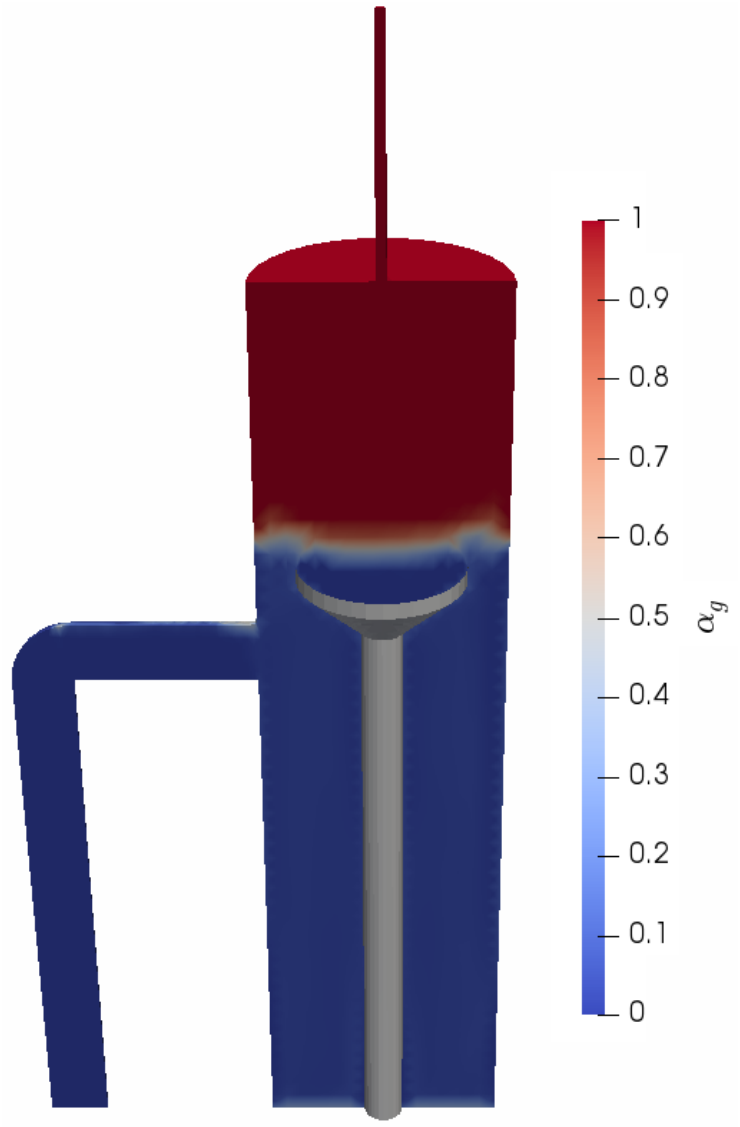

Figure 3.14: Gas volume fraction color map in the air-water system with simple cup (configuration A), $u_{sl} = 0.019$ m/s, $u_{sg} = 0.03$ m/s, $R_r = 0.33$, $d_b = 2.7$ mm.

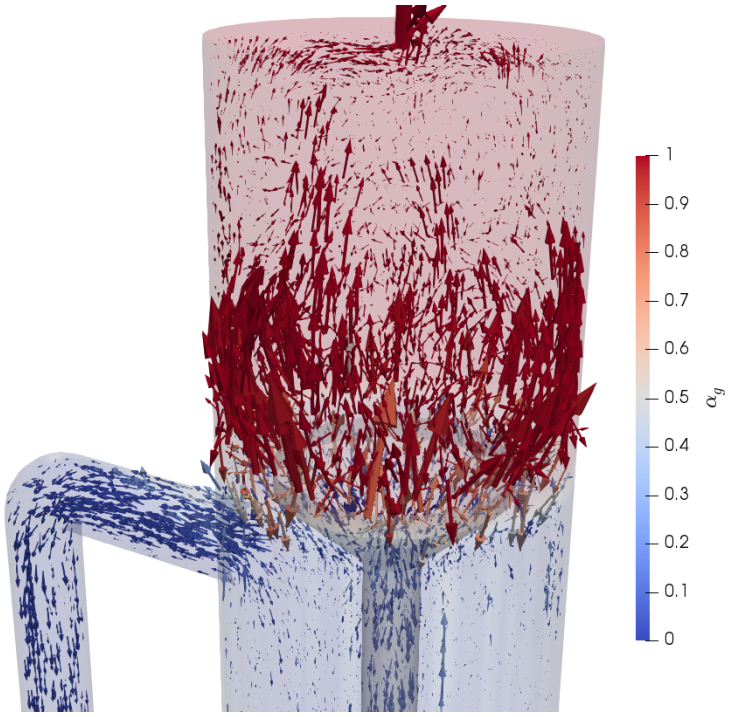

Figure 3.15: Mixture velocity vector field scaled with the local velocity magnitude and colored by the gas phase volume fraction, in the air-water system with simple cup (configuration A), $u_{sl} = 0.019$ m/s, $u_{sg} = 0.03$ m/s, $R_r = 0.33$, $d_b = 2.7$ mm.

of 2.7 mm (case no. II) again the model predicted the gas hold-up in the column accurately. However, as shown in Fig. 3.16, the simulation predicted no gas in the recycle line. Instead, the gas phase was predicted to exit the system from the top and lateral outlets, which was not observed in the experiments. Also, it can be seen that the predicted Q_g^{top} is smaller compared to case I, which confirms that part of gas left from the lateral outlet. In order to assess the effect of average bubble diameter on the predictions of the Euler-Euler model, the air-water system with simulated again using an average bubble diameter of 2 mm (case no. III). It was observed that making the bubble diameter smaller, resulted in over-prediction of the gas hold-up in the column (14% error), while again all the gas left from the top and lateral outlets. These results strengthen the conclusions reached in the previous chapter, namely that the Eulerian model can provide accurate predictions of the gas hold-up in the dispersed flow regime using an experimentally-determined bubble size.

The air-ethanol solution system was also simulated using the Eulerian model with boundary conditions as prescribed in configuration B. Two simulations were carried out in which the average bubble diameter was 1.5 and 1 mm and are referred to as cases no. IV and no. V, respectively. As can be seen from Table 3.2, the gas hold-up is quite sensitive to bubble size. Simulations with average bubble size of 1 mm provide a more accurate prediction of gas hold-up in the column. Again, no gas hold-up was predicted in the recycle line, as all the injected gas left from the top and lateral outlets.

Considering the numerical difficulties and computational complexities associated with controlling the level of the gas/liquid mixture in a system with three outlets (*top*, *lateral*, *bottom*), the following simplification of the system was investigated. Specifically, the computational domain was simplified by sealing the lateral outlet and carrying out simulations using the Eulerian model for the cases listed in Table 3.3. It should be noted that in Table 3.3, configurations A and B refer to the simplified system with the pressure and velocity boundary conditions on the bottom outlet. Since the lateral outlet is ignored in these simulations, the inlet liquid and gas flow rates must be reduced by subtracting the flow rates of liquid and gas leaving from the lateral outlet. In the experimental runs, for Q_l^{inlet} of 20 L/min and the R_r of 0.33, $Q_l^{recycle}$ was set to 6 L/min and consequently $Q_l^{lateral}$ was 14 L/min. Therefore, for the simulation in system without lateral, the inlet flow rate was set to 6 L/min. For the gas phase, since there are three outlets, a mass balance can be written as;

$$Q_g^{inlet} = Q_g^{recycle} + Q_g^{top} + Q_g^{lateral} \tag{3.12}$$

The Q_g^{inlet} and Q_g^{top} were measured experimentally. To calculate $Q_g^{recycle}$, it was assumed that the slip velocity in the recycle line is zero. Therefore, given the experimentally determined value of the gas hold-up in the recycle line, $Q_g^{recycle}$ can be calculated from the

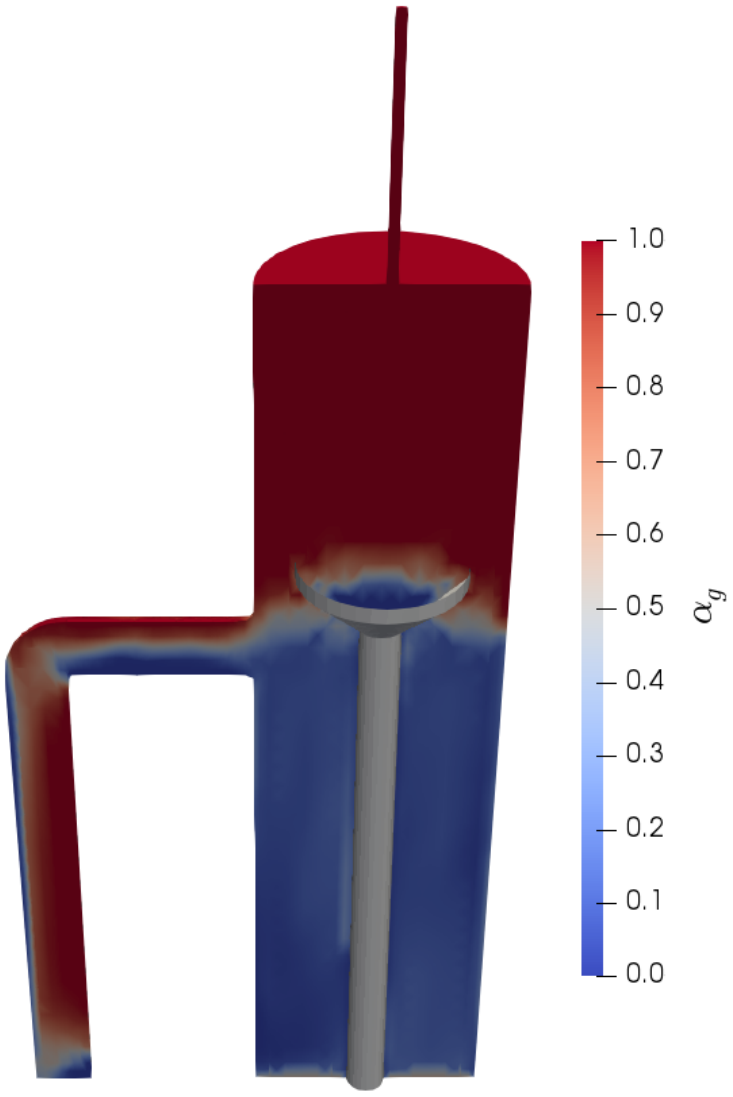

Figure 3.16: Gas volume fraction color map in the air-water system with simple cup (configuration B), $u_{sl} = 0.019$ m/s, $u_{sg} = 0.03$ m/s, $R_r = 0.33$, $d_b = 2.7$ mm.

following equation;

$$\epsilon_g^{recycle} = \frac{Q_g^{recycle}}{Q_l^{recycle} + Q_g^{recycle}} \tag{3.13}$$

As an example, for the air-water system at the operating conditions of interest, $\epsilon_g^{recycle}$ equals 0.061, and using Eq.3.13, $Q_g^{recycle}$ is calculated to be 0.4 L/min. Considering that Q_g^{inlet} and Q_g^{top} are equal to 29.3 and 27 L/min, respectively, $Q_g^{lateral}$ is calculated to be 1.9 L/min. Therefore, for the simulations without lateral outlet the inlet gas flow rate was set to $29.3 - 1.9 = 27.4$ L/min.

The predictions of the Eulerian model for the system with sealed lateral outlet are summarized in Table 3.3. For both air-water and air-ethanol solution systems, the Eulerian model provides accurate predictions of gas hold-up in the column, suggesting that the assumption of no slip in the recycle line was a reasonable one. However, even with a simplified computational domain, the model fails again to predict any gas hold-up in the recycle line. In all the studied cases, all the gas introduced to the system, leaves from the top outlet and Q_g^{top} is Q_g^{inlet}. A typical illustration of the results is provided in Fig. 3.17, which depicts the gas hold-up in the air-ethanol solution system (case no. IX).

Juxtaposition of the Eulerian model's consistent success to predict the average gas hold up in the column to its consistent failure to predict gas hold-up in the recycle line invites two hypotheses. One is related to the appropriateness of the model to accurately represent multiphase flow physics at the length scales of interest. Specifically, the Eulerian model treats phases as inter-penetrating continua, necessitating that discretization of model equations must be such that each cell of the computational domain contain fractions of both continuous and dispersed phases. This implies that the minimum size of a cell (mesh grid) must be larger than a bubble [137]. This requirement is not uniformly met in the simulations described in this chapter, as the mesh in regions close to the recycle cup and inside the recycle line contains cells of size smaller than 1 mm, whereas cell size was at least 3 mm elsewhere. Considering the size of bubbles used in the simulations (1 to 2.7 mm), it is plausible that the failure of the Eulerian model to predict accurately the gas hold up in these parts of the system is the result of discretization that is so coarse that a basic tenet of the model is invalidated. This hypothesis can be tested by carrying out simulations in a scaled-up version of the system, subject to constraints of dynamic and geometric similitude. A second hypothesis is motivated by considerations of significant differences in hydrodynamic conditions near and into the recycle cup, which might result in bubble size reduction. This hypothesis can be tested only by experiment, for example, using optical probes to measure the bubble size inside the recycle line.

Table 3.3: Various cases simulated using the Eulerian model in the system with closed lateral outlet.

Case No.	**System**	d_b (mm)	**B.C.**	$\epsilon_{g,exp.}^{column}$	$\epsilon_{g,sim.}^{column}$	$\epsilon_{g,exp.}^{recycle}$	$\epsilon_{g,sim.}^{recycle}$	$Q_{g,exp.}^{top}$ (L/min)	$Q_{g,sim.}^{top}$ (L/min)
VI	air-water	2.7	config. A	0.085	0.093	0.061	0	27±1	27.4
VII	air-water	2.7	config. B	0.085	0.093	0.061	0	27±1	27.4
VIII	air-water	2	config. B	0.085	0.1	0.061	0	27±1	27.4
IX	air-5wt.% ethanol	1	config. B	0.123	0.126	0.094	0	26±1	26.6

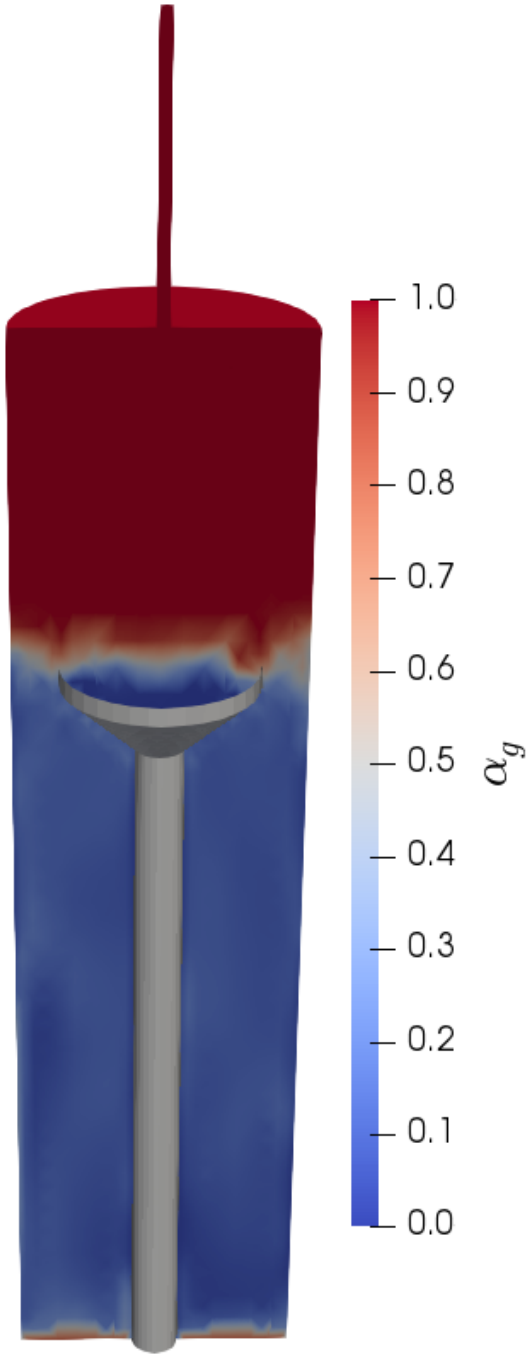

Figure 3.17: Gas volume fraction color map in the air-5wt.% ethanol solution system with simple cup (configuration B), $u_{sl} = 0.019$ m/s, $u_{sg} = 0.03$ m/s, $R_r = 0.33$, $d_b = 1$ mm.

3.6 Conclusion

In this study, experiments were conducted in a pilot scale EBR to investigate the performance of two patented recycle cups (internal gas/liquid separator) over a wide range of operating conditions. Gas hold-up in the recycle line was measured using two pairs of electrical conductivity cells and used to compare the ability of the recycle cups to assist gas/liquid disengagement. It was found that the addition to the simple frustoconical shape recycle cup of two or more vertical conduits (risers) with inlet and outlet at different levels, improved significantly the separation efficiency. Increasing the inlet liquid flow and/or the recycle ratio increased the gas hold-up in the recycle line. Foaming also had a negative impact on the performance of the internal gas/liquid separators. The findings of this study revealed that using a pilot scale system and cost-effective 3-D printing technology, various designs of recycle cup can be created and tested under high gas hold-up conditions. These tests make it possible to screen different designs prior to implementation in the commercial EBRs. Numerical simulation of the pilot scale system using the two-fluid Euler-Euler model resulted in accurate predictions of the overall gas hold-up inside the column. However, the model failed to predict the gas hold-up inside the recycle line. For all the studied cases, all the introduced gas, left from the top and/or lateral outlets. Such results are hypothesized to be the result of small computational cells or mesh grids used in the simulations. Simulations in larger computational domains are required to test the validity of the Eulerian model in predicting the hydrodynamic behavior of such complex systems.

Chapter 4

A Meta-Analysis of Empirical Correlations for Average Gas Hold-up in Three-Phase Fluidized Beds

Amir Mowla, Tanyakarn Treeratanaphitak, Hector M. Budman, Nasser M. Abukhdeir, Marios A. Ioannidis

The contents of this chapter have been published: *Powder Technology, 301:590-595, 2016.*

4.1 Synopsis

Experimental measurements of the average gas hold-up, a key parameter in the design and operation of three-phase (gas-liquid-solid) fluidized beds, are extracted from a multitude of published studies, classified and correlated for the first time. A simple functional, based on power-law dependence of the average gas hold-up on a number of dimensionless variables, successfully correlates gas hold-up during gas flow in fluidized beds of spherical particles with pure water as the liquid phase. Best-fit parameters of such a functional result in prediction of more than 75% of the data with absolute relative error less than 20%, but are shown to depend on the morphology of three-phase flow and may be difficult to generalize.

4.2 Introduction

Three-phase fluidized beds are frequently employed for catalytic reactions in chemical processes such as the upgrading of heavy oils [163, 145], Fischer-Tropsch synthesis [180, 102] and wastewater treatment [160, 191]. A key parameter in the analysis of three-phase (gas-liquid-solid) fluidized beds is the fraction of bed volume occupied by gas, otherwise known as the gas hold-up. Knowledge of the gas hold-up enables the estimation of gas-phase residence time and pressure drop within a fluidized bed. In combination with knowledge of the average bubble diameter, it underpins the estimation of gas-liquid interfacial area associated with inter-phase mass and heat transfer [179]. Design, optimization, and control of three-phase fluidized beds, especially under transport-limited conditions, is thus critically dependent on knowledge of gas-hold up as a function of bed characteristics and operating conditions [53]. Last but not least, validation of CFD models of hydrodynamics in fluidized bed reactors also requires gas hold-up data [144].

The fractional volumetric content (hold-up), as well as the morphology (bubble shape and size distribution), of the gas phase in a three-phase fluidized bed is the outcome of momentum exchange between the gas, liquid and solid phases in motion. Qualitative descriptions of the flow regimes commonly encountered (e.g., dispersed, coalesced or slug flow) have been provided on the basis of visual observations [141, 198, 55] or indirect measurements [190], but the complexity of the hydrodynamic conditions has so far precluded *ab initio* prediction of the gas hold up. Instead, the design of gas-solid-liquid fluidized bed reactors has generally relied on empirical methods [53, 203] grounded on correlations which are informed by dimensional analysis and dynamic similitude [44]. Such correlations are typically derived from experimental data of average gas hold-up obtained under non-reactive cold-flow conditions from measurements of the axial pressure distribution in long columns [44, 161, 176, 151].

Numerous experimental studies have focused on the discovery of empirical correlations between the average gas hold-up, measurable operating parameters and bed characteristics. A comprehensive list of earlier contributions may be found in the reviews of Shah et al. [188] and Fan [53]. More recent work in this area [176, 161, 86, 88, 89, 87, 195, 152] has focused on correlations of gas hold-up as a function of either individual parameters (superficial gas/liquid velocities, liquid properties, particle diameter, column diameter, *etc.*) or combinations of them in the form of dimensionless groups. Table 4.1 summarizes the operating parameters which have been commonly used to correlate the average gas hold-up in three-phase fluidized beds. Notable in Table 4.1 is the absence of any direct measure of bubble size or gas density.

For slurry bubble columns, which by comparison to three-phase fluidized beds are

Table 4.1: Variables commonly used to correlate gas hold-up in three-phase fluidized beds.

Variable	**Symbol**	**Unit**
Liquid velocity	u_{sl}	$\mathrm{m\,s^{-1}}$
Gas velocity	u_{sg}	$\mathrm{m\,s^{-1}}$
Liquid viscosity	μ_l	$\mathrm{Pa\,s}$
Liquid surface tension	$\sigma_{g,l}$	$\mathrm{N/m}$
Liquid density	ρ_l	$\mathrm{kg/m^3}$
Particle diameter	d_p	m
Particle density	ρ_p	$\mathrm{kg/m^3}$
Column diameter	D_c	m
Gas phase buoyancy	$g(\rho_l - \rho_g)$	$\mathrm{kg/(m^2 s^2)}$

characterized by much smaller solid particle sizes (< 0.1 mm) and low solid volume fractions (< 0.1), a compilation and meta-analysis of experimental gas hold-up data from a multitude of literature sources has been provided by Behkish et al. [14]. To our knowledge, a similar effort for gas hold-up in three-phase fluidized bed systems has been undertaken only by Larachi et al. [109]. These authors used an artificial neural network (ANN) approach in an attempt to develop a unified correlation for gas hold-up in three-phase fluidized bed systems.

In this communication we gather and correlate experimental data of average gas hold-up in fluidized beds published in the past 40 years. Hypothesizing that the prevailing flow regime imparts a non-random component to the variability of gas hold-up data, we first classify the experimental observations as suggested by Muroyama and Fan [141]. Although the idea of different correlations for different flow regimes is not new (see also Krishna et al. [103] and Song et al. [198]), determining the transition point and conditions remains a challenge.

We find that the correlations describing gas hold-up in the dispersed and coalesced flow regimes are different. Improved correlations are obtained by considering gas hold-up in systems characterized by small values of the particle Reynolds number ($Re_p \leq 200$) separately from systems characterized by $Re_p > 200$. For both kinds of systems, more than 75% of the experimental observations are predicted by the correlations with absolute relative error less than 20%. Consideration of the average bubble size is shown to improve these correlations only marginally, whereas directly accounting for the density of the gas phase is necessary in order to describe gas hold-up in fluidized beds operating at high pressure. These findings have significant implications for the analysis and design of gas-solid-liquid fluidized beds.

4.3 Methods

From 1399 experimental measurements of gas hold-up in three-phase fluidized beds [136, 198, 138, 161, 176, 41, 164, 89, 87, 88, 195, 86, 151], we select a subset of 342 measurements made in systems involving only spherical particles and pure water as the liquid phase [136, 138, 161, 41, 164, 89, 87, 86, 151]. This choice is motivated by a key hypothesis in this work, namely that the average gas hold-up exhibits a complex dependence on the distribution and morphology of the gas phase (*i.e.* on the flow regime) which cannot be reduced to a simple functional of a small number of variables (see Table 4.1). In a seminal contribution, Muroyama and Fan [141] have described three main regimes of multiphase flow (dispersed, coalesced and slug flow) in gas-liquid-solid fluidized beds. On the basis of visual observations made on systems involving spherical particles and pure water as the liquid phase, these authors have provided a map that could be used to classify the aforementioned 342 measurements (see Fig. 4.1). Using this map, 280 gas hold-up measurements reported in seven different studies [136, 41, 164, 89, 87, 86, 151] are classified as corresponding to the dispersed flow regime. These data, notably include 63 measurements of gas hold-up in fluidized beds operated at pressures higher than atmospheric (up to 6.5 MPa). By comparison to the other regimes, the dispersed flow regime is characterized by limited bubble coalescence, smaller bubble size and more uniform bubble size distribution [53]. Mass transfer in three-phase fluidized beds has been predominately investigated in this regime [53]. In addition to the variables summarized in Table 4.1, the gas density (ρ_g) and the mean bubble diameter (d_b) are also considered.

Accounting for the gas density [175, 86] in the form ($\rho_l - \rho_g$) may be sufficient if the intent is to correlate gas hold-up in atmospheric systems, but may otherwise mask the effect of pressure. Inclusion of gas density as an independent parameter has been recommended for correlating gas hold-up observations made in fluidized beds operated at different pressures [121, 175]. Additionally, the size of bubbles has been linked to gas hold-up, bed expansion and bed mixing in fluidized beds [113, 198], but the standard approach has been to assume that it is dependent on operating parameters and thus implicitly accounted for in gas hold-up correlations [175]. In any case, measurement of the size of bubbles within a fluidized bed is not a straightforward task. Using a conductivity probe [176], for example, one may determine a chord-length distribution, as bubbles of different sizes are intersected by the probe at different locations. Assuming the bubbles are spherical, the underlying bubble size distribution may be then recovered using methods of quantitative stereology [211]. Since the gas hold-up data analyzed here are not accompanied by measurements of bubble chord length, consideration of bubble size must rely on an alternative approach, as explained below.

On the basis of experimental measurements, the radial distribution of time-smoothed bubble chord length within a three-phase fluidized bed has been expressed as follows [226],

$$\frac{l_{vc} - l_v(r)}{l_{vc}} = \frac{l_{vc} - l_{vw}}{l_{vc}} \left(\frac{r}{R}\right)^m, \tag{4.1}$$

where $l_v(r)$ is the time-smoothed chord length at radial position r, l_{vc} and l_{vw} are the time-smoothed bubble chord lengths at the center ($r = 0$) and wall ($r = R$) of the fluidized bed, respectively, and m is an empirical parameter. The values of l_{vc}, l_{vw} and m have been correlated to particle size and fluid velocities as follows (where all quantities are in SI units and m is unitless) [226],

$$l_{vc} = 2.667 \times 10^{-3} d_p^{-0.3} u_{sl}^{-0.072} u_{sg}^{0.221} \tag{4.2}$$

$$l_{vw} = 4.295 \times 10^{-3} d_p^{-0.129} u_{sl}^{-0.060} u_{sg}^{0.124} \tag{4.3}$$

$$m = 3.77 d_p^{0.121} \tag{4.4}$$

Given u_{sl}, u_{sg} and d_p, we estimated l_{vc}, l_{vw} and m from the above equations and subsequently obtained the average bubble chord length from Eq. (4.1) as follows,

$$\langle l_v \rangle = \frac{m}{m+2} l_{vc} + \frac{2}{m+2} l_{vw} \tag{4.5}$$

Finally, assuming that local chord-length measurements follow a Rayleigh probability distribution [100, 116, 118],

$$P(l_v, \sigma_r) = (l_v/\sigma_r) e^{-l_v^2/2\sigma_r^2} \tag{4.6}$$

with scale parameter σ_r given by,

$$\sigma_r = \langle l_v \rangle \sqrt{2/\pi} \tag{4.7}$$

we reconstructed the underlying bubble diameter distribution using Spektors' transformation method [211], obtaining in this manner an estimate of the mean bubble diameter for each measurement of gas hold-up analyzed.

Expanding the set of independent variables (see Table 4.1) to eleven by including the gas density and average bubble diameter and applying the Buckingham Pi theorem [218] we obtain the eight dimensionless groups shown in Table 4.2. Gas hold-up data are assumed to fit a correlation of the form,

$$\epsilon_{gas} = c_0 d_r^{c_1} \beta_g^{c_2} \beta_p^{c_3} u_r^{c_4} Re_l^{c_5} We_l^{c_6} Fr_l^{c_7} \gamma_b^{c_8} \tag{4.8}$$

Table 4.2: Dimensionless groups used in this study.

Name	Symbol	Expression
Liquid-phase Reynolds number	Re_l	$(\rho_l D_c u_{sl})/\mu_l$
Liquid-phase Weber number	We_l	$(\rho_l D_c u_{sl}^2)/\sigma_l$
Liquid-phase Froude number	Fr_l	$(u_{sl}^2 \rho_l)/(g\Delta\rho D_c)$
Gas-liquid density ratio	β_g	ρ_g/ρ_l
Solid-liquid density ratio	β_p	ρ_p/ρ_l
Scaled particle diameter	d_r	d_p/D_c
Scaled bubble diameter	γ_b	d_b/D_c
Gas-liquid velocity ratio	u_r	u_{sg}/u_{sl}

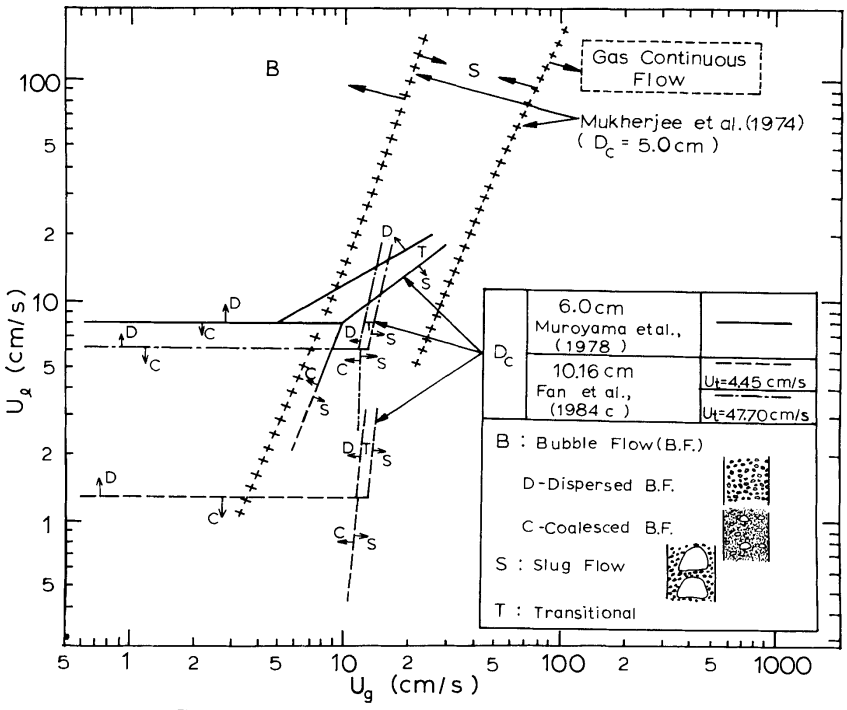

Figure 4.1: Flow regime diagram for co-current three-phase fluidized beds proposed by Muroyama and Fan [141]. Reprinted with permission from . Copyright (1985) John Wiley & Sons, Inc.

where c_i are constants to be determined from a solution to a multiple linear regression model using the least squares method [139]. Functional forms of this kind have been previously fitted to limited experimental data [176, 161, 86, 88, 89, 87, 195].

In order to compare the models found for a specific set of data, Akaike's information criterion (AIC) [30, 117] was calculated for each model,

$$AIC = n\ log(\sigma_\epsilon^2) + 2K \tag{4.9}$$

where n is the sample size, K is the number of estimated parameters included in the model and σ_ϵ^2 is given by,

$$\sigma_\epsilon^2 = \frac{SSR}{n}$$

where SSR is the sum of squared differences between observations and model predictions. For relatively small sample sizes (*i.e.* $n/K < 40$) a corrected form of AIC is used,

$$AIC_c = AIC + \frac{2K(K+1)}{n-K-1} \tag{4.10}$$

The best model is the one with the lowest AIC (or AIC_c). The AIC penalizes for the addition of parameters, and selects a model that fits well but has the minimum number of parameters. Two measures associated with the AIC are used to compare models. One is the delta AIC of the model (Δ_i), which is a measure of each model relative to the best model [30], and is calculated as:

$$\Delta_i = AIC_i - AIC_{min} \tag{4.11}$$

where AIC_i is the value for the model i and AIC_{min} is the value for best model. The other is the Akaike weight (ω_i), which provides another measure of the strength of evidence for each model and represents the ratio of Δ_i values for each model relative to the complete set of r candidate models:

$$\omega_i = \frac{\exp(-\Delta_i/2)}{\sum_{i=1}^{r}(-\Delta_i/2)} \tag{4.12}$$

4.4 Results and Discussion

Here, the performance of different correlations is compared in terms of the coefficient of correlation (R^2), average absolute relative error (AARE), Δ_i and ω_i. The results are summarized in Table 4.3-4.4 and discussed below.

In the first step, all the 342 data points from various flow regimes are fitted to Eq. (4.8), with (Eq. (4.13)) and without (Eq. (4.14)) the parameter accounting for bubble size (γ_b). In either case (Eqs. (4.13),(4.14)), the R^2 and AARE are 0.79 and 21%, respectively. About 35% of the experiential data points, however, are predicted with absolute relative error of greater than 20%.

As can be seen in Table 4.3, inclusion of the parameter accounting for the bubble size seems unnecessary. This supports the original suggestion by Safoniuk et al. [175], that the dependence of gas hold-up on bubble size is captured by other operating parameters such as gas superficial velocity, particle diameter, *etc.*

Next, the gas hold-up data were classified based on the flow map (Fig. 4.1) into dispersed and non-dispersed subsets. Two correlations were developed for each subset: dispersed/coalesced flow (Eq. (4.15))/(Eq. (4.16)) without γ_b and for dispersed/coalesced flow (Eq. (4.17))/(4.18)) including γ_b. Each of these two sets of correlations corresponds to an individual model and thus may be compared in the context of Akaike's information criterion. Some improvement in the values of R^2 and AARE compared to the single correlations mentioned above is evident for systems in the dispersed flow regime.

Past studies focused on three-phase flow regime classification [146, 42, 55] have pointed to a significant effect of particle size on flow morphology. Ostergaard [146] performed flow regime studies using glass particles with diameters 1 mm and 6 mm and found that relatively small particles ($\leq$ 1 mm) were associated with large coalesced bubbles, whereas larger particles ($>$ 2.5 mm) were associated with small uniform bubbles. Darton [42] reported intense bubble coalescence in systems with glass bead particles $<$ 2.5 mm. It was observed in three-phase fluidized beds of small particles that large bubbles moved as a homogeneous fluid of high viscosity, while small bubbles within beds of large particles moved through the bed as in a pure liquid containing obstacles (the solid particles) around which they traveled. Lastly, Zhang et al. [229] observed a significant decrease in the region of the coalesced flow regime in beds with 4.5 mm glass beads particle compared to beds with 1.5 mm particles.

On the basis of these considerations, and in line with our initial hypothesis that the complex dependence of gas hold-up on three-phase flow morphology may be difficult to reduce to a simple functional (*viz.*, Eq. (4.8)), we also split the 342 gas hold-up data in

two groups depending on particle size ($d_p > 2.5$ mm and $d_p \leq 2.5$ mm). Eqs. (4.19) and (4.20), which do not contain γ_b, and Eqs. (4.21) and (4.22), which contain γ_b, make up the two models to predict the gas hold-up for this classification. The obtained R^2 and AARE values for these models (see Table 4.3) demonstrate considerable improvement compared to those based on flow regime classification using the flow map of Muroyama and Fan [141]. The magnitude of Δ_i is also reduced significantly.

Finally, the data points were split based on particle Reynolds number ($Re_p = \frac{\rho_l u_{sl} d_p}{\mu_l}$), using $Re_p = 200$ as the cutoff value, which also corresponds to a transition in the drag coefficient C_d for single free-falling spherical particles in a fluid [75]. This results in a group with 156 data points for the systems with $Re_p \leq 200$ and 186 data points for $Re_p > 200$. Two models, one without γ_b (Eqs. (4.23) and (4.24)) and one containing all the dimensionless groups (Eqs. (4.25) and (4.26)) were developed and are shown in Table (4.4). As can be seen from the table, these models demonstrate the highest R^2 values (up to 88%) and lowest AARE values (about 15%) among all the developed models. They also result in the lowest Δ_i values, with the one without γ_b identified by Akaike's analysis as the best model.

Parity plots comparing the experimentally measured gas hold-up to the predictions of Eqs. (4.23) and (4.24) are shown in Figs. 4.2a–4.2b. Satisfactory agreement across the range of gas hold-up measurements is observed - a significant improvement compared to previously published correlations.

It is worth noting that the experimental data include gas hold-up measurements from systems operated at pressures higher than atmospheric and up to 6.5 MPa. The increased accuracy of the presented generalized correlation is in part due to the inclusion of gas density in the correlation (via the parameter associated with β_g). Gas hold-up in high pressure systems is predicted by Eq. (4.23) or Eq. (4.24) with AARE of 15%. On the contrary, the correlations lacking the β_g term, predict gas hold-up in high pressure systems with AARE of 19%.

Application of Eqs. (4.23) and (4.24) to predict the gas hold-up in three-phase systems involving non-spherical particles or a liquid other than pure water (1057 measurements) resulted in AARE of more than 55%, a result indicative of the limitations of the simple functional, Eq. (4.8), to describe gas hold-up across the full spectrum of bed characteristics and operating conditions. Indeed, even the sophisticated ANN approach used by Larachi et al. [109] does not provide predictions of much better accuracy. This is demonstrated in Figure 4.3, which compares predictions of gas hold-up in experimental systems involving pure water, gas and spherical particles and not available to Larachi et al. [109] at the time of publication of their work, to predictions obtained using Eqs. (4.23) and (4.24) of this study. The obtained AARE was 16.5% for the correlations developed in this study and

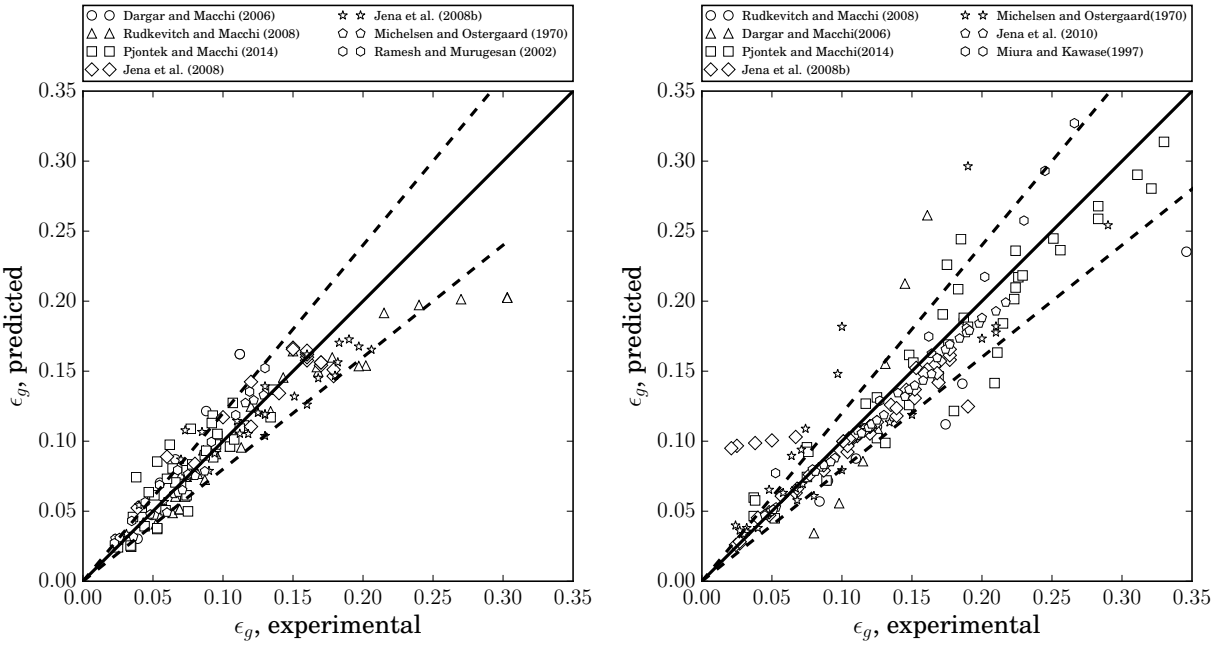

(a) (b)

Figure 4.2: Plots of the literature gas hold-up data (experimental) versus calculated gas hold-up (correlation) for (a) small particle Reynolds number systems (Eq. (4.23)) and (b) large particle Reynolds number systems (Eq. (4.24)). Dashed lines indicate error of $\pm 20\%$.

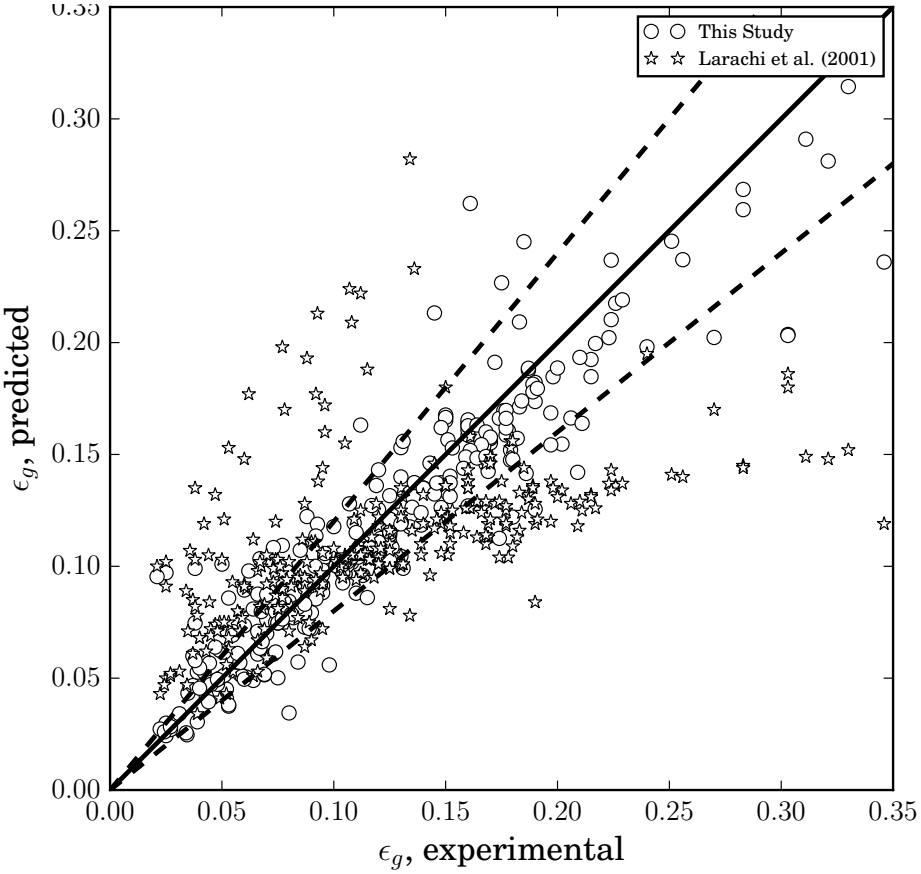

Figure 4.3: Comparison of gas hold-up predictions by Eqs. (4.23) and (4.24) against predictions from the ANN tool developed by Larachi et al. [109]. Dashed lines indicate error of ±20%.

48.5% for the one developed by Larachi et al. [109]. These comparisons suggest a gap in fundamental understanding of the three-way hydrodynamic interactions between bubbles, solid particles and a continuous liquid phase.

4.5 Conclusion

A meta-analysis was performed on experimental data of average gas hold-up in gas-solid-liquid fluidized beds published in numerous studies over the past 40 years. The analysis succeeded in developing statistically significant and acceptably accurate correlations for

the prediction of average gas hold-up in systems involving spherical particles and pure water as the liquid phase. Consideration of average bubble size was found to improve these correlations only marginally. Consideration of the gas density as an independent variable was found to improve significantly the prediction of gas hold up in high pressure systems. At the same time, the analysis illustrated the limitations of a simple functional to approximate the outcome of complex momentum transfer in a three-phase fluidized bed.

Acknowledgements

This research was supported by the Natural Sciences and Engineering Research Council (NSERC) of Canada.

Table 4.3: List of the developed correlations and the comparison measurements

Correlation		R^2	AARE (%)	Δ_i	ω_i
$\epsilon_{gas} = 2771.042\ d_r^{0.415}\beta_g^{0.046}\beta_p^{-1.209}u_r^{0.716}Re_l^{-1.383}We_l^{1.488}Fr_l^{-0.436}$	(4.13)	0.79	21%	39.475	≈ 0
$\epsilon_{gas} = 3040.208\ d_r^{0.40}\beta_g^{0.044}\beta_p^{-1.20}u_r^{0.728}Re_l^{-1.388}We_l^{1.454}Fr_l^{-0.396}\gamma_b^{-0.062}$	(4.14)	0.79	21%	41.535	≈ 0
$\epsilon_{gas} = 4096.153\ d_r^{0.451}\beta_g^{0.027}\beta_p^{-0.936}u_r^{0.696}Re_l^{-1.416}We_l^{1.464}Fr_l^{-0.392}$	(4.15)	0.83	19%	36.145	≈ 0
$\epsilon_{gas} = 67509.128\ d_r^{0.279}\beta_g^{0.096}\beta_p^{-0.963}u_r^{0.849}Re_l^{-1.697}We_l^{1.485}Fr_l^{-0.263}$	(4.16)	0.78	26%		
$\epsilon_{gas} = 4855.582\ d_r^{0.422}\beta_g^{0.023}\beta_p^{-0.877}u_r^{0.722}Re_l^{-1.421}We_l^{1.386}Fr_l^{-0.303}\gamma_b^{-0.23}$	(4.17)	0.83	18%	38.315	≈ 0
$\epsilon_{gas} = 69046.37\ d_r^{0.276}\beta_g^{0.096}\beta_p^{-0.971}u_r^{0.852}Re_l^{-1.698}We_l^{1.476}Fr_l^{-0.253}\gamma_b^{-0.017}$	(4.18)	0.78	25%		
$\epsilon_{gas} = (10^{-4.88})\ d_r^{1.788}\beta_g^{0.037}\beta_p^{0.536}u_r^{0.635}Re_l^{0.487}We_l^{1.659}Fr_l^{-1.569}$	(4.19)	0.86	16%	28.885	≈ 0
$\epsilon_{gas} = 0.151\ d_r^{0.190}\beta_g^{0.076}\beta_p^{0.764}u_r^{0.774}We_l^{0.285}Fr_l^{0.05}$	(4.20)	0.82	19%		
$\epsilon_{gas} = (10^{-4.72})\ d_r^{1.803}\beta_g^{0.039}\beta_p^{0.546}u_r^{0.627}Re_l^{0.410}We_l^{1.749}Fr_l^{-1.623}\gamma_b^{0.033}$	(4.21)	0.86	16%	23.575	≈ 0
$\epsilon_{gas} = 37414.75\ d_r^{-2.25}\beta_g^{-0.067}\beta_p^{0.136}u_r^{2.79}We_l^{-6.272}Fr_l^{7.237}\gamma_b^{-11.393}$	(4.22)	0.82	18%		

Table 4.4: Correlations and comparison measurements for data points classified using Re_p.

Correlation		R^2	AARE (%)	Δ_i	ω_i
$\epsilon_{gas} = 17.153\ d_r^{0.722}\beta_g^{0.072}\beta_p^{-2.108}u_r^{0.679}Re_l^{-1.207}We_l^{2.202}Fr_l^{-1.237}$	(4.23)	0.88	15%	0	0.586
$\epsilon_{gas} = 433.253\ d_r^{0.158}\beta_g^{0.061}\beta_p^{0.833}u_r^{0.738}Re_l^{-1.106}We_l^{0.914}Fr_l^{-0.06}$	(4.24)	0.83	18%		
$\epsilon_{gas} = 17.199\ d_r^{0.735}\beta_g^{0.073}\beta_p^{-2.112}u_r^{0.673}Re_l^{-1.219}We_l^{2.237}Fr_l^{-1.267}\gamma_b^{0.024}$	(4.25)	0.88	15%	0.6948	0.414
$\epsilon_{gas} = 52.843\ d_r^{-2.316}\beta_g^{-0.079}\beta_p^{2.383}u_r^{2.697}Re_l^{0.869}We_l^{-6.984}Fr_l^{7.464}\gamma_b^{-11.049}$	(4.26)	0.82	18%		

Chapter 5

Effect of Particle Wettability on the Hydrodynamics of Three-Phase Fluidized Beds Subject to Foaming

Amir Mowla, Marios A. Ioannidis

The contents of this chapter are being submitted for publication in *Powder Technology*.

5.1 Synopsis

We studied the effect of particle wettability on the hydrodynamics of gas-liquid-solid fluidized beds in a cold-flow pilot scale setup. Overall phase hold-up data in the bed region and in the freeboard (solid-free) region was measured and compared for the systems operating with hydrophobic and hydrophilic glass beads. Experiments were conducted in air-water as well as air-5wt.% ethanol aqueous solution systems. It was observed that rendering the particles hydrophobic resulted in more than 20% decrease in the overall gas hold-up in the bed region. Attachment of bubbles to particles and formation of bubble-particle agglomerates with lower apparent density compared to the bare particles is found as the main reason of such gas hold-up reduction. Due to the lower density of these agglomerates, they have lower tendency toward bubble break-up, in turn, larger bubble size distribution is expected in the bed of hydrophobic particles. The extension of such larger bubbles into the freeboard region, was also found to reduce the foam thickness above the freeboard region in the air-ethanol solution system. According to the semi-empirical models on dynamics of foam formation, foam thickness is inversely proportional to the bubble

size. The models predicted that the bubble size in the freeboard region of the system with hydrophobic particles is about 15% greater than the system of hydrophilic particles.

5.2 Introduction

Three-phase fluidized beds are frequently employed for catalytic reactions in chemical processes such as upgrading of heavy oils [163], Fischer-Tropsch synthesis [102, 180], wastewater treatment [191], coal liquefaction [101] and methanol production [205]. They are well-known for promoting contact among the gas, liquid and solid phases, thus facilitating heat and mass transfer. Various aspects of three-phase fluidized beds have been studied extensively and described in several books and reviews [146, 51, 141, 53]. In gas-liquid-solid fluidized beds, bubble dynamics affect the hydrodynamics as well as the rate of reactions significantly. A bubble size distribution is understood to emerge from the interactions between bubbles and particles [224]. In this context, not only the bulk but also the surface properties of the solid particles and bubbles play a role in determining the behavior of these systems [23, 210]. To date, studies investigating the hydrodynamics of three-phase fluidized beds have involved particles that are strongly wetted by the liquid phase [124, 41, 151, 87, 88, 195] with very few exceptions.

Bhatia et al. [23] compared the hydrodynamics of 1 mm wettable and non-wettable (coated with Teflon) glass beads in an air-water system. They reported that when gas is introduced in the bed of the Teflon-coated particles, the bed expanded, whereas an initial bed contraction was observed for the case of wettable particles. Armstrong et al. [11] studied a bed of 6 mm Teflon-coated glass beads in an air-water system. They reported smaller values of the gas hold-up in the three-phase system comprising hydrophobic particles as compared to hydrophilic ones. Adhesion of bubbles to hydrophobic particles was also observed and it was suggested that the concomitant decrease in the apparent density of the particles was the cause of increased bed expansion and reduced gas hold-up. Armstrong et al. [11] invoked work of adhesion arguments to explain the attachment of gas bubbles to hydrophobic particles. The work of adhesion (W) is the energy required to separate a liquid from a solid and is given as follows [183],

$$W = \sigma_{g,l}(1 + \cos\theta) \tag{5.1}$$

where $\sigma_{g,l}$ is the gas-liquid surface tension and θ is the contact angle, defined as the angle between the solid surface and the gas-liquid interface measured through the liquid phase. According to Eq.5.1, as the particles become more hydrophobic (*i.e.* θ increases), the work of adhesion decreases thereby facilitating bubble attachment. Formation of bubble-particle

aggregates has also been observed by Tsutsumi et al. [209, 210] who studied the effect of particle wettability on the rise velocity and wake characteristics of single bubbles rising in a liquid-solid fluidized bed. They reported that for bubbles smaller than 1.5 cm, the bubble rise velocity is lower in the case of hydrophobic particles ($\theta = 93^{\circ}$) due to the attachment of particles to bubbles and the resulting increase in drag. For larger bubbles, however, the rise velocity was found independent of the particle wettability, as for such fast rising bubbles the fluid shear effects prevented particle attachment. The observations of Tsutsumi et al. [210] are conditioned by particle size, which in their study was less than 1 mm (400 and 700 µm). As will be discussed next, such small particles cannot penetrate or break-up bubbles upon collision and, if they are hydrophobic, they remain attached to bubbles. This may be seen by comparing the force required to separate a hydrophobic particle from the gas/liquid interface [9] to the net force due to gravity and buoyancy of the particle. Assuming, for example, a 700 µm spherical glass particle attached at the air-water interface with $\theta = 93^{\circ}$, the magnitude of these forces is estimated as follows;

$$F_{detachment} = \pi \ d_p \ \sigma_{g,l} \ cos^2(\frac{\theta}{2}) = 7.5 \times 10^{-5} N, \tag{5.2a}$$

$$F_{gravitational} - F_{buoyant} = \frac{\pi}{6} d_p^3 \rho_p g - \frac{\pi}{6} d_p^3 \rho_l g = 3.52 \times 10^{-6} N \tag{5.2b}$$

Chen and Fan [37] have developed a mechanistic model for the collision between a single spherical-cap bubble (with radius of curvature R) and a single particle (with diameter d_p) in a liquid medium. The model was initially developed for the case where the particle is wetted completely by the liquid ($\theta = 0^{\circ}$). This implies that the particle is not in direct contact with the gas bubble and a liquid film is always present between the dispersed phases. Fig. 5.1 illustrates particle penetration into a bubble at a depth h. In their model, Chen and Fan [37] consider the following forces acting on the particle at depth h:

$$F = m_p a = \frac{\pi}{6} d_p^3 \rho_l g - \frac{\pi}{6} d_p^3 \rho_p g + \sigma_{g,l} \pi d_p + (\frac{2\sigma_{g,l}}{R} - \rho_l g h) \frac{\pi}{4} d_p^2, \tag{5.3}$$

where the first two terms on the right-hand side of Eq.5.3 are the buoyant and gravitational forces, respectively. The third term is the surface tension force and the forth term is a pressure term which consists of the capillary pressure given by the Young-Laplace equation and the liquid head due to penetration at depth h. The particle is thus subjected to a net force, F, which results in particle acceleration a.

When the particle collides with the bubble, the particle either bounces off the gas-liquid interface or it penetrates it, which may or may not lead to bubble breakage. According

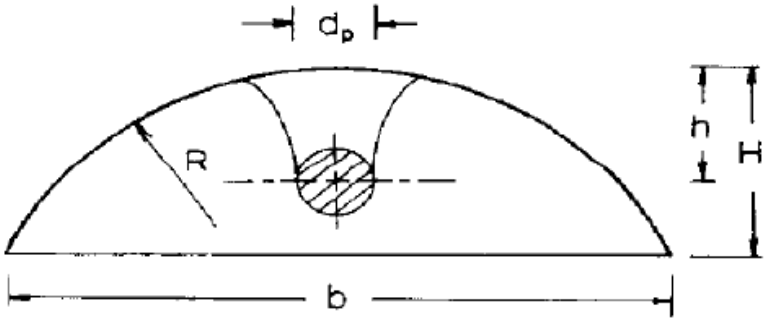

Figure 5.1: Diagram of a particle colliding with a spherical-cap bubble [37]

to the model, the particle penetrates the bubble if any of the following criteria is satisfied [37]:

1- the particle acceleration is downward

2- the relative velocity of the particle to the bubble is downward

3- the particle penetration depth is larger than the deformed bubble height ($h > H$)

If the particle penetrates the bubble, the bubble is considered to assume a donut shape with height, H_d (see Fig. 5.2). According to the model of Chen and Fan, if the particle diameter is larger than H_d, the bubble breaks up, otherwise it reforms to its original shape. The model was tested against observations of the bubble behavior when colliding with particles of varying diameter (2 to 11 mm) and density, and was found to provide fair predictions. It was concluded that in single bubble-single particle collision, penetration is a necessary, but not sufficient condition for bubble break-up. Importantly, the model of Chen and Fan predicts that lowering the surface tension favors the penetration of the bubble by the colliding particle. If the condition for bubble break-up is also met, lowering of surface tension should be expected to increase the bubble break-up rate. This prediction was not tested, as Chen and Fan [37] performed experiments using distilled water and air only. It should be noted that bubble break-up is independent of surface tension in the model of Chen and Fan.

The model described above was extended for application to non-wettable particles [36]. In this case, it was assumed that half of the particle's surface is not wetted by the liquid

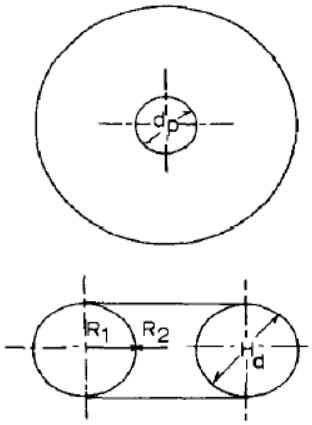

Figure 5.2: Diagram of a donut-shape bubble [37]

$\theta = 90°$). Consequently, the buoyant force acting on the particle is smaller, the contact time between the bubble and particle is longer and the interaction is stronger. The more hydrophobic the particle, the smaller the buoyant force and the easier it is for the particle to penetrate the bubble, as also expected from considerations of the work of adhesion and verified experimentally [36]. If the condition for bubble break-up is also met, and since this condition is independent of wettability, one expects hydrophobic particles to increase the bubble break-up rate, leading to higher gas hold-up. The fact that this expectation is not experimentally verified [11] suggests that bubble break-up in fluidized beds of hydrophobic particles is not determined by bare particle-bubble collisions, but rather by the collisions between bubbles and particle-bubble agglomerates.

The above mentioned investigations of the effect of particle wettability on the hydrodynamics of gas-liquid fluidized beds have been limited to the system of water and air. Industrial three-phase fluidized bed systems generally contain multicomponent liquids with different physical properties. The range of gas hold-up is also higher. Very few studies are found in literature which examine the effect of particle wettability under conditions similar to industrial fluidized bed reactors, specifically ebullated bed reactors (EBR), which are fluidized bed systems used in hydrocracking (upgrading) of heavy oil and bitumen.

The hydrogen gas and liquid (diluted bitumen) feeds enter the EBR through a plenum chamber below the distributor grid, mix with a recycled liquid stream and flow upward through an expanded bed of catalysts [134]. The EBR consists of a three-phase section (reaction region) and a catalyst-free section (freeboard region). An internal recycle line in the freeboard region directs a fraction of the liquid to a recycle pump below the distributor grid. At the top of the reactor, a gas/liquid separator (recycle cup) connected to the

recycle line serves to disengage gas from the recycle liquid stream [134]. Industrial scale EBRs reportedly operate with gas hold-up values in excess of 25% in the three-phase section [198, 134]. Higher gas hold-up values have also been observed in the freeboard region (Fig. 5.3). Such high volumes of hydrogen and vapor products in the reaction zone are undesirable because they decrease the bitumen conversion significantly. Entrainment of gas in the recycled liquid stream has been associated with high values of gas hold-up. Excessive gas entrainment in the recycle line leads to instability in the operation of industrial hydroprocessors, caused by large liquid flow fluctuations through the pump. Excessive gas entrainment is aggravated by foaming in the freeboard region of the EBRs [201]. Given the low surface tension of the liquid phase and the likely presence of surface-active substances (such as naphthenic acid), foaming is inherent to hydroprocessing reactors [201, 72].

Considering the detrimental effects of foaming on EBR operability, only a few studies have examined methods to suppress the foam layer under conditions of high gas hold-up. The use of foam control chemicals is not practical, since these agents are cracked under the severe operating conditions prevailing in hydrocracking units, resulting in contamination of the gas and liquid phases [41]. Guitian and Joseph [72] were able to reproduce the high gas hold-up condition in the freeboard region of a CANMET commercial system (see Fig. 5.3, data of Pruden [157]) in a cold-slit bubble column reactor by adding sodium dodecyl sulfate (SDS) and pentanol to water. Beyond a critical gas superficial velocity, they observed a foam/bubbly mixture interface at the top of the reactor, with foam above and a bubbly mixture below the interface. It was noticed that the foam height in the bubble column was reduced significantly when they fluidized fine hydrophobic particles (plastic spheres of diameter equal to 532 µm) in the bubbly mixture below the foam. The same reactor was also used to compare the effect of fluidizing hydrophobic and hydrophilic particles of fine sand (diameter ranging from 300 to 800 µm) on foaming [128]. Both kinds of particles, but more so hydrophobic ones, were found to reduce foaming. It is important to note that the hydrodynamics of EBRs are very different from the systems used in these studies. In EBRs, the catalyst particles are confined in the three-phase zone below the freeboard region and are *not* in contact with the foam layer above the freeboard region. The effect of particle hydrophobicity on gas hold-up in the three-phase section and its relation to foam formation in the freeboard region has not been adequately studied.

In this study we investigate the effect of particle wettability on the fluid dynamics of three-phase fluidized beds operating with distilled water as well as 5wt.% aqueous ethanol solution. Ethanol is added to the system in order to simulate the high gas hold-up, foaming condition occurring in the EBRs used in the hydrocracking of bitumen. Using a pilot-scale gas-liquid-solid fluidized bed system, we report on the overall gas hold-up in the three-

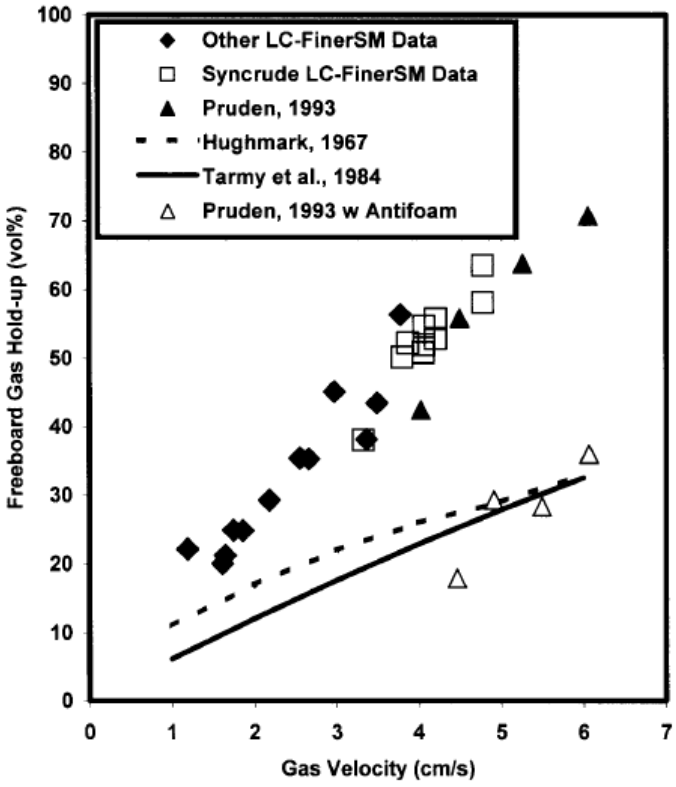

Figure 5.3: Gas hold-up in the freeboard region of commercial EBRs with recycle cup [134]

phase and freeboard regions for both hydrophilic and hydrophobic particles. We compare the fluidization behavior of particles with different wettability and analyze its effect on foam formation using measurements of foam thickness. The latter data are shown to be consistent with semi-empirical models of foam dynamics [150, 12]. A conceptual model of particle-bubble interaction, according to which bubble break-up in beds of hydrophobic particles is determined by collisions between bubbles and gas-padded particles (particles covered by small gas bubbles), is consistent with the experimental data and is supported by photographic evidence.

5.3 Experimental Setup and Procedure

5.3.1 Experimental Setup

In this study, experiments were carried out in a cold-flow pilot scale fluidized bed system shown in Fig. 5.4. The fluidization column is made from clear PVC with an ID of 15.2 cm and height of 220 cm. The column consists of three main regions: the gas/liquid distributor (plenum chamber), the particle bed region and the freeboard region. The plenum chamber section has the same diameter as that of the column and is 20 cm in height. A perforated plate is fitted between the bed section and the plenum chamber to evenly distribute gas and liquid within the column. Compressed air (Rigid, model OF50150TS) at superficial velocities ranging from 0.01 to 0.16 m/s was used as the gas phase. Two gas spargers with openings of 100 µm were installed symmetrically in the plenum chamber to introduce the gas to the system. Distilled water or 5wt.% aqueous ethanol solution at superficial velocities of 0.057 and 0.095 m/s was employed as the liquid phase. A 1-hp centrifugal pump (Goulds, model 2ST1E4F4) transported the liquid from a storage tank to the bottom of the plenum chamber. The liquid and gas flow rates were controlled by control valves and monitored by rotameters (Blue-White, models F-43040LNS and F-55376-GP). Clear glass beads of diameter equal to 4 mm were used as the solid particles in the fluidized bed. The glass beads were rendered hydrophobic by coating with octadecyltrichlorosilane (OTS) using pentane as the solvent [133]. The operating conditions investigated are summarized in Table 5.1. Liquid superficial velocities for the experiments were selected based on preliminary tests aimed at determining the minimum liquid superficial velocity required to make the bed of particles fluidized (*i.e.* minimum liquid fluidization velocity, u_{lmf}). Gas superficial velocities were selected to observe the transition from dispersed to coalesced bubble flow regime [129, 141].

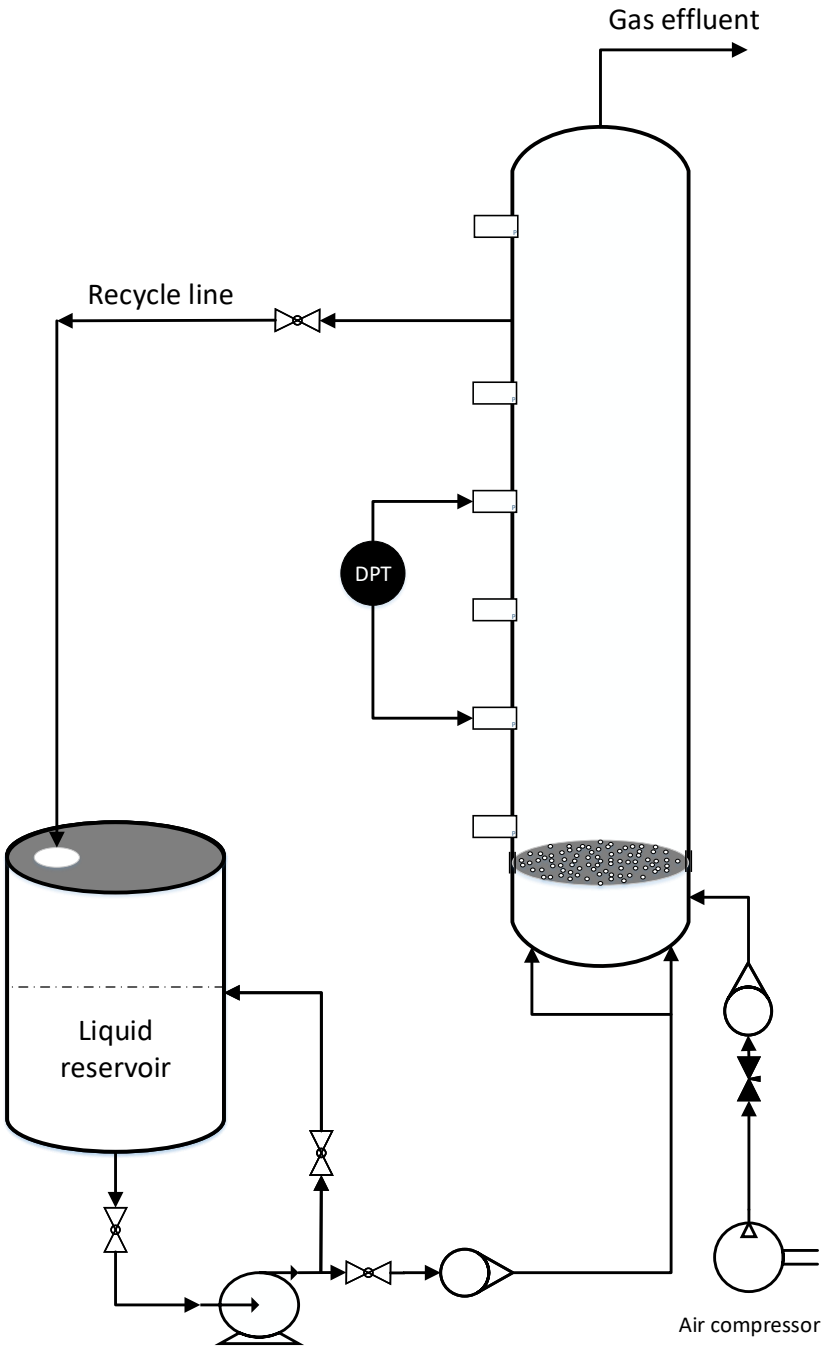

Figure 5.4: Schematics of the experimental set-up

Table 5.1: Studied operating condition and phase physical properties.

Parameter	Symbol	Values	Unit
Superficial liquid velocity	u_{sl}	0.057, 0.095	m/s
Superficial gas velocity	u_{sg}	0-0.16	m/s
Liquid viscosity	μ_l	1.004×10^{-3}	kg/m s
Gas-liquid surface tension (water)	$\sigma_{g,l}$	0.072	N/m
Gas-liquid surface tension (5 wt.% aqueous ethanol solution)	$\sigma_{g,l}$	0.055	N/m
Liquid density (water)	ρ_l	998.3	kg/m^3
Liquid density (5 wt.% aqueous ethanol solution)	ρ_l	989	kg/m^3
Gas density	ρ_g	1.205	kg/m^3
Solid density	ρ_s	2500	kg/m^3

5.3.2 Overall Phase Hold-up Measurement

Overall phase hold-ups are typically determined via dynamic pressure drop measurement along the bed and the freeboard regions. In this study, the overall phase hold-ups were obtained using a differential pressure transducer (Rosemount, model 3051CD2A22A1AM5C6Q4). Seven pressure ports were installed axially along the column height at 25 cm intervals. The solid volume fraction can be expressed in terms of the total mass of solid particles (W_s), bed cross section (A_c), solid density and the expanded bed height (H_e) as follows:

$$\epsilon_s = \frac{W_s}{\rho_s A_c H_e} \tag{5.4}$$

In the above equation, the expanded bed height can be determined using pressure profiles or by visual observation of the bed-freeboard interface. Neglecting the frictional drag force on the column wall [53], the gas hold-up is then related to the dynamic pressure drop (ΔP), as follows:

$$\epsilon_g = \frac{\epsilon_s(\rho_s - \rho_l) + \frac{\Delta P}{g\Delta z}}{\rho_l - \rho_g} \tag{5.5}$$

Since the only phases present in the fluidized bed are gas, liquid and solid, we have:

$$\epsilon_l = 1 - \epsilon_s - \epsilon_g \tag{5.6}$$

The dynamic pressure drop in the freeboard was also measured and used to calculate the gas hold-up in that region, as follows,

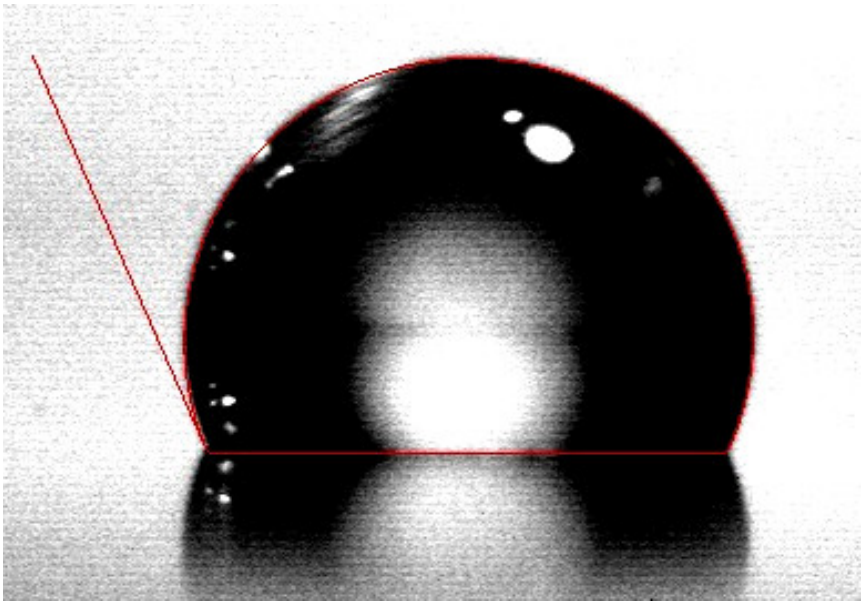

Figure 5.5: Drop of water sitting on a glass substrate coated with OTS according to the procedure described by [133]

$$\epsilon_g = \frac{\frac{\Delta P}{g\Delta z}}{\rho_l - \rho_g} \tag{5.7}$$

5.3.3 Contact Angle Measurement

The degree of wettability of a particles is generally evaluated in terms of the contact angle. In this study, the contact angle of drops of water and 5wt.% aqueous ethanol solution on glass slides (with and without coating by OTS) was measured by image analysis of sessile drops using a tensiometer (AST Products, model VCA 2500 XE) equipped with a CCD camera. An example of contact angle measurements is shown in Fig. 5.5 for a drop of water on the OTS-coated glass substrate. The average contact angle for the coated substrates was 115±6 degrees, which implies that the coating was effective at rendering the particles hydrophobic. Addition of ethanol to water did not change the average contact angle (θ = 113±5 degrees). The contact angle of either liquid phase on uncoated glass substrates (washed with 30% V/V aqueous HCl solution) was zero.

5.4 Results and Discussion

5.4.1 Phase Hold-up Measurement in Gas-Liquid-Solid Region

Global hold-up values obtained in this study are shown in Figs. 5.6 to 5.9. The results of our study are in good agreement with measurements of previous studies exploring similar operating conditions conditions [41]. For the air-water system operating with the smaller liquid velocity (u_{sl} = 0.057 m/s), a change in the slope of gas hold-up data was observed with increasing gas velocity, indicating transition from the dispersed to the coalesced flow regime. By increasing the inlet gas flow rate, the number of bubbles increases, the distance between individual bubbles decreases and consequently the intensity of bubble collisions increases [229]. Bubble coalescence phenomena result in formation of large bubbles and a wide bubble size distribution is observed. Similar trend were noted in previous studies in the system of air-water-glass bead system [87, 41, 151]. Due to the low residence time of the large bubbles in the coalesced system, gas hold-up did not increase significantly in this flow regime. The calculated standard errors for the gas hold-up data are also larger in the coalesced regime as enhanced pressure fluctuations were observed. The change of slope in gas hold-up trend was not as clear in the system with the higher liquid superficial velocity (Fig. 5.6b). This could be due to the fact that at higher liquid velocities the dispersed flow regime is delayed and the transition occurs at higher gas velocities [129]. Smaller fluctuations in pressure readings and consequently smaller standard errors were noted in this system. A comparison of Fig. 5.6a to Fig. 5.6b reveals the effect of liquid flow rate. By increasing the liquid superficial velocity from 0.057 to 0.095 m/s, the gas hold-up decreased. As the liquid rises faster, the residence time of bubbles in the system decreases and the gas hold-up drops. The effect of liquid velocity on gas hold-up is a complex phenomena and various trends has been observed in the literature. Safoniuk et al. [176] reported that the gas hold-up is almost independent of liquid velocity, except for the very high values of liquid velocities. Gas hold-up has also been reported to increase with the liquid velocity [41, 195, 151]. Pjontek et al. [151] mentioned that the delayed transition to the coalesced regime at higher liquid velocities results in greater number of small bubbles in the system which in turn causes the higher gas hold-ups.

As mentioned before, industrial fluidized bed reactors such as the ones used for heavy oil upgrading generally operate with gas hold-up values greater than 25%. Research aimed at elucidating the hydrodynamics of such systems have therefore sought to simulate high gas hold-up conditions in pilot scale systems using fluids with similar physical properties or by adjusting the bubble coalescence behavior using surface-active components [54, 124, 165, 166, 164, 152]. In this study, ethanol was used to modify the surface tension of water and experiments were conducted with 5wt.% aqueous ethanol solution as the liquid phase.

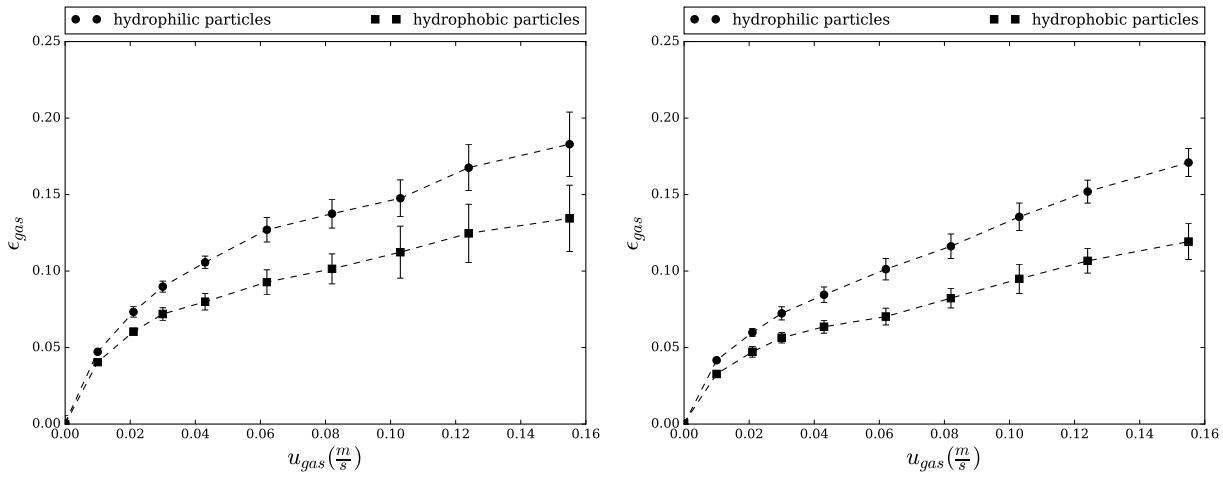

Figure 5.6: Gas hold-up in the bed region of air-water system for (a) $u_{sl} = 0.057$ m/s and (b) $u_{sl} = 0.095$ m/s (Note: dashed lines are a guide to the eye.)

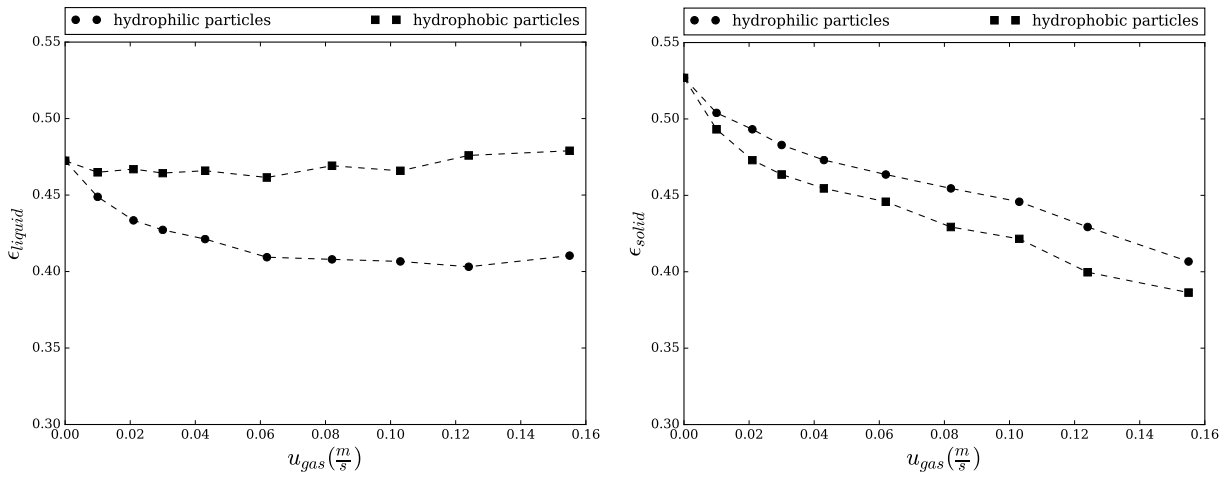

Figure 5.7: Liquid hold-up (a) and solid hold-up (b) in the bed of air-water system at u_{sl} = 0.057 m/s.

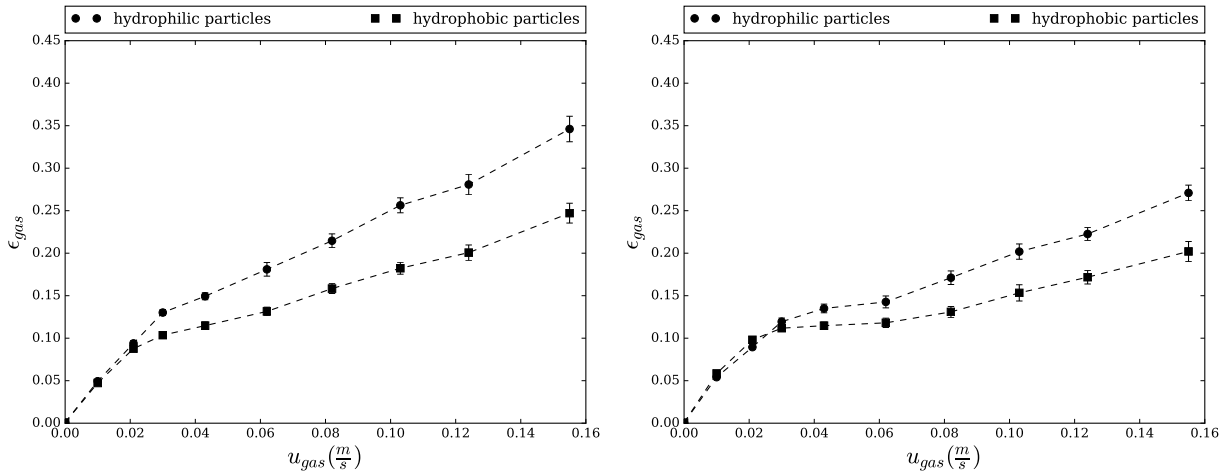

Figure 5.8: Gas hold-up in the bed region of air-5wt.% ethanol solution system for (a) u_{sl} = 0.057 m/s and (b) u_{sl} = 0.095 m/s (Note: dashed lines are a guide to the eye.)

Addition of ethanol to water decreased the surface tension from 0.072 N/m to 0.055 N/m. The phase hold-up values are shown in Figs. 5.8 and 5.9. Gas hold-up values of up to 35% obtained in the bed region which show significant increase compared to the distilled water system (see Fig. 5.10). Also, the results confirm that using the ethanol solution was effective in creating a high gas hold-up condition in the fluidized bed - condition associated with reduced average bubble size [189, 152].

For the ethanol system operating at the smaller liquid velocity, the change in slope of gas hold-up data is not as obvious as the water system. This implies a smaller number of large bubbles in the system as bubble coalescence was inhibited. Pressure fluctuations over the whole range of gas velocities were also smaller for the surfactant system compared to water system. Consequently, the standard error of measurement is lower. For the case of larger liquid velocity, gas hold-up initially increased with gas velocity, became constant (from 0.04 and to 0.06 cm/s), and then increased again. It seems that at this liquid velocity, a transition flow regime [198] prevailed over a short range of gas velocities in the ethanol system. Such trend can be seen in the results of Dargar and Macchi [41] and Fan et al. [54] who also used alcohol solutions (ethanol and n-butanol, respectively). Increasing the liquid velocity from 0.057 to 0.095 m/s, had a minor effect on the gas hold-up for low gas velocities of up to 0.03 m/s. After this value, the ethanol system behaved similar to the the distilled water system and the gas hold-up decreased with increasing liquid velocity.

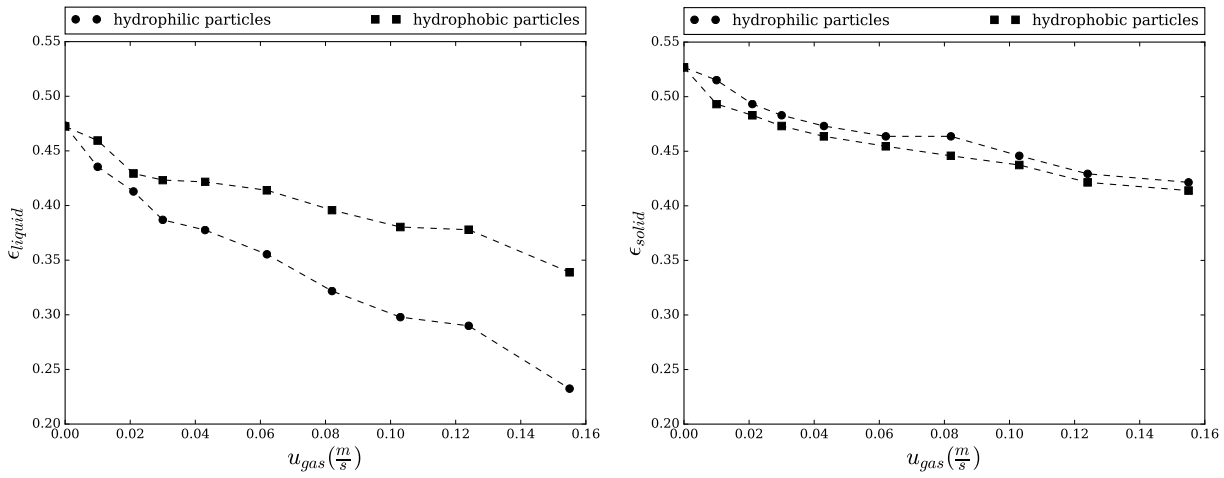

(a) (b)

Figure 5.9: Liquid hold-up (a) and solid hold-up (b) in the bed of air-5wt.% ethanol solution system at $u_{sl} = 0.057$ m/s (Note: dashed lines are a guide to the eye.)

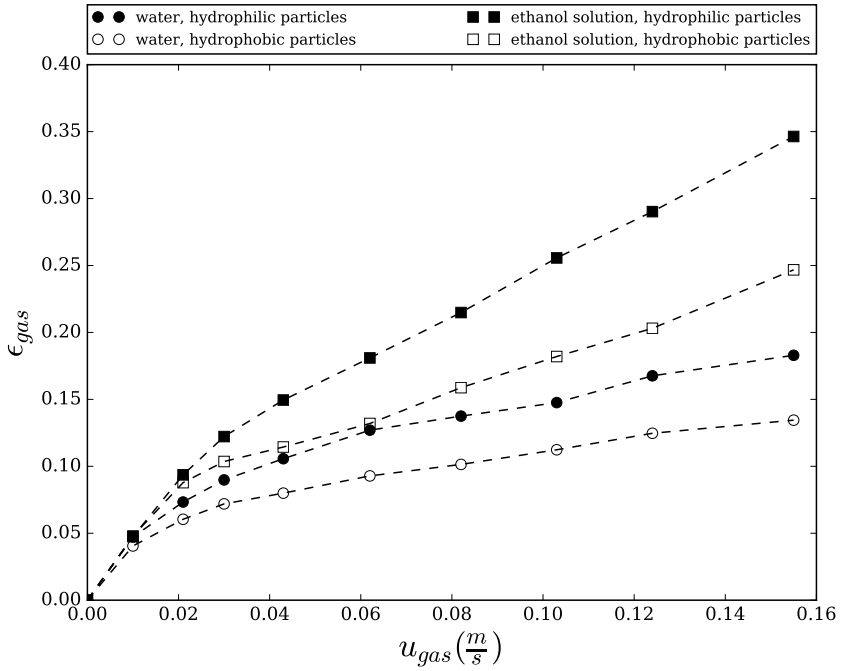

Figure 5.10: Comparison of gas hold-up in the bed region for air-water and air-5wt.% ethanol solution systems at $u_{sl} = 0.057$ m/s (Note: dashed lines are a guide to the eye.)

5.4.2 Prediction of Overall Gas Hold-up with Empirical Correlations

A recent meta-analysis study [140] has provided a set of empirical correlations to predict the overall gas hold-up in three-phase fluidized beds of spherical particles with water as the liquid phase. It was found that classification of data points based on the particle Reynolds number ($Re_p = \frac{\rho_l u_{sl} d_p}{\mu_l}$) produced correlations with the least average absolute relative error (AARE). These correlations are tested here for their ability to predict the overall gas hold-up data of the air-water-glass bead systems for both hydrophobic and hydrophilic particles. As shown in Fig. 5.11, the correlations are able to predict gas hold-up values of up to 15% with less than 25% error and the AARE is 24% for the case of hydrophilic particles. However, for the system of hydrophobic particles, the correlations failed to predict gas hold-up values of more than 8% and the AARE exceeds 56%. The results implied that the empirical correlations cannot capture the hydrodynamics of gas-liquid-solid fluidized beds operating with hydrophobic particles. This is expected as there is no parameter in the correlations to account for the effect of wettability on the average bubble size, a key determinant of gas hold-up.

5.4.3 Effect of Particle Wettability on the Overall Phase Hold-up Values

Operating the fluidized bed with the hydrophobic glass beads decreased the overall gas hold-up by an average of about 26% and 21% for the systems of air-water and air-5wt.% ethanol solution, respectively. Larger bed expansion was observed for the case of hydrophobic particles. Consequently the liquid hold-up values were higher in these systems (see Figs. 5.7a and 5.9a). Solid hold-ups were also slightly smaller for the bed of hydrophobic particles which again implies a larger bed expansion. The experimental results for the air-water systems are similar to the findings of Armstrong et al. [11]. Adhesion of bubbles to hydrophobic particles and formation of bubble-particle agglomerates was observed frequently, especially at the bed/freeboard interface (see Fig. 5.12). The bubble-particle adhesion can be explained by considering the definition of work of adhesion described in Eq.5.1. Increasing the contact angle from 0 to 115 degrees at a constant surface tension decreases the energy of adhesion by more than 70%. Therefore, much less energy is required to separate liquid and solid phases, facilitating attachment of bubbles to particles upon collision. It should also be noted that in the systems studied here, the effect of contact angle on the work of adhesion is much more pronounced than the effect of surface tension.

For the large particles used in this study, a single bubble attached to the particle

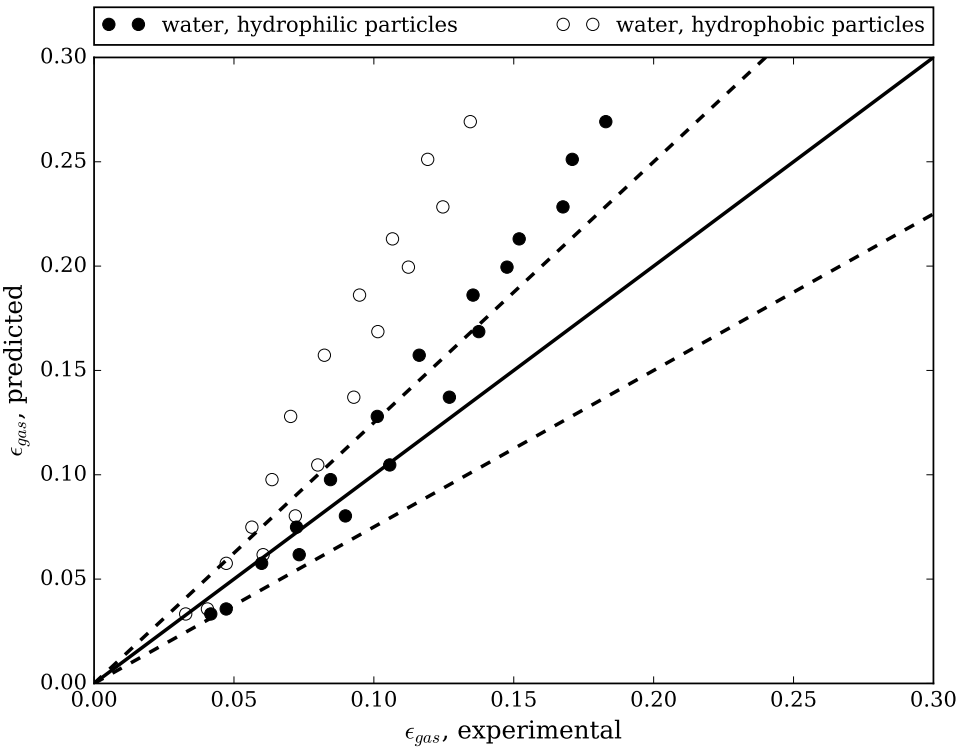

Figure 5.11: Comparison of gas hold-up predictions by correlations of Mowla et al. [140] with the experimental data for the air-water-glass beads system obtained in this study. Dashed lines indicate error of ±25%.

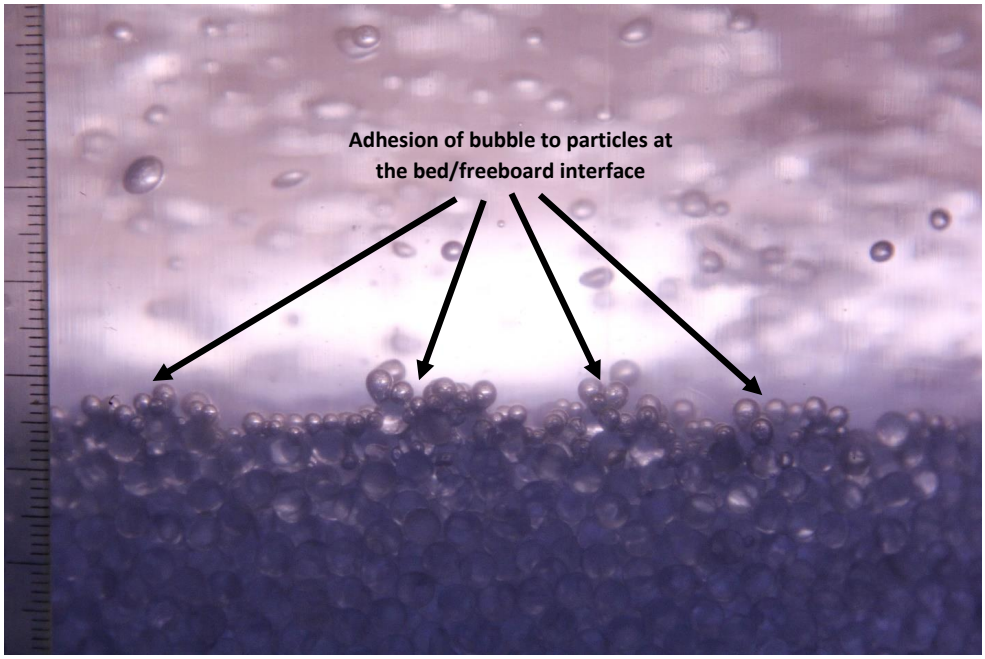

Figure 5.12: Adhesion of air bubbles to the hydrophobic glass beads in the air-water system

was not able to float the particle, separating it from the bed and transferring it in the freeboard region. However, in cases where three or more bubbles were attached to one particle (see Fig. 5.13), it was observed that the bubble-particle agglomerate left the bed and was temporarily suspended in the freeboard region. This behavior is consistent with the interpretation of Armstrong et al. [11], according to whom formation of particle-bubble agglomerates with lower apparent density than bare particles is the cause of greater bed expansion in systems of hydrophobic particles. Assuming attachment of three bubbles of average diameter of 2 mm to a 4 mm particle, the bubble-particle agglomerate has an apparent density which is about 40% lower than the density of the bare particle. Because of the poor wettability of the particles, gas bubbles attached to particles cannot be completely removed and small gas "pads" remain on the particles held by strong capillary forces. In the context of the model of Chen and Fan [36], gas-padded particles are less able to penetrate large bubbles because of decreased apparent density. As a result, a reduction of the bubble break-up rate in the bed region should be expected, leading to larger average bubble size and lower gas hold-up. In the context of this model, one must conclude that bubble-particle collisions in fluidized beds of hydrophobic particles involve predominantly gas-padded rather than bare particles. Because such collisions may involve the interaction between two gas-liquid interfaces (of the free and attached bubble), as shown in Fig. 5.14,

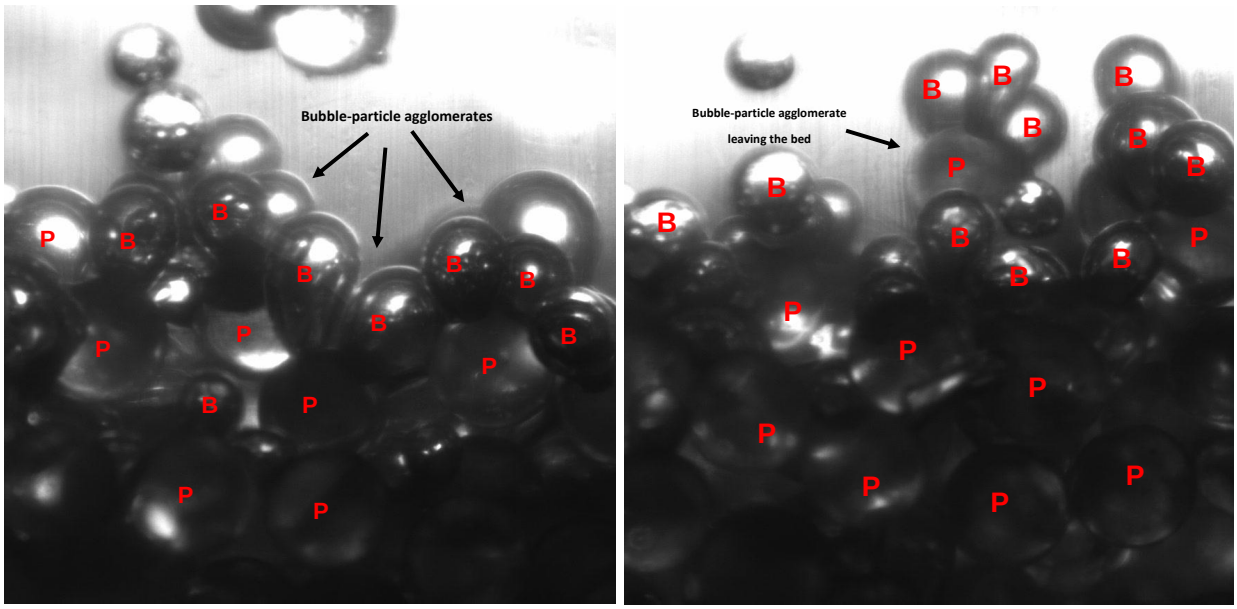

(a) (b)

Figure 5.13: Adhesion of multiple bubbles (B) to the hydrophobic particles (P)

it is reasonable to expect differences between the behavior of coalescing (air-water) and non-coalescing (air-5wt.% aqueous ethanol solution) systems.

5.4.4 Gas Hold-up and Foam Thickness in the Freeboard Region

The overall gas hold-up as well as the foam thickness at steady state were measured in the freeboard region of the fluidized bed in order to observe if particle wettability has an effect on the hydrodynamics of this region. The gas hold-up data are presented in Figs. 5.15 and 5.16. Considering the findings of section 5.4.3, one expects the gas hold-up in the freeboard region (gas-liquid flow) to be lower when the bed consists of hydrophobic particles, for in this case the average size of bubbles introduced in the freeboard region is larger [169], as a result of reduced bubble break-up rate. This is indeed observed in the data, with the exception of the air-water system at the higher inlet liquid velocity (see Fig. 5.15b). Apparently, under such conditions the bubble break-up rate is not significantly reduced by bubble-particle attachment. It is possible that a reduction in bubble break-up rate due to a reduction of apparent density is compensated by additional forces at play during the coalescence of an attached and a free bubble [149]. Since bubble coalescence

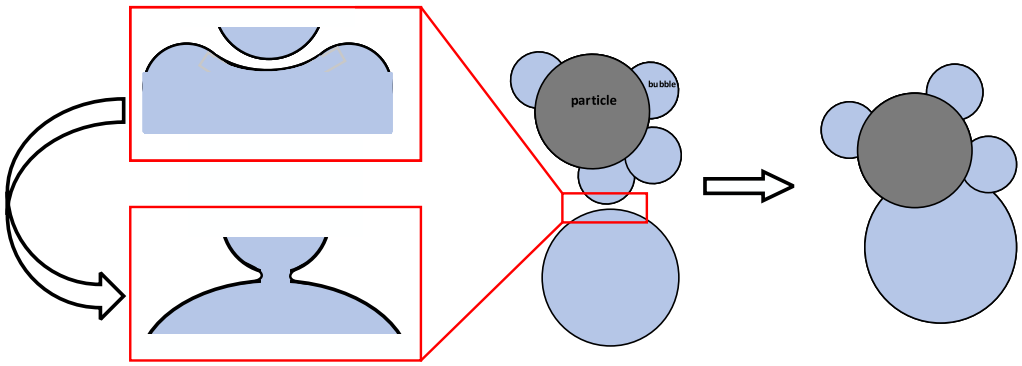

Figure 5.14: Interaction between attached and free bubbles

is inhibited in the ethanol system, the effect of hydrophobic particles is more prominent in the freeboard region of the ethanol system, in which the gas hold-up is reduced by an average of 25% compared to the case of hydrophilic particles.

If the bubble diameter in the freeboard region is larger when the bed contains hydrophobic particles, one expects differences in the steady state foam thickness (H_∞) generated at the macroscopic interphase at the top of the freeboard region. This is borne out of theoretical considerations described below.

Pilon et al. [150] have proposed a semi-empirical model for the prediction of foam thickness in isothermal gas-liquid solutions at steady state. According to these authors, the time evolution of the top and bottom boundaries of a layer of foam formed by gas injection at the bottom of a vertical column containing liquid (see Fig. 5.17), is described by the following equations (z_1 and z_2)[22];

$$\begin{aligned} \frac{dz_1}{dt} &= \frac{\epsilon_g(z_1,t)q_{PB}(z_1,t)}{1-\epsilon_g(z_1,t)} \\ \frac{dz_2}{dt} &= \frac{u_{sg}}{\epsilon_g(z_2,t)} - q_{PB}(z_2,t) \end{aligned} \tag{5.8}$$

where $\epsilon_g(z,t)$ and $q_{PB}(z,t)$ are the gas fraction and the mass flow rate of liquid through the Plateau borders at location z and time t. The foam thickness may be written as $H_\infty = z_2 - z_1$. Therefore, using Eq.5.8, one can obtain the following evolution equation for the foam thickness;

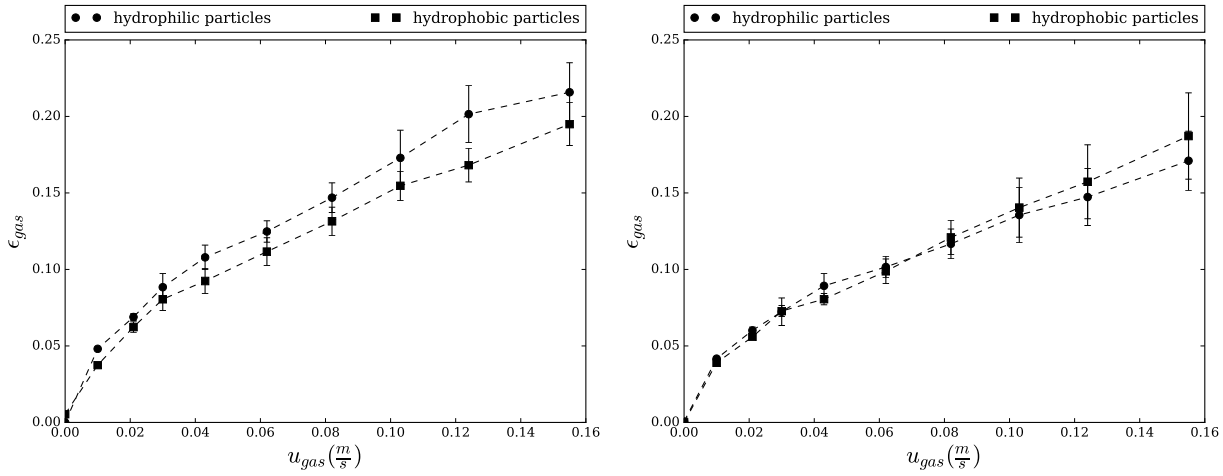

(a) (b)

Figure 5.15: Gas hold-up in the freeboard region of air-water system for (a) $u_{sl} = 0.057$ m/s and (b) $u_{sl} = 0.095$ m/s (Note: dashed lines are a guide to the eye.)

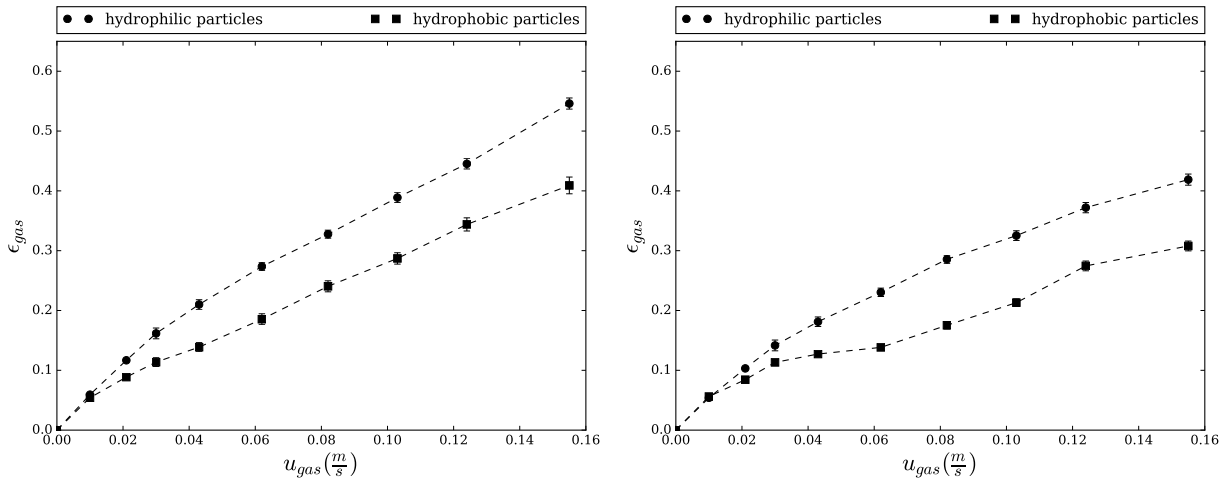

(a) (b)

Figure 5.16: Gas hold-up in the freeboard region of air-5wt.% ethanol solution system for (a) $u_{sl} = 0.057$ m/s and (b) $u_{sl} = 0.095$ m/s (Note: dashed lines are a guide to the eye.)

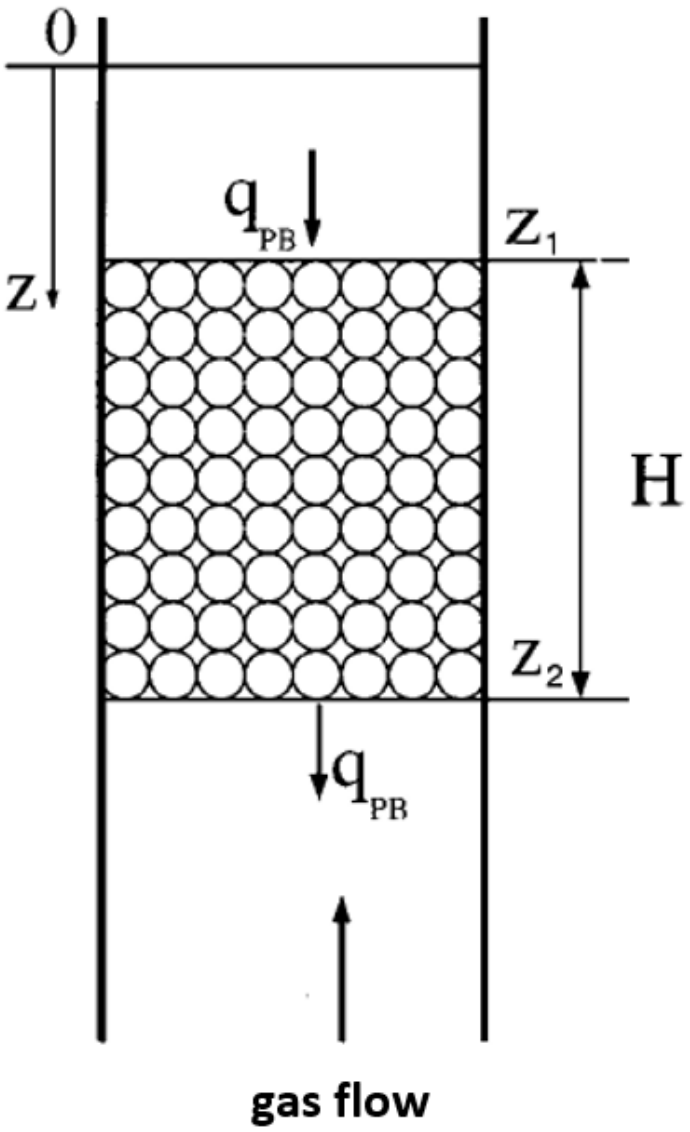

Figure 5.17: Schematic of a foam layer formed by gas injection into liquid in a vertical column (modified from Pilon et al. [150])

$$\frac{dH}{dt} = \frac{d(z_2 - z_1)}{dt} = \frac{u_{sg}}{\epsilon_g(z_2, t)} - q_{PB}(z_2, t) - \frac{\epsilon_g(z_1, t) q_{PB}(z_1, t)}{1 - \epsilon_g(z_1, t)} \tag{5.9}$$

where the first term on the right-hand side is the increase of the foam thickness due to the addition of gas at the bottom boundary and the last two terms are the decrease of the foam thickness due to liquid drainage through the Plateau borders and gas flow due to bubble rupture at the top boundary of the foam. Additionally, the flow rate $q_{PB}(z, t)$ may be expressed as follows,

$$q_{PB}(z, t) = \frac{3}{15} N r_b n_p u_f \tag{5.10}$$

where r_b is the bubble radius, N is the number of bubbles per unit volume, n_p is the number of Plateau borders per bubble, a_p is the cross-sectional area of a Plateau border, and u_f is the velocity of the fluid through the Plateau border due to gravity drainage. Simplified expressions for the terms in Eq.5.10 are given in the literature [143]. Replacing Eq.5.10 in Eq.5.9 using the simplified expressions and rendering Eq.5.9 dimensionless by applying the Buckingham-Pi theorem, one may express H_∞ in terms of two dimensionless numbers (Π) as follows,

$$\begin{aligned} \Pi_2 &= c_1 \ \Pi_1^{c_2}, \\ \Pi_1 &= \frac{Re}{Fr}, \\ \Pi_2 &= Ca \ (\frac{H_\infty}{r_b}) \end{aligned} \tag{5.11}$$

where c_1 and c_2 are constants to be determined by fitting to experimental data, and Ca, Re and Fr are the capillary, Reynolds and Froude numbers, respectively, which are defined as,

$$Re = \frac{\rho_l \ (u_{sg} - u_{sg}^{min}) \ r_b}{\mu_l}, \tag{5.12a}$$

$$Fr = \frac{(u_{sg} - u_{sg}^{min})^2}{g r_b}, \tag{5.12b}$$

$$Ca = \frac{\mu_l \ (u_{sg} - u_{sg}^{min})}{\sigma_{g,l}} \tag{5.12c}$$

where u_{sg}^{min} is the gas superficial velocity at the onset of foaming and g is the gravitational constant. Pilon et al. [150] found c_1 and c_2 to be 2905 and -1.8, when they fit their model to experimental data of foam thickness for high-viscosity fluids available in the literature. Using the fitted constants, the following semi-empirical model is obtained for the foam height at steady state;

$$H_\infty = 2905 \, \frac{\sigma_{g,l}}{r_b^{2.6}} \, \frac{\mu_l (u_{sg} - u_{sg}^{min})^{0.8}}{(\rho_l g)^{1.8}} \tag{5.13}$$

The model described above takes into account viscous, gravitational and capillary forces, but neglects the effects of foam coarsening. This may be acceptable for high-viscosity fluids providing thick and stable liquid films between bubbles in the foam [215]. An extension of this model to low-viscosity liquids (e.g. aqueous foam) by Attia et al. [12] has considered a third dimensionless number to account for foam coarsening driven by Ostwald ripening that is common in surfactant foams. Coarsening of gas-liquid foam by Ostwald ripening is a process in which large bubbles consume adjacent smaller bubbles and grow in size [199] via solute diffusion through the intervening liquid films. Unlike high-viscosity liquids in which the size of bubble remains constant through the foam height, in low-viscosity fluids bubble size increases from bottom to top within a foam layer (see Fig. 5.18). The third Π introduced by Attia et al. [12] is as follows,

$$\Pi_3 = \frac{DS}{r_b (u_{sg} - u_{sg}^{min})} \tag{5.14}$$

where D is the diffusion coefficient of gas in liquid and S is the dimensionless Ostwald coefficient of solubility which is defined as the volume of gas absorbed by unit volume of pure liquid at a given pressure and temperature [13]. To find H_∞ a power law relation was assumed between the three dimensionless numbers,

$$\Pi_2 = m_1 \Pi_1^{m_2} \Pi_3^{m_3} \tag{5.15}$$

where m_1, m_2, m_3 are the empirical constants to be determined from experimental data. Attia et al. [12] found these constants to be equal to 118, -1.8 and -0.96, respectively, by fitting their model to experimental data of low viscosity liquids from literature. Using these values, Eq.5.15 is written in dimensional form as follows;

$$H_\infty = 118 \, \frac{\sigma_{g,l}}{r_b^{1.64}} \, \frac{\mu_l^{0.8} (u_{sg} - u_{sg}^{min})^{1.76}}{(\rho_l g)^{1.8} (DS)^{0.96}} \tag{5.16}$$

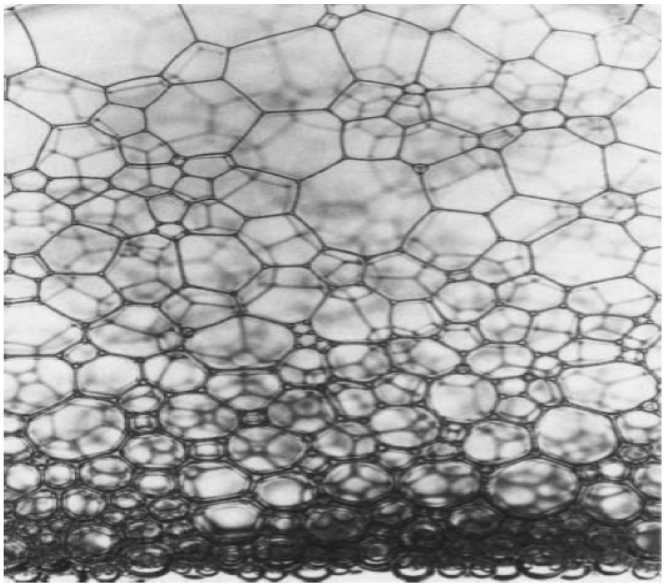

Figure 5.18: Photograph of a stable foam of an aqueous 5% SDS solution [177]

It may be noted in both Eq.5.13 and Eq.5.16 that H_∞ is inversely proportional to bubble radius, *i.e*, decreasing as r_b increases. Therefore, if the average bubble diameter in the freeboard region of a three-phase fluidized bed of hydrophobic particles is larger than in a bed of hydrophilic particles, the steady-state foam thickness should be smaller. This is indeed the case as observed in Fig. 5.19. The figure shows the thickness of foam layer above the gas/liquid bubbly mixture in the freeboard region. These results suggest the possibility to reduce foaming in the freeboard region (and gas hold up in the three-phase region) of industrial fluidized bed systems by controlling the particle wettability.

Another observation from Fig. 5.19 is that the foam thickness decreased as the liquid velocity increased. The onset of foaming was also delayed at the higher liquid velocity. Such observations are consistent with the findings of Guitian and Joseph [72], who established experimentally that a critical gas velocity for the onset of foam formation depends on liquid velocity as follows;

$$u_{sg}^{min} = b_1 + b_2\ u_{sl} \tag{5.17}$$

where b_1 and b_2 are empirical constants which depend only on the liquid phase physical properties. A system operating at u_{sg} less than u_{sg}^{min} does not experience foaming. When u_{sg} exceeds the critical value in Eq.5.17, foam begins to appear and the foam layer expands with increasing u_{sg}. It may also be inferred from the model that the critical gas velocity

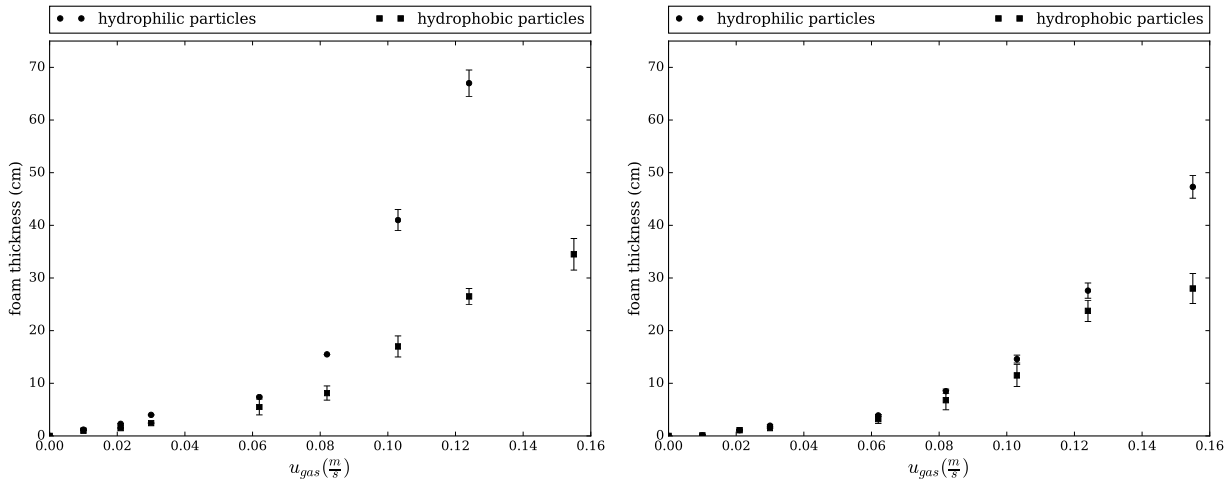

(a) (b)

Figure 5.19: Foam thickness above the freeboard region of air-5wt.% ethanol solution system for (a) $u_{sl} = 0.057$ m/s and (b) $u_{sl} = 0.095$ m/s

for the onset of foaming is higher when the liquid velocity is increased.

The foam thickness data (Fig. 5.19) obtained in this work may be analyzed quantitatively using Eqs.5.11 and 5.15. On the basis of visual observations, we took u_{sg}^{min} as 0 and 0.01 m/s for the systems operating with inlet liquid velocity of 0.057 and 0.095 m/s, respectively. Assuming spherical bubbles, the average bubble diameter was estimated by solving the following equation,

$$C_{do}Re_b^2 = \frac{4}{3}Ar \tag{5.18}$$

where Re_b and Ar are the bubble Reynolds number and Archimedes number, respectively, defined as;

$$Re_b = \frac{\rho_l u_o d_b}{\mu_l} \tag{5.19a}$$

$$Ar = \frac{d_b^3 \rho_l (\rho_l - \rho_g)}{\mu_l^2} \tag{5.19b}$$

where d_b is the bubble diameter and u_o is the bubble terminal velocity. Also, C_{do} in Eq. 5.18 is the drag coefficient acting on an isolated bubble, which is assumed to be given by the Tomiyama empirical correlation for slightly contaminated gas-liquid systems as follows [207],

$$C_{do} = \max\left\{\min\left[\frac{24}{Re_b}(1+0.15Re_b^{0.687}), \frac{72}{Re_b}\right], \left[\frac{8}{3}\frac{Eo}{Eo+4}\right]\right\},$$
$$Eo = \frac{g(\rho_l - \rho_g)d_b^2}{\sigma_{g,l}} \tag{5.20}$$

The terminal velocity can be calculated by considering the balance between buoyancy and drag forces. The steady state mass balance for an incompressible and non-reacting gas phase in a vertical column yields [169]:

$$\epsilon_g = \frac{u_{sg}}{u_o}\ f(\epsilon_g)^{0.5} \tag{5.21}$$

where $f(\epsilon_g)$ is a swarm correction factor defined as C_d/C_{do}. Here, C_d represents the drag force acting on a bubble under actual operating conditions. In this study we consider the swarm factor proposed by Gemello et al. [62],

$$f(\epsilon_g) = max\left[(1-\epsilon_g)\ \left\{(1-\epsilon_g)^{25} + (4.8\ \frac{\epsilon_g}{1-\epsilon_g})^{25}\right\}^{-\frac{2}{25}},\ 0.12\right] \tag{5.22}$$

Using Eqs.5.21 and 5.22, a value of u_o may be calculated for a given value of u_{sg} and ϵ_g in the freeboard region. Subsequently, the bubble diameter (and r_b) may be calculated by solving Eq. 5.18 using Eqs.5.19 and 5.20. The values of Π_1 and Π_2 may then be obtained from the values of r_b and other parameters listed in Table 5.1. Proceeding in this manner, Eq.5.11 was fitted to the experimental foam height data with c_1 = 147.94 and c_2 = -1.86 with correlation coefficient (R^2) of 0.98. Replacing the constants in Eq.5.11, H_∞ can be expressed as,

$$H_\infty = 147.94\ \frac{\sigma_{g,l}}{r_b^{2.72}}\ \frac{\mu_l(u_{sg} - u_{sg}^{min})^{0.86}}{(\rho_l g)^{1.86}} \tag{5.23}$$

For air at atmospheric pressure and room temperature, D and S in Eq.5.14 may be taken equal to 1.45×10^{-9} m^2/s and 1.69×10^{-2}, respectively [12]. Eq.5.15 may then be fitted to the experimental data to obtain m_1 = 0.614, m_2 = -1.632 and m_3 = -0.344, and with R^2 of 0.98. Again, H_∞ can be written in dimensional form as,

$$H_\infty = 0.614\ \frac{\sigma_{g,l}}{r_b^{1.92}}\ \frac{\mu_l^{0.632}(u_{sg} - u_{sg}^{min})^{0.976}}{(\rho_l g)^{1.632}(DS)^{0.344}} \tag{5.24}$$

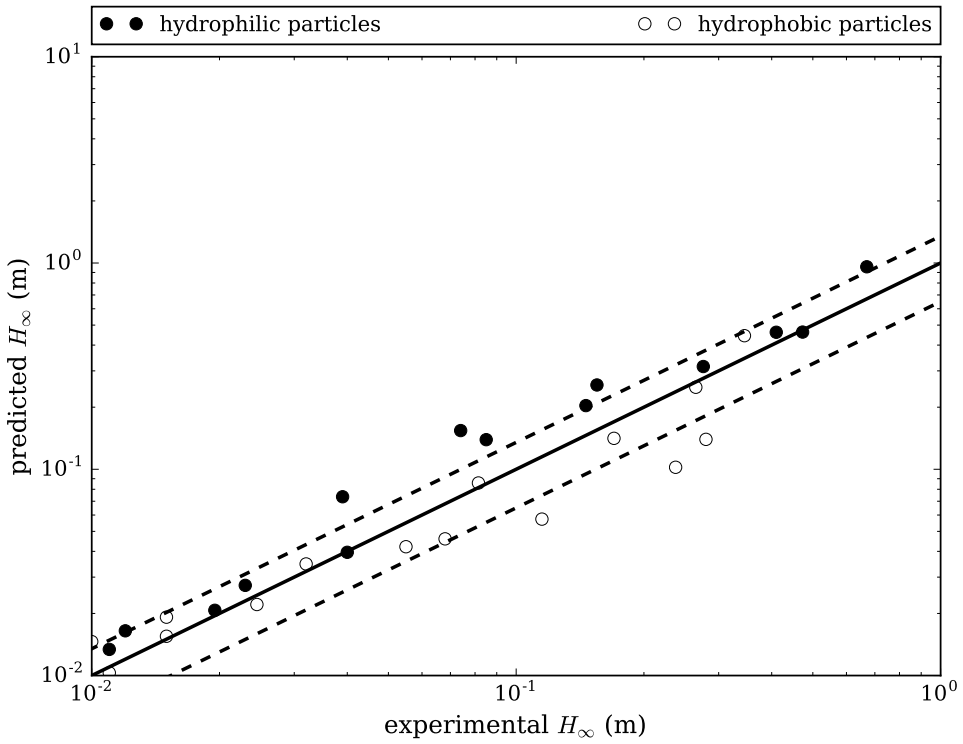

Figure 5.20: Comparison between experimental data and predictions of the steady state foam thickness from Eq.5.23. Dashed lines indicate error of ±35%.

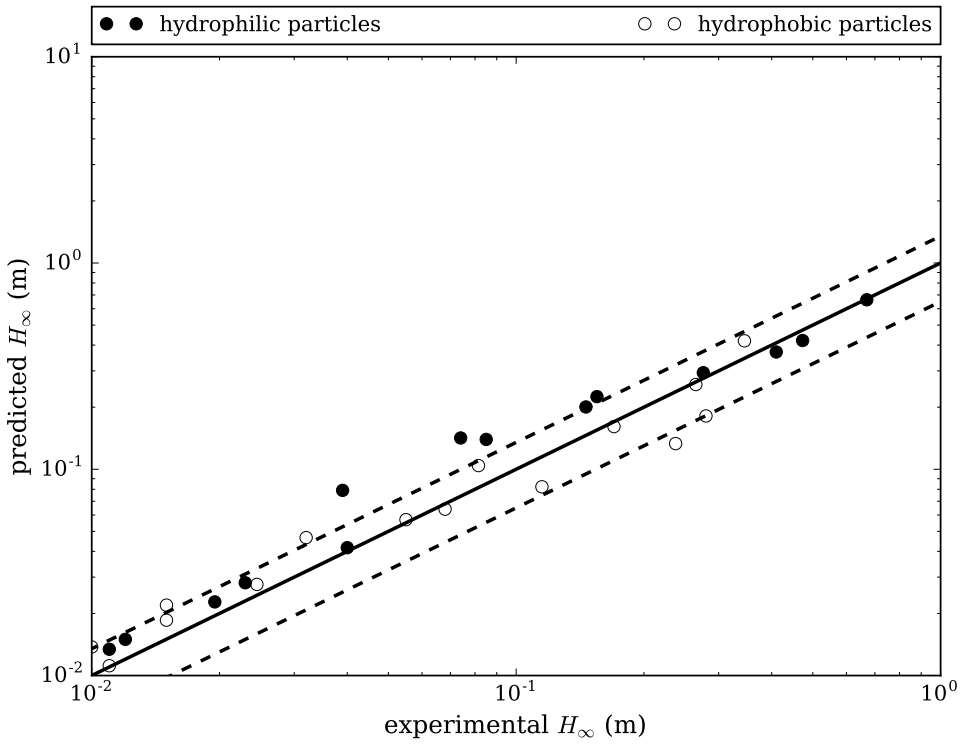

Figure 5.21: Comparison between experimental data and predictions of the steady state foam thickness from Eq.5.24. Dashed lines indicate error of ±35%.

Table 5.2: Average bubble diameter, estimated by semi-empirical models, in the freeboard region of the air-5wt.% ethanol solution system

Model	d_b for system of hydrophilic particles (mm)	d_b for system of hydrophobic particles (mm)
Eq.5.23	0.91	1.02
Eq.5.24	0.96	1.13

The accuracy of the two models in predicting the foam height at steady state, H_∞, is similar. This is shown in Figs. 5.20 and 5.21 which compare experimental data to predictions of Eqs.5.23 and 5.24, respectively. Analysis of our data as proposed by Pilon et al. [150] and Attia et al. [12] enables estimation of r_b by rearranging Eqs.5.23 and 5.24. The estimated bubble diameters for the foaming air-5wt.% ethanol system in the freeboard region are about 1 mm. These values, which are tabulated in Table 5.2 agree with the literature findings for air-ethanol solutions in gas-liquid flows [189]. Also, the average bubble diameter estimated using Eq.5.18 in the freeboard region of the system operating with hydrophobic particles is about 15% greater than the one in the freeboard region of the system operating with hydrophilic particles. Considering the sensitivity of the steady state foam thickness to the bubble diameter in the context of the semi-empirical models, the difference in the foam thickness can be explained by the difference in the calculated average bubble diameters.

5.5 Conclusion

In this study, the effect of particle wettability on the hydrodynamics of a gas-liquid-solid fluidized bed system operating with distilled water and 5wt.% aqueous ethanol solution was studied. For both systems, making the particles hydrophobic via coating with OTS, reduced the gas hold-up by more than 20%. Attachment of bubbles to particles and formation of bubble-particle agglomerates was observed. According to previous studies, the lower density of such agglomerates compared to individual particles, decreases their tendency towards bubble break-up. Hence, larger bubbles are produced and the gas hold-up dropped. Similar trend was observed for the overall gas hold-up in the freeboard region. The thickness of foam layer formed on top of the gas/liquid interface in the aqueous ethanol system was also measured. It was observed that the foam thickness decreased with increasing the inlet liquid superficial velocity as well as by making the particles hydrophobic. The foam thickness data were consistent with available semi-empirical models of foam height dynamics. The models revealed the great sensitivity of foam thickness to the bubble diameter in the gas-liquid flow system, such that a small increase in the average bubble size

decreases the foam thickness notably. It was concluded that a larger average bubble size in the bed of hydrophobic particles caused by reduction of the bubble break-up rate, leads to a reduction of the gas hold-up in the freeboard region and a reduction of the foam thickness. The results of this study suggest that reduction of both gas hold-up and foaming in three-phase fluidized bed reactors is possible by tailoring particle wettability.

Acknowledgements

This research was supported by the Natural Sciences and Engineering Research Council (NSERC) of Canada.

Chapter 6

Conclusions and Recommendations

6.1 Summary and Conclusions

The present thesis sought to improve the understanding of the fluid dynamics of the EBRs used in the hydroprocessing of bitumen through combination of experimental investigation and CFD simulations. To do so, a pilot scale cold-flow EBR was designed and constructed. The system was able to operate in both two-phase (gas-liquid) and three-phase (gas-liquid-solid) modes. Therefore, experiments were conducted in both modes and over a wide range of operational parameters to study the hydrodynamics of the bed section as well as the freeboard region of the EBRs.

First, the experimental measurements of the overall gas hold-up were obtained for air-water and air-0.5wt.% ethanol aqueous solution in the pilot scale system in both homogeneous and heterogeneous flow regimes. The objective was to validate a two-fluid Eulerian model in prediction of the hydrodynamics of the gas-liquid flows for operation either as bubble column or in co-current flow. In the homogeneous flow regime ($u_{sg} \leq 0.03$ m/s), the bubble diameter was measured via image analysis employing a digital camera. Using the measured bubble diameters, the model was able to predict the overall gas hold-up to within 10% of the experimental measurements. It was also found that the bubble diameter was considerably sensitive to the change in surface tension. Decreasing the surface tension by only 4%, resulted in about 30% decrease in the average bubble diameter. Such sensitivity to surface tension (and possibly to other parameters such as sparger design) was recognized as the main limitation in the predictive ability of the Eulerian model in the homogeneous regime. For the heterogeneous flow regime, as the image analysis method was not applicable, an empirical correlation was used to determine the bubble size. However,

the main limitation to the predictive ability of the model in this flow regime was originates from uncertainty in selection of the swarm correction factor. Including a well-known swarm correction factor (by Simonnet et al. [193]) in the model resulted in accurate predictions of the overall gas hold-up in the bubble column mode (to within 10%). However, in the co-current flow, which has not been studied as much in the literature, the average error between the experiments and the model predictions was about 22%. Changing a constant parameter in the swarm correction equation, resulted in accurate prediction of the overall gas hold-up in one of the studied cases. Considering that the swarm correction models are generally derived for bubble columns, development of improved equations for co-current gas-liquid flows requires further investigation.

The modular design of the pilot scale EBR in this study allowed the implementation and examining the performance of various recycle cup designs in gas/liquid disengagement. We designed two patented recycle cups according to the information available in the patent literature. The recycle cups were then printed using a desktop 3-D printer and 3 mm ABS filaments. The recycle cups were tested over a wide range operational parameters (gas and liquid flow rates and recycle ratio) and in air-water and air-5wt.% ethanol aqueous solution systems. The performance of the cups were compared by measuring the gas hold-up in the recycle line. Two-pairs of electrical conductivity cells which were installed in the recycle line, made the gas hold-up measurements possible. As expected, the gas hold-up in the recycle line increased by increasing the gas hold-up in the EBR. In the ethanol solution system, at gas velocities of over 0.05 m/s, a layer of foam was formed in the freeboard region. It was observed that in such cases more gas was entrained in the recycle stream. Therefore, foam formation negatively affect the performance of the recycle cups. Gas hold-up in the recycle line also increased with an increase in the inlet liquid flow rate and/or recycle ratio. Bubbles has less time to escape from the liquid, consequently more bubbles trapped in the recycled liquid. The Eulerian model was also employed to predict the gas hold-up in the column and inside the recycle line. In the homogeneous regime, given the correct bubble diameter, the model predicted the column gas hold-up with great accuracy (less than 10% error). However, the model failed in estimation of the recycle line gas hold-up. These observations are hypothesize to be the results of using small grid size in the computational domain, especially inside the recycle line, as if the size of computational cells is smaller than a single bubble, the basic principles of Eulerian model is invalidated.

Due to the complicated hydrodynamic behavior of the gas-liquid-solid fluidized bed systems, *ab initio* prediction of the overall gas hold-up in these systems is not possible yet. Instead, prediction of this key parameter in design and operation of multiphase flows is still relied on empirical correlations which are developed based on the experimental measurements in pilot scale system. In order to develop accurate empirical correlations,

a meta-analysis was performed on the experimental data of the overall gas hold-up data in the gas-liquid-solid fluidized beds published in numerous studies over the past 40 years. As finding a single unified correlation to capture the hydrodynamic behavior of all the collected data points was impractical, the data points were classified according to several criteria (flow regime, particle diameter and particle Reynolds number). It was found that the classification of the data points according to the particle Reynolds number resulted in the most accurate and statistically significant correlations. Consideration of gas density in the correlations, improved the prediction of gas hold-up notably. However, considering bubble diameter as an independent variable, did not affect the accuracy of the correlations.

Finally, we studied the effect of particle wettability on the hydrodynamics of a gas-liquid-solid fluidized bed system operating with distilled water and 5wt.% aqueous ethanol solution. It was observed that gas hold-up was dropped by an average of about 20% in the fluidized bed of hydrophobic particles, compared to the hydrophilic ones. Adhesion of bubbles to particles and formation of bubble-particle agglomerates were observed frequently. According to the previous literature, the lower density of such agglomerates compared to bare particles, decreases their ability to penetrate and break-up the bubbles in the system. Therefore, the system of hydrophobic particles is associated with a larger bubble size distribution and consequently smaller gas hold-up. In this study, we have also measured the thickness of foam layer formed on top of the gas/liquid interface in the system of aqueous ethanol solution. The foam thickness decreased by rendering the particles hydrophobic as well as by increasing the inlet liquid flow rate. The experimental foam thickness data were then used to find the constants of two semi-empirical models for steady state foam thickness prediction. The models were significantly sensitive (and inversely proportional) to changes in bubble diameter. It was discussed that since a larger bubble size distribution exists in the bed of hydrophobic particles, the bubble size in the freeboard region of such systems should be larger. Hence, the foam thickness is smaller. The results of this study confirms the ability of hydrophobic particles in reduction of gas hold-up and foam thickness in the fluidized bed reactors.

6.2 Recommendations

The following subjects are recommended for future studies:

- Development of improved swarm correction models for the co-current gas-liquid flows is highly recommended. Almost all of the swarm correction equations available in the literature are empirical fits to experimental data in bubble columns. Comprehensive

set of experiments are required in co-current gas-liquid flows in order to develop improved swarm correction factors for this operation mode.

- Addition of a recycle pump to the scaled down EBR in order to return the recycled stream to the EBR is also recommended. Doing so, one can study the influence of separation efficiency of the recycle cups on the dynamics of the bed section. It was reported in the patent literature that poor performance of recycle cups in the foaming systems can result in instability of the bed of particles. Investigating such statement was not possible using the current setup. This can be done by installation of a recycle pump. An effort can also be made to develop more complicated recycle cups and test them in scaled down EBRs. Considering the low cost of 3-D printing technology, various designs can be tested in the pilot systems prior to implementation in the commercial units.

- It was observed that due to the small size of the experimental setup in this study, very small mesh grids were used in the computational domain (in the recycle line section) which resulted in failure of the Eulerian model. Future works can scale-up the computational domain and examine the validity of the model in prediction of gas hold-up in the recycle line using the experimental data provided here. Satisfying the dynamic and geometry similitude between the scaled-up system and the pilot scale system here, similar gas hold-up values are expected.

- In this study, we have developed a set of empirical correlations for the gas-liquid-solid system operating with water and spherical particles. From about 1400 data points collected, we have only used 342 points to develop the correlations presented here. Similar attempt can be made to find accurate empirical correlations for other systems, especially for the ones with gas hold-up values of over 25%, *i.e.*, operating with surface active agents or the low surface tension liquids.

- Although it is not possible to operate an industrial EBR with a bed of hydrophobic particles, the findings of this study informed that foam reduction is possible through even a slight increase in the bubble size distribution. Studies on particle segregation in gas-liquid-solid fluidized bed provided insights that fluidizing particles of same density but with different diameters can lead to great segregation among particles, with the smaller particles on top of the large particles. A hypothesis would be to fluidize a small fraction of hydrophobic particles (with smaller diameter) along with larger hydrophilic particles. According to particle segregation studies, a layer of hydrophobic particles is predicted to form on top of large hydrophilic particles. Presence of this layer could lead to an increase in size of the bubbles which enter the

freeboard region. Therefore, foam thickness is expected to decrease. Further studies and experiments to test this hypothesis are recommended.

References

[1] Alberta's energy reserves 2007 and supply/demand outlook 2008-2017. Technical report, Energy Resources Conservation Board: Calgary, AB, 2008.

[2] *Implementation of a Complete Wall Function for the Standard κ-ε Turbulence Model in OpenFOAM 4.0.* Chalmers University of Technology, 2016.

[3] Openfoam: Open source field operation and manipulation library. The OpenFoam Foundation, 2017.

[4] M. Agnaou, T. Treeratanaphitak, A. Mowla, M. Ioannidis, N. M. Abukhdeir, and H. Budman. On the use of physical boundary conditions for two-phase flow simulations: integration of control feedback. *Comput. Chem. Eng.*, 118:268 – 282, 2018.

[5] H. Akita and F. Yoshida. Bubble size, interfacial area, and liquid-phase mass transfer coefficient in bubble columns. *Ind. Eng. Chem. Process Des. Dev.*, 13(1):84–91, 1974.

[6] F. Al-Oufi. *An investigation of gas void fraction and transition condition for two-phase flow in a annular gap bubble column.* PhD thesis, Loughborough University, 2008.

[7] F.M. Al-Oufi, C.D. Rielly, and I.W. Cumming. Experimental srudy of void fraction behaviour in vertical bubbly gas-liquid flow using conductivity and maeasurments. In A.M. Al-Yami, editor, *Processdings of the Saudi Innovation Conference, Newcastle upon Tyne, UK.*, 2007.

[8] H.B. AlBa'ba'a, T. Elgammal, and R.S. Amano. Correlations of bubble diameter and frequency for air-water system based on orifice diameter and flow rate. *J. Fluids Eng.*, 138(11):114501–114501–7, 2011.

[9] J. Ally, M. Kappl, H. Butt, and A. Amirfazli. Detachment force of particles from air-liquid interfaces of films and bubbles. *Langmuir*, 26(23):1813518143, 2010.

[10] J. Ancheyta and J.G. Speight. *Hydroprocessing of heavy oils and residua*. CRC Press, Taylor & Francis Group, 2007.

[11] E. R. Armstrong, C.G.J. Baker, and M.A. Bergougnou. Effects of solids wettability on the characteristics of three-phase fuidization. In D.L. Kearins, editor, *Fluidization Technology*, pages 405–409, Hmisphere, 1976.

[12] J. A. Attia, S. Kholi, and L. Pilon. Scaling laws in steady-state aqueous foams including ostwald ripening. *Colloids Surf. A Physicochem. Eng. Asp.*, 436:1000 – 1006, 2013.

[13] R. Battino. The ostwald coefficient of gas solubility. *Fluid Phase Equilib.*, 15(3):231 – 240, 1984.

[14] A. Behkish, R. Lemoine, R. Oukaci, and B. I. Morsi. Novel correlations for gas holdup in large-scale slurry bubble column reactors operating under elevated pressures and temperatures. *Chem. Eng. J.*, 115:157–171, 2006.

[15] A. Behzadi. Turbulence modelling at high phase fractions. *Technical Report, BRITE/EURAM III (BE 4322), III-30*, 2001.

[16] A. Behzadi, R.I. Issa, and H. Rusche. Modelling of dispersed bubble and droplet flow at high phase fractions. *Chem. Eng. Sci.*, 59(4):759 – 770, 2004.

[17] G. Besagni, P. Brazzale, A. Fiocca, and F. Inzoli. Estimation of bubble size distributions and shapes in two-phase bubble column using image analysis and optical probes. *Flow Meas. Instrum.*, 52(Supplement C):190 – 207, 2016.

[18] G. Besagni and F. Inzoli. Bubble size distributions and shapes in annular gap bubble column. *Exp. Therm. Fluid Sci.*, 74(Supplement C):27 – 48, 2016.

[19] G. Besagni, F. Inzoli, G. De Guido, and L. A. Pellegrini. The dual effect of viscosity on bubble column hydrodynamics. *Chem. Eng. Sci.*, 158:509 – 538, 2017.

[20] G. Besagni, F. Inzoli, and T. Ziegenhein. Two-phase bubble columns: A comprehensive review. *ChemEngineering*, 2(2), 2018.

[21] G. Besagni, F. Inzoli, T. Ziegenhein, and D. Lucas. Computational fluid-dynamic modeling of the pseudo-homogeneous flow regime in large-scale bubble columns. *Chem. Eng. Sci.*, 160:144–160, 2017.

[22] A. Bhakta and E. Ruckenstein. Drainage and coalescence in standing foams. *J. Colloid Interface Sci.*, 191(1):184 – 201, 1997.

[23] V. K. Bhatia, K. A. Evans, N. Epstein, and P. Dakshinamurty. Effect of solids wettability on expansion of gas-liquid fluidized beds. *Ind. Eng. Chem. Process Des. Dev.*, 11(1):151–152, 1972.

[24] V.H. Bhusare, M.K. Dhiman, D.V. Kalaga, S. Roy, and J.B. Joshi. CFD simulations of a bubble column with and without internals by using openfoam. *Chem. Eng. J.*, 317:157 – 174, 2017.

[25] M. Bouaifi, G. Hebrard, D. Bastoul, and M. Roustan. A comparative study of gas hold-up, bubble size, interfacial area and mass transfer coefficients in stirred gas-liquid reactors and bubble columns. *Chem. Eng. Process.*, 40(2):97 – 111, 2001.

[26] J. Bredberg. On the wall boundary condition for turbulence models. Internal Report 00/4, Chalmers University of Technology, Department of Thermo and Fluid Dynamics., Goteberg, 2000.

[27] L. A. Briens and N. Ellis. Hydrodynamics of three-phase fluidized bed systems examined by statistical, fractal, chaos and wavelet analysis methods. *Chem. Eng. Sci.*, 60(22):6094–6106, 2005. 7th International Conference on Gas-Liquid and Gas-Liquid-Solid Reactor Engineering7th International Conference on Gas-Liquid and Gas-Liquid-Solid Reactor Engineering.

[28] N. Brunard, T. Gauthier, and J. LePage. Internal device for separating a mixture that comprises at least one gaseous phase and one liquid phase, 2006.

[29] R. Burckhart and W. Deckwer. Bubble size distribution and interfacial areas of electrolyte solutions in bubble columns. *Chem. Eng. Sci.*, 30(3):351 – 354, 1975.

[30] K. P. Burnham and D. R. Anderson. *Model Selection and Multimodel Inference: a practical information-theoretic approach*. Springer-Verlag, New York, 2nd edition, 2002.

[31] R. D. Buttke and J. R. Frey. Reduced gas holdup in ebullated reactor, 1995.

[32] R. D. Buttke and J.R. Frey. Process for collecting vapor in ebullated bed reactors, 1989.

[33] G. Cerne, S. Petelin, and I.Tiselj. Coupling of the interface tracking and the two-fluid models for the simulation of incompressible two-phase flow. *J. Comput. Phys.*, 171(2):776 – 804, 2001.

[34] T.Y. Chan. Liquid degasser in an ebullated bed process, 11 1991.

[35] P. Chen, J. Sanyal, and M.P. Dudukovic. Numerical simulation of bubble columns flows: effect of different breakup and coalescence closures. *Chem. Eng. Sci.*, 60(4):1085 – 1101, 2005.

[36] Y. Chen and L.-S. Fan. Bubble breakage due to particle collision in a liquid medium: particle wettability effects. *Chem. Eng. Sci.*, 44(11):2762 – 2767, 1989.

[37] Y. Chen and L.-S. Fan. Bubble breakage mechanisms due to collision with a particle in liquid medium. *Chem. Eng. Sci.*, 44(1):117 – 132, 1989.

[38] M. C. Chervenak and A. G. Comolli. Catalytic hydrogenation process and apparatus with improved vapor liquid separation, 9 1980.

[39] M. Colombo and M. Fairweather. Multiphase turbulence in bubbly flows: Rans simulations. *Int. J. Multiphase Flow*, 77:222 – 243, 2015.

[40] P. Dargar. Effect of surfactants on hydrodynamics of bubble columns and three-phase fluidibeds beds. Master's thesis, University of Ottawa, 2005.

[41] P. Dargar and A. Macchi. Effect of surface-active agents on the phase holdups of three-phase fluidized beds. *Chem. Eng. Process.*, 45(9):764 – 772, 2006.

[42] R.C. Darton. The physical behaviour of three-phase fluidized beds. In J.F. Davidson, R. Clift, and D. Harrison, editors, *Fluidization*, chapter 15, pages 495–528. Academic Press, 2nd edition, 1985.

[43] E. D. Deckwer and R. W. Field. *Bubble Column Reactos.* Wiley, 1992.

[44] W.-D. Deckwer and A. Schumpe. Improved tools for bubble column reactor design and scale-up. *Chem. Eng. Sci.*, 48:889–911, 1993.

[45] N. Devanathan, C.A. McKnight, W.B. VanderHeyden, L.P. Hackman, P.J. Klomans, and R.W. Skwarok. Hydrocarbon processing apparatus, 4 1997.

[46] D.A. Drew and R.T. Lahey. The virtual mass and lift force on a sphere in rotating and straining inviscid flow. *Int. J. Multiphase Flow*, 13(1):113 – 121, 1987.

[47] W. Du, X. Bao, J. Xu, and W. Wei. Computational fluid dynamics (CFD) modeling of spouted bed: assessment of drag coefficient correlations. *Chem. Eng. Sci.*, 61(5):1401 – 1420, 2006.

[48] K. Ekambara and M.T. Dhotre. CFD simulation of bubble column. *Nucl. Eng. Des.*, 240(5):963 – 969, 2010.

[49] S.H. Eltahry. k-epsilon equation for compressible reciprocating engine flows. *J. Energy*, 7(4):345–353, 1983.

[50] H. Enwald, E. Peirano, and A.-E Almstedt. Eulerian two-phase flow theory applied to fluidization. *Int. J. Multiphase Flow*, 22(Supplement):21 – 66, 1996.

[51] N. Epstein. Three-phase fluidization: Some knowledge gaps. *Can. J. Chem. Eng.*, 59(6):649–657, 1981.

[52] J.R. Fair. Desinging gas-sparged reactors. *Chem. Eng.*, 74:67–72, 1976.

[53] L.-S. Fan. *Gas-liquid-solid Fluidization Engineering*. Butterworth, Stoneham, MA, 1989.

[54] L.-S. Fan, F. Bavarian, R.L. Gorowara, B.E. Kreischer, R.D. Buttke, and L.B. Peck. Hydrodynamics of gas-liquid-solid fluidization under high gas hold-up conditions. *Powder Technol.*, 53(3):285 – 293, 1987.

[55] L.-S. Fan, S. Satija, and K. Wisecarver. Pressure fluctuation measurements and flow regime transitions in gas-liquid-solid fluidized beds. *AIChE J.*, 32:338–340, 1986.

[56] L.-S. Fan and G. Yang. Gas–liquid–solid three-phase fluidization. In Wen-Ching Yang, editor, *Handbook of Fluidization and Fluid-Particle Systems*. Marecl DeKker, Inc., 2003.

[57] D. F. Fletcher, D. D. McClure, J. M. Kavanagh, and G. W. Barton. CFD simulation of industrial bubble columns: numerical challenges and model validation successes. *Appl. Math. Model.*, 44:25 – 42, 2017.

[58] M. S. Fraguío, M. C. Cassanello, F. Larachi, and J. Chaouki. Flow regime transition pointers in three-phase fluidized beds inferred from a solid tracer trajectory. *Chem. Eng. Process.*, 45(5):350–358, 2006.

[59] A. B. Gandhi and J. B. Joshi. Unified correlation for overall gas hold-up in bubble column reactors for various gas-liquid systems using hybrid genetic algorithm-support vector regression technique. *Can. J. Chem. Eng.*, 88:758–776, 2010.

[60] E. Garnier, P. Sagaut, and M. Deville. Large eddy simulation of shock/homogeneous turbulence interaction. *Comput. Fluids*, 31(2):245 – 268, 2002.

[61] T. Gauthier, J. Verstraete, and S. Maget. Heavy feed hydroconversion method in ebullated bed mode with feed injection at the reactor top, 2015.

[62] L. Gemello, V. Cappello, F. Augier, D. Marchisio, and C. Plais. CFD-based scale-up of hydrodynamics and mixing in bubble columns. *Chem. Eng. Res. Des.*, 136:846 – 858, 2018.

[63] L. Gemello, C. Plais, F. Augier, A. Cloupet, and D.L. Marchisio. Hydrodynamics and bubble size in bubble columns: Effects of contaminants and spargers. *Chem. Eng. Sci.*, 184:93 – 102, 2018.

[64] S. Gerber, F. Behrendt, and M. Oevermann. A comparative study of euler-euler and euler-lagrange modelling of wood gasification in a dense fluidized bed. In Guangxi Yue, Hai Zhang, Changsui Zhao, and Zhongyang Luo, editors, *Proceedings of the 20th International Conference on Fluidized Bed Combustion*, 2010.

[65] B. Gonzalez, N. Calvar, E. Gomez, and A. Dominguez. Density, dynamic viscosity, and derived properties of binary mixtures of methanol or ethanol with water, ethyl acetate, and methyl acetate at t=(293.15, 298.15, and 303.15)k. *J. Chem. Thermodyn.*, 39(12):1578 – 1588, 2007.

[66] R. L. Gorowara and L.-S. Fan. Effect of surfactants on three-phase fluidized bed hydrodynamics. *Ind. Eng. Chem. Res.*, 29:882–891, 1990.

[67] J. R. Grace and F. Taghipour. Verification and validation of CFD models and dynamic similarity for fluidized beds. *Powder Technol.*, 139(2):99 – 110, 2004.

[68] M. R. Gray. *Upgrading Oilsands Bitumen and Heavy Oil*. The University of Alberta Press, 2015.

[69] A. A. Gregoli and W. R. Mounce. Vapor liquid separation apparatus, 1972.

[70] G. R. Guedon, G. Besagni, and F. Inzoli. Prediction of gas-liquid flow in an annular gap bubble column using a bi-dispersed eulerian model. *Chem. Eng. Sci.*, 161:138 – 150, 2017.

[71] S. Guet, S. Luther, and G. Ooms. Bubble shape and orientation determination with a four-point optical fibre probe. *Exp. Therm Fluid Sci.*, 29(7):803 – 812, 2005. Two Phase Flow.

[72] J. Guitian and D. Joseph. How bubbly mixtures foam and foam control using a fluidized bed. *Int. J. Multiphase Flow*, 24(1):1–16, 1998.

[73] A. Gupta and S. Roy. Euler-euler simulation of bubbly flow in a rectangular bubble column: experimental validation with radioactive particle tracking. *Chem. Eng. J.*, 225(Supplement C):818 – 836, 2013.

[74] L. H. Guzman and R. P. van Driesen. Apparatus for treatment of liquid with gas, 3 1964.

[75] A. Haider and O. Levenspiel. Drag coefficient and terminal velocity of spherical and nonspherical particles. *Powder Technology*, 58(1):63–70, 1989.

[76] G.F. Hewitt. Multiphase flow in the energy industries. *J. Eng. Thermophysics*, 17(1):12–23, 2008.

[77] T. Hibiki, M. Ishii, and Z. Xiao. Axial interfacial area transport of vertical bubbly flows. *Int. J. Heat Mass Transfer*, 44(10):1869 – 1888, 2001.

[78] H. Hikita, S. Asai, K. Tanigawa, K. Segawa, and M. Kitao. Gas hold-up in bubble columns. *Chem. Eng. J.*, 20(1):59 – 67, 1980. An International Journal of Research and Development.

[79] H. Hikita and H. Kikukawa. Liquid-phase mixing in bubble columns: Effect of liquid properties. *Chem. Eng. J.*, 8(3):191 – 197, 1974.

[80] T.S. Horozov. Foams and foam films stabilised by solid particles. *Curr. Opin. Colloid Interface Sci.*, 13(3):134–140, 2008.

[81] Z. Huang, D. D. McClure, G. W. Barton, D.F. Fletcher, and J. M. Kavanagh. Assessment of the impact of bubble size modelling in cfd simulations of alternative bubble column configurations operating in the heterogeneous regime. *Chem. Eng. Sci.*, 186:88 – 101, 2018.

[82] C.L. Hyndman, F. Larachi, and C. Guy. Understanding gas-phase hydrodynamics in bubble columns: a convective model based on kinetic theory. *Chem. Eng. Sci.*, 52(1):63 – 77, 1997.

[83] M. Ishii and T. Hibiki. *Thermo-Fluid Dynamics of Two-Phase Flow*. Springer, 2nd edition, 2011.

[84] H. A. Jakobsen. Phase distribution phenomena in two-phase bubble column reactors. *Chem. Eng. Sci.*, 56(3):1049 – 1056, 2001.

[85] H. A. Jakobsen, H. Lindborg, and C.A. Dorao. Modeling of bubble column reactors: progress and limitations. *Ind. Eng. Chem. Res.*, 44:5107–5151, 2005.

[86] H.M. Jena, G.K. Roy, and S.S. Mahapatra. Determination of optimum gas holdup conditions in a three-phase fluidized bed by genetic algorithm. *Comput. Chem. Eng.*, 34:476–484, 2010.

[87] H.M. Jena, G.K. Roy, and B.C. Meikap. Prediction of gas holdup in a three-phase fluidized bed from bed pressure drop measurement. *Chem. Eng. Res. Des.*, 86(11):1301–1308, 2008.

[88] H.M. Jena, G.K. Roy, and B.C. Meikap. Hydrodynamics of a gas-liquid-solid fluidized bed with hollow cylindrical particles. *Chem. Eng. Process. Process Intensif.*, 48:279–287, 2009.

[89] H.M. Jena, B.K. Sahoo, G.K. Roy, and B.C. Meikap. Characterization of hydrodynamic properties of a gas-liquid-solid three-phase fluidized bed with regular shape spherical glass bead particles. *Chem. Eng. J.*, 145:50–56, 2008.

[90] X. Jia, J. Wen, , W. Feng, and Q. Yuan. Local hydrodynamics modeling of a gas-liquid-solid three-phase airlift loop reactor. *Ind. Eng. Chem. Res.*, 46(15):5210–5220, 2007.

[91] J.B. Joshi. Computational flow modelling and design of bubble column reactors. *Chem. Eng. Sci.*, 56:5893 – 5933, 2001.

[92] E. K.T. Kam, M. H. Al-Mashan, and H. Al-Azmi. The mixing aspects of NiMo and CoMo hydrotreating catalysts in ebullated-bed reactors. *Catal. Today*, 48(14):229 – 236, 1999.

[93] E. K.T. Kam, F. Jasam, and M. Al-Mashan. Catalyst attrition in ebullated-bed hydrotreator operations. *Catal. Today*, 64:297–308, 2001. Special Issue: Multiphase Catalytic Reactor Engineering.

[94] N. Kantarci, F. Borak, and K. O. Ulgen. Bubble column reactors. *Process Biochem.*, 40(7):2263 – 2283, 2005.

[95] S. I. Karakashev, O. Ozdemir, M. A. Hampton, and A. V. Nguyen. Formation and stability of foams stabilized by fine particles with similar size, contact angle and different shapes. *Colloid. Surface. A*, 382(13):132 – 138, 2011.

[96] G. Keitel and U. Onken. The effect of solutes on bubble size in air-water dispersions. *Chem. Eng. Commun.*, 17(1-6):85–98, 1982.

[97] M.J.H. Khan, M.A. Hussain, Z. Mansourpour, N. Mostoufi, N.M. Ghasem, and E.C. Abdullah. CFD simulation of fluidized bed reactors for polyolefin production - A review. *Ind. Eng. Chem. Res*, 20(6):3919 – 3946, 2014.

[98] Z. Khan, V. H. Bhusare, and J. B. Joshi. Comparison of turbulence models for bubble column reactors. *Chem. Eng. Sci.*, 164:34 – 52, 2017.

[99] R. Kikuchi, A. Tsutsumi, and K. Yoshida. Fractal aspect of hydrodynamics in a three-phase fluidized bed. *Chem. Eng. Sci.*, 51(11):2865–2870, 1996. Chemical Reaction Engineering: From Fundamentals to Commercial Plants and Products.

[100] H. Kobayashi, B.L. Mark, and W. Turin. *Probability, Random Processes, and Statistical Analysis*. Cambridge University Press, New York, 2012.

[101] M. Kouzu, K. Koyama, M. Oneyama, T. Aramaki, T. Hayashi, M. Kobayashi, H. Itoh, and H. Hattori. Catalytic hydrogenation of recycle solvent in a 150t/d pilot plant of the NEDOL coal liquefaction process. *Fuel*, 79(34):365–371, 2000.

[102] R. Krishna. A scale-up strategy for a commercial scale bubble column slurry reactor for fischer-tropsch synthesis. *Oil Gas Sci. Tech.*, 55(4):359–393, 2000.

[103] R. Krishna, P.M. Wilkinson, and L.L. Van Dierendonck. A model for gas holdup in bubble columns incorporating the influence of gas density on flow regime transitions. *Chem. Eng. Sci.*, 46(10):2491–2496, 1991.

[104] A. V. Kulkarni. Design of a pipe/ring type of sparger for a bubble column reactor. *Chem. Eng. Technol.*, 33(6):1015–1022, 2010.

[105] S. Kumar, R. A. Kumar, P. Munshi, and A. Khanna. Gas hold-up in three phase co-current bubble columns. *Proc. Eng.*, 42:782 –794, 2012.

[106] S.B. Kumar, D. Moslemian, and M. P. Dudukovic. Gas-holdup measurements in bubble columns using computed tomography. *AIChE J.*, 43(6):1414–1425, 1997.

[107] P.L.C. Lage and R.O. Esposito. Experimental determination of bubble size distributions in bubble columns: prediction of mean bubble diameter and gas hold up. *Powder Technol.*, 101(2):142 – 150, 1999.

[108] C.D. Lane, C.A. McKnight, J. Wiens, K. Reid, and A.A. Donaldson. Parametric analysis of internal gas separation within an ebullated bed reactor. *Chem. Eng. Res. Des.*, 105:44 – 54, 2016.

[109] F. Larach, L. Belfares, I. Iliuta, and B.P. A. Grandjean. Three-phase fluidization macroscopic hydrodynamics revisited. *Ind. Eng. Chem. Res.*, 40(3):993–1008, 2001.

[110] Y.M. Lau, N.G. Deen, and J.A.M. Kuipers. Development of an image measurement technique for size distribution in dense bubbly flows. *Chem. Eng. Sci.*, 94(Supplement C):20 – 29, 2013.

[111] B. E. Launder and D. B. Spalding. The numerical computation of turbulent flows. In S. V. Patankar, A. Pollard, A. K. Singhal, and S. P. Vanka, editors, *Numerical Prediction of Flow, Heat Transfer, Turbulence and Combustion*, pages 96 – 116. Pergamon, 1983.

[112] D. Law, S.T. Jones, T.J. Heindel, and F.A. Battaglia. A combined numerical and experimental study of hydrodynamics for an air-water external loop airlift reactor. *J. Fluids Eng.*, 133(2):021301–021301–8, 2011.

[113] S. L. P. Lee, A. Soria, and H. I. De Lasa. Evolution of bubble length distributions in three-phase fluidized beds. *AIChE J.*, 36:1763–1767, 1990.

[114] D. Li and H. Christian. Simulation of bubbly flows with special numerical treatments of the semi-conservative and fully conservative two-fluid model. *Chem. Eng. Sci.*, 174:25 – 39, 2017.

[115] M. Lichti and H. Bart. Bubble size distributions with a shadowgraphic optical probe. *Flow Meas. Instrum.*, 60:164 – 170, 2018.

[116] W. Liu, N.N. Clark, and A.I. Karamavruc. General method for the transformation of chord-length data to a local bubble-size distribution. *AIChE J.*, 42:2713–2720, 1996.

[117] L. Ljung. *System Identification: Theory for the User*. Prentice Hall, 1987.

[118] C. Lo and S. Hwang. Local hydrodynamic properties of gas phase in an internal-loop airlift reactor. *Chem. Eng. J.*, 91:3–22, 2003.

[119] D. A. Lote, V. Vadakanchery, and A. W. Patwardhan. Computational fluid dynamics simulations of the air-water two-phase vertically upward bubbly flow in pipes. *Ind. Eng. Chem. Res.*, 57(31):10609–10627, 2018.

[120] D. Lucas, E. Krepper, and H.-M. Prasser. Development of co-current air-water flow in a vertical pipe. *Int. J. Multiphase Flow*, 31(12):1304 – 1328, 2005.

[121] X. Luo, P. Jiang, and L.-S. Fan. High-pressure three-phase fluidization: Hydrodynamics and heat transfer. *AIChE J.*, 43:2432–2445, 1997.

[122] X. Luo, D.J. Lee, R. Lau, G. Yang, and L.-S. Fan. Maximum stable bubble size and gas holdup in high-pressure slurry bubble columns. *AIChE J.*, 45(4):665–680, 1999.

[123] D. Ma, M. Liu, Y. Zu, and C. Tang. Two-dimensional volume of fluid simulation studies on single bubble formation and dynamics in bubble columns. *Chem. Eng. Sci.*, 72:61 – 77, 2012.

[124] A. Macchi, H. Bi, J.R. Grace, C.A. McKnight, and L. Hackman. Dimensional hydrodynamic similitude in three-phase fluidized beds. *Chem. Eng. Sci.*, 56(2122):6039 – 6045, 2001. Proceedings of the 5th International Conference on Gas-Liquid and Gas-Liquid-Solid Reactor Engineering.

[125] M.M. Marchese, A. Uribe-Salas, and J.A. Finch. Measurement of gas holdup in a three-phase concurrent downflow column. *Chem. Eng. Sci.*, 47(13):3475 – 3482, 1992.

[126] H. Marschall, R. Mornhinweg, A. Kossmanna, S. Oberhauser, K. Langbein, and O. Hinrichsen. Numerical simulation of dispersed gas/liquid flows in bubble columns at high phase fractions using openfoam. part ii - numerical simulations and results. *Chem. Eng.Technol.*, 34(8):1321–1327, 2011.

[127] J. Martinez, J.L. Sanchez, J. Ancheyta, and R.S. Ruiz. A review of process aspects and modeling of ebullated bed reactors for hydrocracking of heavy oils. *Catal. Rev.*, 52:60–105, 2010.

[128] C. Mata and D.D. Joseph. Foam control using a fluidized bed of hydrophobic particles. *Int. J. Multiphase Flow*, 25(1):63–85, 1999. cited By 3.

[129] A. Matsuura and L.-S. Fan. Distribution of bubble properties in a gasliquidsolid fluidized bed. *AIChE J.*, 30(6):894–903, 1984.

[130] E. D. Mattix and L. Charles. Reaction vessel for improved temperature regulation in exothermic reactions, 12 1968.

[131] J.C. Maxwell. *A Treatise of Electricity and Magnetism*, volume 1. Oxford University Press, 3rd edition, 1982.

[132] D.D. McClure, H. Norris, J.M. Kavanagh, D. Fletcher, and G.W. Barton. Validation of a computationally efficient computational fluid dynamics (CFD) model for industrial bubble column bioreactors. *Ind. Eng. Chem. Res.*, 53(37):14526–14543, 2014.

[133] M.E. McGovern, K.M.R. Kallury, and M. Thompson. Role of solvent on the silanization of glass with octadecyltrichlorosilane. *Langmuir*, 10(10):3607–3614, 1994.

[134] C.A. McKnight, L. Hackman, J.R. Grace, A. Macchi, D. Kiel, and J. Tyler. Fluid dynamic studies in support of an industrial three-phase fluidized bed hydroprocessor. *Can. J. Chem. Eng.*, 81(3-4):338–350, 2003.

[135] P.C. Mena, M.C. Ruzicka, F.A. Rocha, J.A. Teixeira, and J. Drahoš. Effect of solids on homogeneous–heterogeneous flow regime transition in bubble columns. *Chem. Eng. Sci.*, 60(22):6013–6026, 2005. 7th International Conference on Gas-Liquid and Gas-Liquid-Solid Reactor Engineering7th International Conference on Gas-Liquid and Gas-Liquid-Solid Reactor Engineering.

[136] M.L. Michelsen and K. Ostergaard. Hold-up and fluid mixing in gas-liquid fluidised beds. *Chem. Eng. J.*, 1:37–46, 1970.

[137] M. Mielli. *A numerical analysis of confined turbulent bubble plumes*. PhD thesis, Swiss Federal Institute of Technology Zurich, 2002.

[138] H. Miura and Y. Kawase. Hydrodynamics and mass transfer in three-phase fluidized beds with non-Newtonian fluids. *Chem. Eng. Sci.*, 52:4095–4104, 1997.

[139] D. C. Montgomery. *Design and Analysis of Experiments*. Wiley, 7th edition, 2008.

[140] A. Mowla, T. Treeratanaphitak, H. M. Budman, N. M. Abukhdeir, and M. A. Ioannidis. A meta-analysis of empirical correlations for average gas hold-up in three-phase fluidized beds. *Powder Technol.*, 301(Supplement C):590 – 595, 2016.

[141] K. Muroyama and L.-S. Fan. Fundamentals of gas-liquid-solid fluidization. *AIChE J.*, 31:1–34, 1985.

[142] K. Muroyama, E. Shibutani, T. Tsuji, and M. Shimizu. Performance evaluation of a full-scale deep u-tube utilizing ozonated oxygen as the process gas for treating drinking water. *Chem. Biochem. Eng. Q.*, 21(4):383–393, 2007.

[143] G. Narsimhan and E. Ruckenstein. Hydrodynamics, enrichment, and collapse in foams. *Langmuir*, 2(2):230–238, 1986.

[144] E. Olmos, C. Gentric, C. Vial, G. Wild, and N. Midoux. Numerical simulation of multiphase flow in bubble column reactors. influence of bubble coalescence and break-up. *Chem. Eng. Sci.*, 56:6359–6365, 2001. Proceedings of the 5th International Conference on Gas-Liquid and Gas-Liquid-Solid Reactor Engineering.

[145] H. Ortiz-Moreno, J. Ramírez, R. Cuevas, G. Marroquín, and J. Ancheyta. Heavy oil upgrading at moderate pressure using dispersed catalysts: Effects of temperature, pressure and catalytic precursor. *Fuel*, 100:186–192, 2012. ISAHOF 2011 Feed and Processes for the Production of Clean Fuels.

[146] K. Ostergaard. Three-phase fluidization. In J.F. Davidson and D. Harrison, editors, *Fluidization*, chapter 18, pages 751–778. Academic Press, 1971.

[147] V. G. Pangarkar. *Design of Multiphase Reactors*. John Wiley & Sons, Inc., 2015.

[148] J. Parekh and R. Rzehak. Euler-euler multiphase cfd-simulation with full reynolds stress model and anisotropic bubble-induced turbulence. *Int. J. Multiphase Flow*, 99:231 – 245, 2018.

[149] J. D. Paulsen, R. Carmigniani, A. Kannan, J. C. Burton, and S. R. Nagel. Coalescence of bubbles and drops in an outer fluid. *Nat. Commun.*, 5(3182), 2014.

[150] L. Pilon, A. G. Fedorov, and R. Viskanta. Steady-state thickness of liquidgas foams. *J. Colloid Interface Sci.*, 242(2):425 – 436, 2001.

[151] D. Pjontek and A. Macchi. Hydrodynamic comparison of spherical and cylindrical particles in a gas-liquid-solid fluidized bed at elevated pressure and high gas holdup conditions. *Powder Technology*, 253:657–676, 2014.

[152] D. Pjontek, C. A. McKnight, J. Wiens, and A. Macchi. Ebullated bed fluid dynamics relevant to industrial hydroprocessing. *Chem. Eng. Sci.*, 126:730–744, 2015.

[153] D. Pjontek, V. Parisien, C. Farrell, C.A. McKnight, J. Wiens, and A. Macchi. Particle agglomeration in gas-liquid-solid fluidized beds with a dispersed immiscible liquid: Study on particle size, shape and material. *Powder Technol.*, 266:45–60, 2014.

[154] M. Pourtousi, P. Ganesan, and J.N. Sahu. Effect of bubble diameter size on prediction of flow pattern in euler-euler simulation of homogeneous bubble column regime. *Measurement*, 76(Supplement C):255 – 270, 2015.

[155] M. Pourtousi, J.N. Sahu, and P. Ganesan. Effect of interfacial forces and turbulence models on predicting flow pattern inside the bubble column. *Chem. Eng. Process.*, 75(Supplement C):38 – 47, 2014.

[156] H.-M. Prasser, D. Scholz, and C. Zippe. Bubble size measurement using wire-mesh sensors. *Flow Meas. Instrum.*, 12(4):299 – 312, 2001.

[157] B.B. Pruden. The canmet hydrocracking process: Recent developments. In *Proc. Conf. Oil Sands Our Petroleum Future*, pages 276–282, Edmonton, Alberta, 1993.

[158] N. Qi, H. Zhang, B. Jin, and K. Zhang. CFD modelling of hydrodynamics and degradation kinetics in an annular slurry photocatalyticreactor for wastewater treatment. *Chem. Eng. J.*, 172(1):84–95, 2011.

[159] P. Maximiano Raimundo, A. Cartellier, D. Beneventi, A. Forret, and F. Augier. A new technique for in-situ measurements of bubble characteristics in bubble columns operated in the heterogeneous regime. *Chem. Eng. Sci.*, 155:504 – 523, 2016.

[160] M. Rajasimman and C. Karthikeyan. Aerobic digestion of starch wastewater in a fluidized bed bioreactor with low density biomass support. *J. Hazard. Mater.*, 143:82–86, 2007.

[161] K. Ramesh and T. Murugesan. Minimum fluidization velocity and gas holdup in gas-liquid-solid fluidized bed reactors. *J. Chem. Technol. Biotechnol.*, 77:129–136, 2002.

[162] M.R. Rampure, A.A. Kulkarni, and V.V. Ranade. Hydrodynamics of bubble column reactors at high gas velocity: experiments and computational fluid dynamics (CFD) simulations. *Ind. Eng. Chem.*, 46(25):8431–8447, 2007.

[163] M. S. Rana, V. Sámano, J. Ancheyta, and J.A.I. Diaz. A review of recent advances on process technologies for upgrading of heavy oils and residua. *Fuel*, 86:1216–1231, 2007. Special Issue: Mexican Congress on Chemical Reaction Engineering 2006.

[164] D. Rudkevitch and A. Macchi. Hydrodynamics of a high pressure three-phase fluidized bed subject to foaming. *Can. J. Chem. Eng.*, 86:293–301, 2008.

[165] R.S. Ruiz, F. Alonso, and J. Ancheyta. Effect of high pressure operation on overall phase holdups in ebullated-bed reactors. *Catal. Today*, 98(12):265 – 271, 2004. International Symposium on Advances in Hydroprocessing of Oil Fractions (ISAHOF 2004).

[166] R.S. Ruiz, F. Alonso, and J. Ancheyta. Pressure and temperature effects on the hydrodynamic characteristics of ebullated-bed systems. *Catal. Today*, 109:205–213, 2005. Hydroprocessing of Heavy Oil Fractions Hydroprocessing of Heavy Oil Fractions.

[167] H. Rusche. *Computational fluid dynamics of dispersed two-phase flows at high phase fractions.* PhD thesis, Imperial College London, 2002.

[168] F. Russo and N. T. Basse. Scaling of turbulence intensity for low-speed flow in smooth pipes. *Flow Meas. Instrum.*, 52:101 – 114, 2016.

[169] M.C. Ruzicka. On stability of a bubble column. *Chem. Eng. Res. Des.*, 91(2):191 – 203, 2013.

[170] R. Rzehak, M. Krauß, P. Kovats, and K. Zhringer. Fluid dynamics in a bubble column: new experiments and simulations. *Int. J. Multiphase Flow*, 89:299 – 312, 2017.

[171] R. Rzehak and E. Krepper. Closure models for turbulent bubbly flows: A CFD study. *Nucl. Eng. Des.*, 265:701 – 711, 2013.

[172] R. Rzehak and S. Kriebitzsch. Multiphase CFD-simulation of bubbly pipe flow: A code comparison. *Int. J. Multiphase Flow*, 68:135 – 152, 2015.

[173] M. Saberian-Broudjenni, G. Wild, J.-C. Charpentier, Y. Fortin, J.-P. Euzen, and R. Patoux. Contribution to the hydrodynamic study of gas-liquid-solid fluidized bed reactor. *Int. Chem. Eng.*, 27(3):423–440, 1987.

[174] M. Safoniuk. *Dimensional simultitude and the hydrodynamics of three-phase fluidized Beds*. PhD thesis, The University of British Columbia, 1999.

[175] M. Safoniuk, J.R. Grace, L. Hackman, and C.A. McKnight. Use of dimensional similitude for scale-up of hydrodynamics in three-phase fluidized beds. *Chem. Eng. Sci.*, 54:4961–4966, 1999.

[176] M. Safoniuk, J.R. Grace, L. Hackman, and C.A. McKnight. Gas holdup in a three-phase fluidized bed. *AIChE J.*, 48:1581–1587, 2002.

[177] A. Saint-James, D. J. Durian, and D. A. Weitz. *Kirk-Othmer Encyclopedia of Chemical Technology*, chapter Foams. Wiley, 2000.

[178] A. Sarrafi, M. Jamialahmadi, H. Mller-Steinhagen, and J.M. Smith. Gas holdup in homogeneous and heterogeneous gas-liquid bubble column reactors. *Can. J. Chem. Eng.*, 77(1):11–21, 1999.

[179] C. N. Satterfield. *Mass Transfer in Heterogeneous Catalysis*, volume 82. MIT Press, Cambridge, MA, 1970.

[180] S. C. Saxena. Bubble column reactors and fischer-tropsch synthesis. *Catal. Rev.*, 37:227–309, 1995.

[181] S. M. Sayles. Gas-liquid separation in an ebullated bed process, 1989.

[182] R. Schafer, C. Merten, and G. Eigenberger. Bubble size distributions in a bubble column reactor under industrial conditions. *Exp. Therm. Fluid Sci.*, 26(6):595 – 604, 2002.

[183] M. E. Schrader. Young-dupre revisited. *Langmuir*, 11(9):3585–3589, 1995.

[184] L.L. Schramm and F. Wassmuth. *Foams:Fundamentals and Applications in the Petroleum Industry*, chapter Foams: Basic Principles. American Chemical Society, 1994.

[185] A. Schumpe and G. Grund. The gas disengagement technique for studying gas holdup structure in bubble columns. *Can. J. Chem. Eng.*, 64(6):891–896, 1986.

[186] J. Schweitzer and S. Kressmann. Ebullated bed reactor modeling for residue conversion. *Chem. Eng. Sci.*, 59(22):5637 – 5645, 2004. ISCRE18.

[187] B. Selma, R. Bannari, and P. Proulx. A full integration of a dispersion and interface closures in the standard k-epsilon model of turbulence. *Chem. Eng. Sci.*, 65(20):5417 – 5428, 2010.

[188] Y. T. Shah, B. G. Kelkar, S. P. Godbole, and W.-D. Deckwer. Design parameters estimations for bubble column reactors. *AIChE J.*, 28(3):353–379, 1982.

[189] Y.T. Shah, J. Sebastian, D.N. Smith, and J.A. Ruether. On the behavior of the gas phase in a bubble column with ethanol-water mixtures. *Ind. Eng. Chem. Process Des. Dev.*, 24(4):1140–1148, 1985.

[190] A. Shaikh and M.H. Al-Dahhan. A review on flow regime transition in bubble columns. *Int. J. Chem. Reactor Eng.*, 5, 2007.

[191] Y.-J. Shih, M.-T. Tsai, and Y.-H. Huang. Mineralization and defluoridation of 2,2,3,3-tetrafluoro -1-propanol (TFP) by UV oxidation in a novel three-phase fluidized bed reactor (3P-FBR). *Water Res.*, 47(7):2325–2330, 2013.

[192] M. K. Silva, M. A. d'Avila, and M. Mori. Study of the interfacial forces and turbulence models in a bubble column. *Comput. Chem. Eng.*, 44:34–44, 2012.

[193] M. Simonnet, C. Gentric, E. Olmos, and N. Midoux. Experimental determination of the drag coefficient in a swarm of bubbles. *Chem. Eng. Sci.*, 62(3):858 – 866, 2007.

[194] M. Simonnet, C. Gentric, E. Olmos, and N. Midoux. CFD simulation of the flow field in a bubble column reactor: Importance of the drag force formulation to describe regime transitions. *Chem. Eng. Process.*, 47(9):1726 – 1737, 2008.

[195] V. Sivakumar, K. Senthilkumar, and T. Kannadasan. Prediction of gas holdup in the three-phase fluidized bed: air/newtonian and non-newtonian liquid systems. *Pol. J. Chem. Technol.*, 12:64–71, 2010.

[196] A. Sokolichin, G. Eigenberger, and A. Lapin. Simulation of buoyancy driven bubbly flow: Established simplifications and open questions. *AIChE J.*, 50(1):24–45, 2004.

[197] A. Sokolichin, G. Eigenberger, A. Lapin, and A. Lubert. Dynamic numerical simulation of gas-liquid two-phase flows euler/euler versus euler/lagrange. *Chem. Eng. Sci.*, 52(4):611 – 626, 1997.

[198] G. Song, F. Bavarian, L.-S. Fan, R.D. Buttke, and L.B. Peck. Hydrodynamics of three-phase fluidized bed containing cylindrical hydrotreating catalysts. *Can. J. Chem. Eng.*, 67:265–275, 1989.

[199] P. Stevenson. Inter-bubble gas diffusion in liquid foam. *Curr. Opin. Colloid Interface Sci.*, 15(5):374 – 381, 2010.

[200] N. C. Stewart. H-Oil process, 1975.

[201] J. C. Strickland. Liquid inventory control in an ebullated bed process, 1990.

[202] M. V. Tabib, S. A. Roy, and J. B. Joshi. CFD simulation of bubble column-an analysis of interphase forces and turbulence models. *Chem. Eng. J.*, 139(3):589 – 614, 2008.

[203] F. Taghipour, N. Ellis, and C. Wong. Experimental and computational study of gas-solid fluidized bed hydrodynamics. *Chem. Eng. Sci.*, 60:6857–6867, 2005.

[204] B.L. Tarmy, M. Chang, C.A. Coulaloglou, and P.R. Ponzi. Three phase hydrodynamic characteristics of the eds coal liquefaction reactors. In *Inst. Chem. Eng. Symp. Ser.*, volume 87, pages 303–317, 1984.

[205] P.J.A Tijm, F.J Waller, and D.M Brown. Methanol technology developments for the new millennium. *Applied Catalysis A: General*, 221(12):275–282, 2001. Hoelderich Special Issue.

[206] A. Tomiyama. Struggle with computational bubble dynamics. In *Third International Conference on Multiphase Flow, Lyon, France*, June 1998.

[207] A. Tomiyama, I. Kataoka, I. Zun, and T. Sakaguchi. Drag coefficients of single bubbles under normal and micro gravity conditions. *JSME Int. J. Ser. B Fluids Therm. Eng.*, 41(2):472–479, 1998.

[208] A. Tomiyama, H. Tamai, I. Zun, and S. Hosokawa. Transverse migration of single bubbles in simple shear flows. *Chem. Eng. Sci.*, 57(11):1849 – 1858, 2002.

[209] A. Tsutsumi, A. G. Dastidar, and L.-S. Fan. Characteristics of gas-liquid-solid fluidization with nonwettable particles. *AIChE J.*, 37(6):951–952, 1991.

[210] A. Tsutsumi, J. Nieh, and L.-S. Fan. Particle wettability effects on bubble wake dynamics in gas-liquid-solid fluidization. *Chem. Eng. Sci.*, 46(9):2381 – 2384, 1991.

[211] E. E. Underwood. *Quantitative Stereology*. Addison-Wesley, 1970.

[212] A. Uribe-Salas, C.O. Gomez, and J.A. Finch. A conductivity technique for gas and solids holdup determination in three-phase reactors. *Chem. Eng. Sci.*, 49(1):1 – 10, 1994.

[213] A. Vaidheeswaran and T. Hibiki. Bubble-induced turbulence modeling for vertical bubbly flows. *Int. J. Heat Mass Transfer*, 115:741 – 752, 2017.

[214] B.G.M. van Wachem and A.E. Almstedt. Methods for multiphase computational fluid dynamics. *Chem. Eng. J.*, 96:81 – 98, 2003.

[215] J. Wang, A. V. Nguyen, and S. Farrokhpay. A critical review of the growth, drainage and collapse of foams. *Adv. Colloid Interface Sci.*, 228:55 – 70, 2016.

[216] Q. Wang and W. Yao. Computation and validation of the interphase force models for bubbly flow. *Int. J. Heat Mass Transfer*, 98:799 – 813, 2016.

[217] H. Weller. Derivation, modelling and solution of the conditionally averaged two-phase flow equations. Technical report, OpenCFD Limited, 2005.

[218] F. M. White. *Fluid Mechanics*. McGraw-Hill, 1999.

[219] P. M. Wilkinson, A.P. Spek, and L.L. van Dierendonck. Design parameters estimation for scale-up of high-pressure bubble columns. *AIChE J.*, 38(4):544–554, 1992.

[220] A. J. Wilson. *Foams: Physics, Chemistry and Structure*. Springer, 1989.

[221] E.S. Winkel, S.L. Ceccio, D.R. Dowling, and M. Perlin. Bubble-size distributions produced by wall injection of air into flowing freshwater, saltwater and surfactant solutions. *Exp. Fluids*, 37(6):802–810, Dec 2004.

[222] F. Yamashita, Y. Mori, and S. Fujita. Size and distributions of bubbles in bubble column. *J. Chem. Eng. Jpn.*, 12(5-9), 1979.

[223] S. Yamoah, R. Martinez-Cuenca, G. Monros, S. Chiva, and R. Macian-Juan. Numerical investigation of models for drag, lift, wall lubrication and turbulent dispersion forces for the simulation of gas-liquid two-phase flow. *Chem. Eng. Res. Des.*, 98:17 – 35, 2015.

[224] G.Q. Yang, B. Du, and L.-S. Fan. Bubble formation and dynamics in gas-liquid-solid fluidization – A review. *Chem. Eng. Sci.*, 62:2–27, 2007. Fluidized Bed Applications.

[225] L.P. Yarin, A. Mosyak, and G. Hetsroni. *Fluid Flow, Heat Transfer and Boiling in Micro-Channels*. Spriger, Berlin, 2009.

[226] Y. Yu and S. D. Kim. Bubble characteristics in the radial direction of three-phase fluidized beds. *AIChE J.*, 34:2069–2072, 1988.

[227] Y. Yu and S. D. Kim. Bubble properties and local liquid velocity in the radial direction of cocurrent gasliquid flow. *Chem. Eng. Sci.*, 46(1):313 – 320, 1991.

[228] D. Zhang, N. Deen, and J. Kuipers. Numerical simulation of the dynamic flow behavior in a bubble column: a study of closures for turbulence and interface forces. *Chem. Eng. J.*, 61(23):7593–7608, 2006.

[229] J.-P. Zhang, J.R. Grace, N. Epstein, and K.S. Lim. Flow regime identification in gas-liquid flow and three-phase fluidized beds. *Chem. Eng. Sci.*, 52(21):3979 – 3992, 1997.

[230] X. Zhang, K. Guo, W. Qi, T. Zhang, and C. Liu. Gas holdup, bubble behaviour, and mass transfer characteristics in a two-stage internal loop airlift reactor with different screens. *Can. J. Chem. Eng.*, 95(6):1202–1212, 2017.

APPENDICES

Appendix A

Pilot Scale Multiphase Flow System and Used Equipment

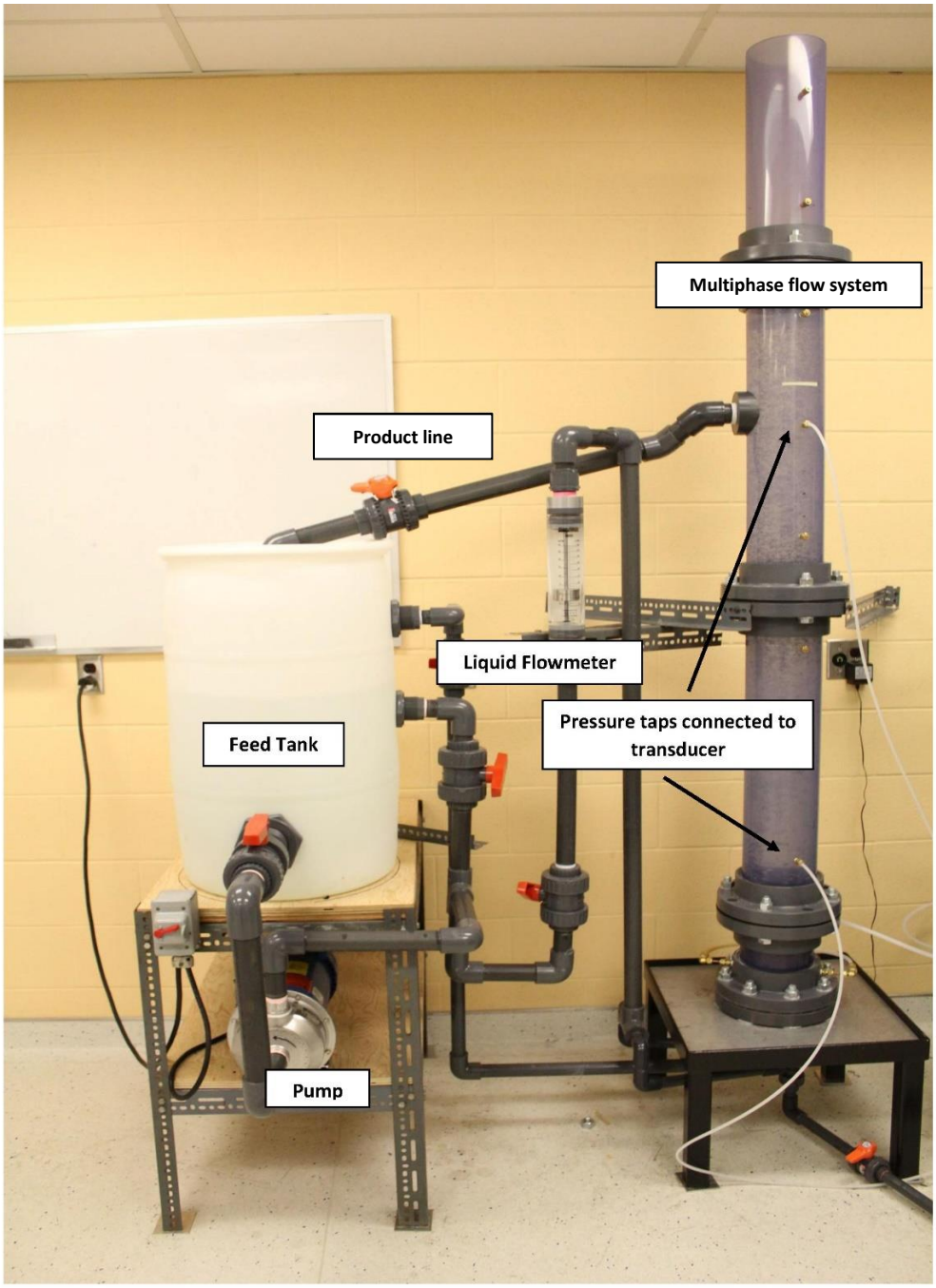

Figure A.1: Pilot scale multiphase flow system used in this study

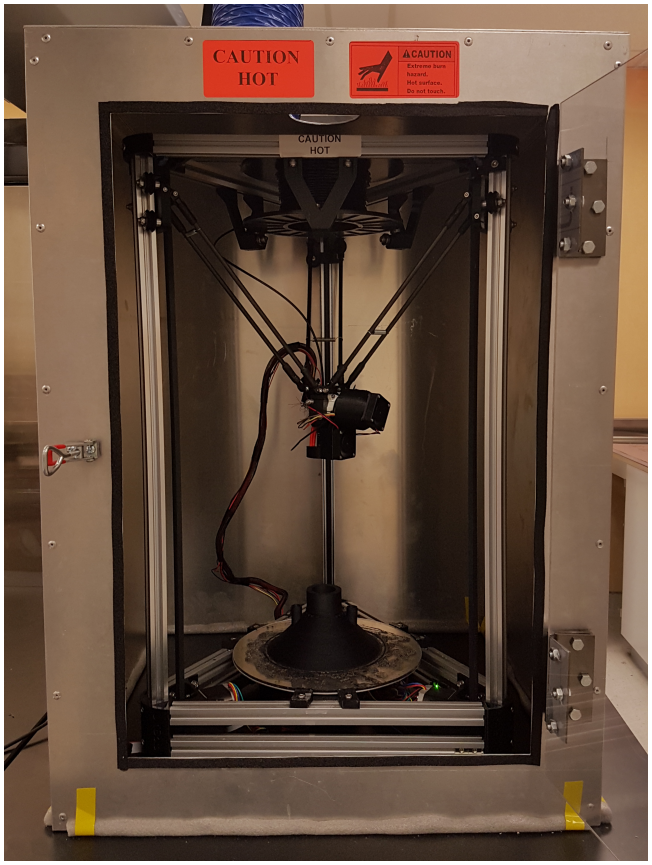

Figure A.2: 3-D printer used in this study to fabricate recycle cups

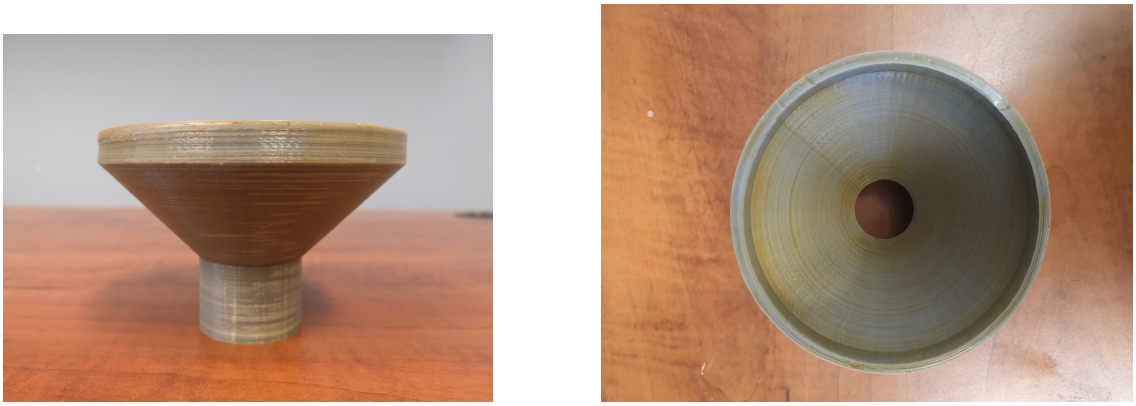

(a) (b)

Figure A.3: Simple cup used in Chapter 3

(a) (b)

Figure A.4: Cup with risers used in Chapter 3

Figure A.5: LCR meter used in this study to measure gas hold-up in the recycle line

Appendix B

Sample Raw Data for Bubble Diameter Measurements Using Image Analysis

Fig. B.1 shows the bubble diameter measurements for the sample case of air-water system operating at $u_{sl} = 0$, $u_{sg} = 0.03$ m/s. The histogram of the data is also shown in Fig. B.2. For the sample case shown here the average bubble diameter was calculated as 2.7±0.7.

For each set of operational parameters, several photographs were taken. From the two best photographs, more than 100 bubbles were selected. Considering the bubbles as ellipse, the major and minor axes were measured. The resolution of images were about 21 pixels/mm. Following is a sample calculation:

Assuming a bubble with $2a = 68$ pixels and $2b = 59$ pixels. Bubble diameter is calculated as:

$d_b = 2\sqrt[3]{a^2 b} \rightarrow d_b = 65$ pixels $\rightarrow d_b = \frac{65\ pixels}{21 \frac{pixels}{mm}} = 3.1$ mm.

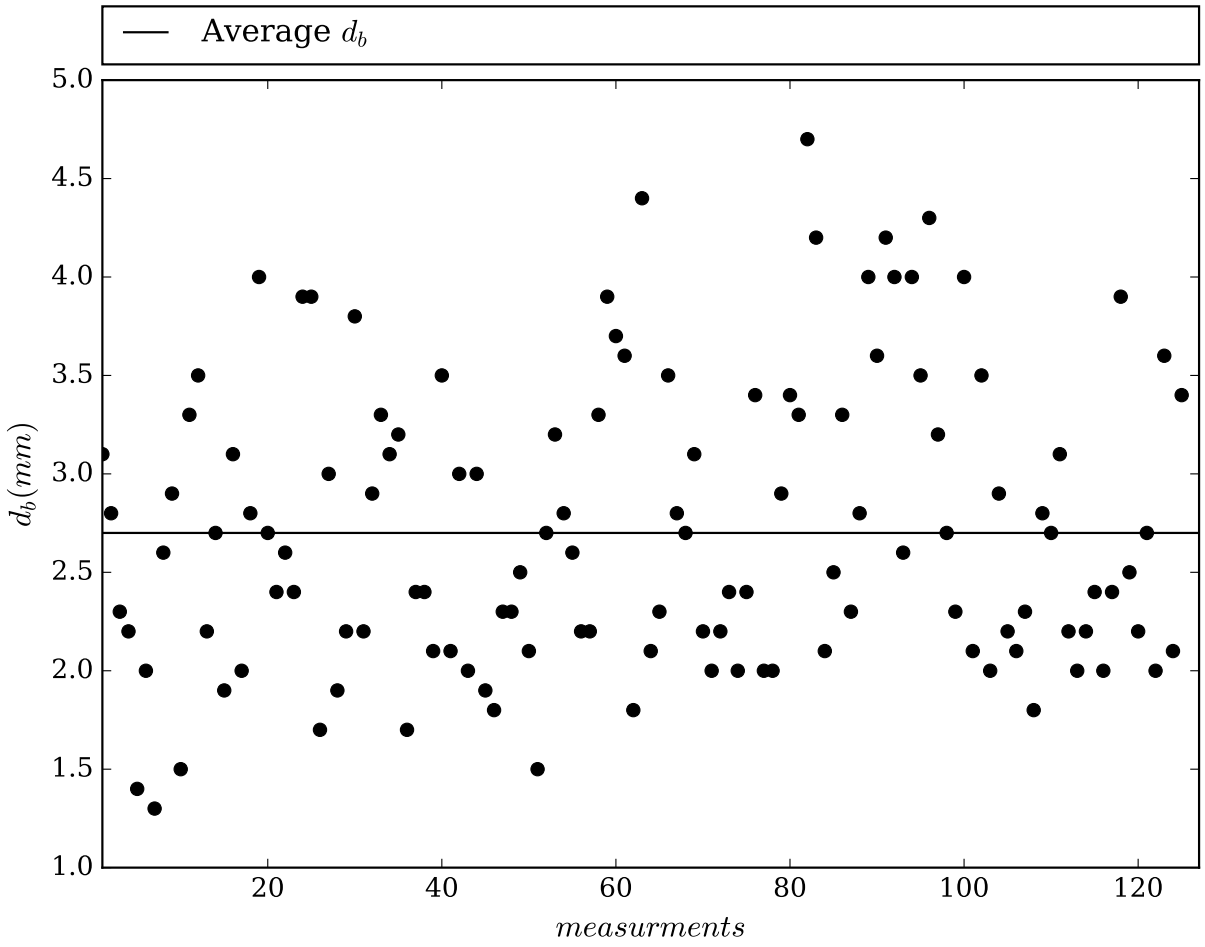

Figure B.1: Bubble diameter measurements for air-water system operating at $u_{sl} = 0$, $u_{sg} = 0.03$ m/s.

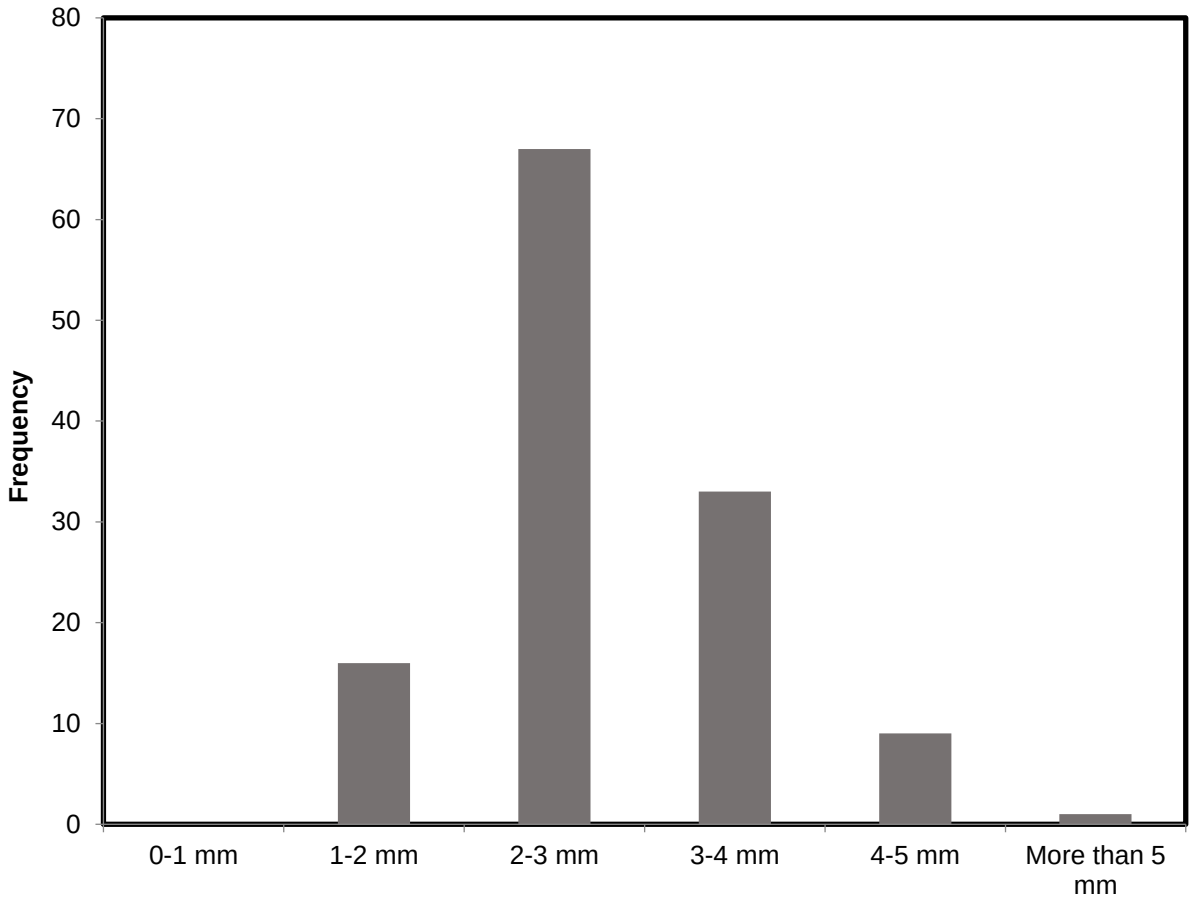

Figure B.2: Histogram of bubble diameter measurements for air-water system operating at $u_{sl} = 0$, $u_{sg} = 0.03$ m/s.

Appendix C

Sample Raw Data for Gas Hold-up in the Recycle Line

Fig. C.1 shows the conductance values from the LCR meter for calculation of gas hold-up in the recycle line for the sample case of air-5wt.% aqueous ethanol solution system and operating under $u_{sl} = 0.028$ m/s, $u_{sg} = 0.075$ m/s and $R_r = 0.5$.

For each set of operational parameters, two or three repetitions were taken for each pair of electrical conductivity cells. For each trial, between 40 to 50 readings were obtained from the LCR meter in a period of 3 minutes. The average of the readings were then calculated and used for gas hold-up measurement. For the case shown in Fig. C.1, the conductance for the liquid was $1.16\pm1 \times 10^{-3}$ Siemens (Si). The average of conductance readings for the gas-liquid mixture (G_m) from the pair of electrical conductivity installed in the top of recycle line was $1.067\pm0.033\times 10^{-3}$ Si and for the one installed in the bottom of the recycle line was $1.061\pm0.04\times 10^{-3}$ Si. Using the average G_m values and employing Eq.3.4 for the data in Fig. C.1, the gas hold-up was reported as 0.056 ± 0.003.

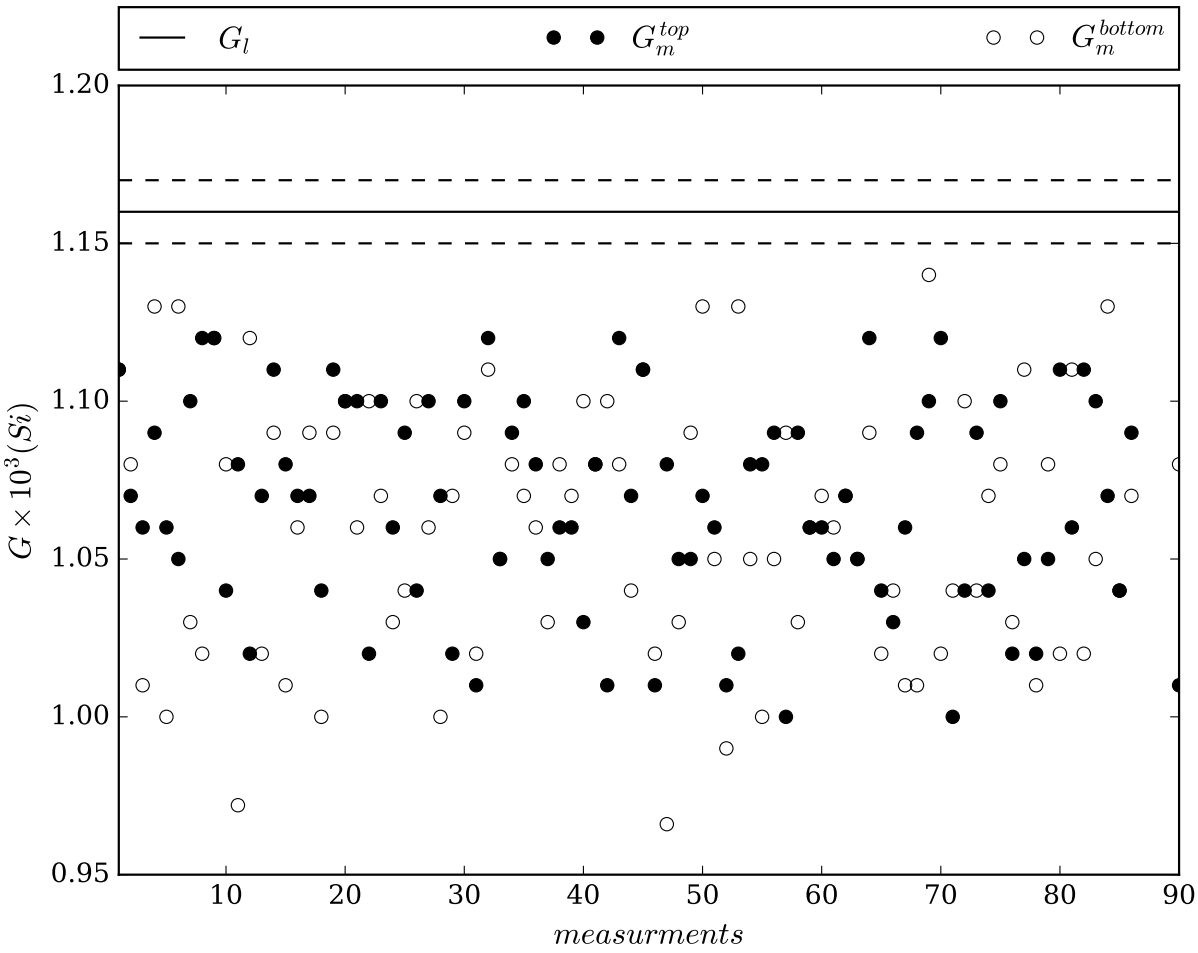

Figure C.1: Readings from electrical conductivity cells installed inside the recycle line (Dashed lines show the uncertainty in readings of G_l).